

Widely tunable multi-wavelength thulium-doped mode-locked all-fiber laser

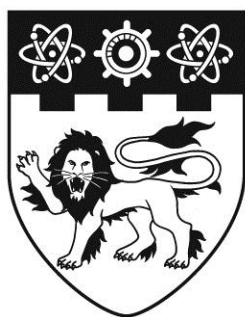
Yan, Zhiyu

2017

Yan, Z. (2017). Widely tunable multi-wavelength thulium-doped mode-locked all-fiber laser.
Doctoral thesis, Nanyang Technological University, Singapore.

<http://hdl.handle.net/10356/72052>

<https://doi.org/10.32657/10356/72052>



**NANYANG
TECHNOLOGICAL
UNIVERSITY**

**WIDELY TUNABLE MULTI-WAVELENGTH
THULIUM-DOPED MODE-LOCKED
ALL-FIBER LASER**

ZHIYU YAN

SCHOOL OF ELECTRICAL & ELECTRONIC ENGINEERING

2016

**WIDELY TUNABLE MULTI-WAVELENGTH
THULIUM-DOPED MODE-LOCKED
ALL-FIBER LASER**

ZHIYU YAN

SCHOOL OF ELECTRICAL & ELECTRONIC ENGINEERING

**A THESIS SUBMITTED TO
THE NANYANG TECHNOLOGICAL UNIVERSITY
IN PARTIAL FULFILLMENT OF THE REQUIREMENTS FOR THE DEGREE OF
DOCTOR OF PHILOSOPHY**

Acknowledgement

I would like to take this opportunity to express my sincere gratitude to my supervisor -- Prof. Wang Qi Jie. I was inspired by his passion for research. He loved it, bore down everything before him and enjoyed the success. I also benefitted much from his way of thinking. I knew how to come out, evaluate and carry on an idea. I knew how to well design an experiment by considering all the influencing factors, leaving margins and planning in advance for the unforeseen circumstances. He trusted me and gave me many chances to practice, so that I can deepen the understanding of fundamental knowledge, strength the problem-solving ability, and finally handle the project independently. He is willing to listen to my thoughts and difficulties, and he is always around to give me a hand. He also made effort to lead our team very well, by building the collaborations and finding a lot of resources, keeping the fairness, and bringing us the positive energy. His supervision is not only on research itself, but also on personal improvement from various aspects. I feel so lucky to have him to be my supervisor.

I am very grateful to my co-supervisors: Prof. Shum Ping Perry and Dr. Yu Xia. They gave me many opportunities to join the academic seminars, workshops and society activities, to exchange ideas with outstanding scholars all around the world. They also gave me many valuable suggestions on how to conduct the experiments, analysis the results, and present scientific papers.

I want to thank my teammates: Hu Xiaonan, Li Huizi, Li Xiaohui, Luo Jiaqi, Liang Guozhen, Liu Kun, Liu Tao, Meng Bo, Shen Youde, Sun Biao, Tang Yulong, Tao Jin, Yu Xuechao, Zeng Yongquan, Zhou Yanyan, *et al.* We together explored the secrets of the world, shared happiness and hardships, and celebrated our achievements. They made my Ph.D. journey very pleasant, meaningful and unforgettable.

I also want to thank Prof. Tang Dingyuan, Prof. Dong Xinyong, Qi Wenliang, Shao Guodong, and Wang Lulu for the use of their equipment.

Thanks to technicians in our labs: Mr. Chong Lui Tat, Anthony, Mr. Muhd Fauzi Bin Abdullah, Mr. Palaniraj, Ms. Seet Lye Ping and Ms. Yee Yang Boey. They managed lab in a well-organized way, dealt with all experimental issues carefully and patiently, and created a nice working environment for us.

Last but not least, thanks to my grandparents, father, mother and husband. They are always by my side. Thanks for their endless love.

Tables of Contents

Acknowledgement	i
Tables of Contents	ii
List of Figures	iv
List of Tables	vi
Summary	vii
Chapter 1	
Introduction.....	1
1.1 Background and Motivation.....	1
1.2 Challenges and Objective.....	4
1.3 Thesis organization	5
Chapter 2	
Theory on Passively Mode-Locked Fiber Laser	6
2.1 Pulse Propagation in Single-Mode Fiber	6
2.1.1 Pulse Propagation Equation in Single-Mode Fiber	6
2.1.2 Chromatic Dispersion	8
2.1.3 Optical Soliton	10
2.2 Pulse Propagation in Gain Fiber	11
2.2.1 Three-, Four-, and Quasi-Three- Level System	11
2.2.2 Gain Coefficient and Amplification Factor.....	14
2.2.3 Ginzburg–Landau Equation	15
2.3 Passively Mode-Locked Fiber Laser.....	18
2.3.1 Fiber Laser Cavity.....	18
2.3.2 Laser Threshold.....	19
2.3.3 Mode Locking	21
2.3.4 Passive Mode Locking Enabled by Nonlinear Polarization Evolution	23
2.3.4.1 Fiber Birefringence	24
2.3.4.2 Pulse shaping by nonlinear polarization evolution	28
Chapter 3	
Literature Review.....	30
3.1 Nonlinear Polarization Evolution Based Technique	30
3.2 Nonlinear Amplifier Loop Mirror Based Technique	32
3.3 Grating Based Technique.....	33
3.4 Fiber Taper Based Technique	34
3.5 Fabry-Perot Interferometer Based Technique	35
3.6 Special Fibers Based Technique	35

3.7 Other Techniques in Tunable Multi-Wavelength Fiber Lasers.....	36
Chapter 4	
The Configuration of Experimental Setup	39
4.1 The Energy Level, Absorption and Emission of Thulium-Doped Fibers	39
4.2 The Transmission of Polarization-Dependent Isolator	41
4.3 The Transmission of Coupler.....	43
4.4 The Scheme for Multi-Wavelength Emission.....	44
4.5 The Scheme for Tunable Operation	48
4.6 The Experimental Setup.....	51
Chapter 5	
Tunable Single-Wavelength Mode Locking	54
5.1 The Experimental Results	54
5.2 The Mechanisms	57
Chapter 6	
Multi-Wavelength Mode Locking	60
6.1 Tunable Multi-Wavelength Mode Locking	60
6.1.1 The Experimental Results	60
6.1.2 The Mechanisms	61
6.2 Switchable Multi-wavelength Mode Locking.....	64
6.3 The Quasi-Five-Wavelength Q-Switched Mode Locking	67
Chapter 7	
The Extended Results and Discussions.....	70
7.1 Soliton Dynamics.....	70
7.1.1 The Peak Sidebands	70
7.1.2 The Dip Sidebands	74
7.2 The Observation of Noise-Like Pulses	74
7.3 The Laser Stability and Repeatability	76
Chapter 8	
Conclusion and Future Works	78
8.1 The Conclusion	78
8.2 The Future Works	79
Reference	81
Publications.....	91
Journal Papers	91
Conference Proceedings.....	92
Conference Talks	92

List of Figures

Figure 1. 1. Synthetic stick absorption spectrum of a simple gas mixture corresponding to the Earth's atmosphere composition based on HITRAN data created using HITRAN on the Web system. Green color: water vapor, WN: wavenumber (caution: lower wavelengths on the right, higher on the left). Water vapor concentration for this gas mixture is 0.4% [1].....	2
Figure 1. 2. The scheme of telecommunication with the multi-wavelength light source.	2
Figure 2. 1. The dispersion and group-velocity dispersion of fused silica.....	9
Figure 2. 2. The energy level diagrams of (a) three-level system, (b) four-level system, and (c) quasi-three-level system.....	12
Figure 2. 3. The schematic of (a) Fabry-Perot cavity, (b) fiber ring cavity, and (c) figure-8 cavity. WDM: wavelength-division multiplexer.	18
Figure 2. 4. The power change in a Fabry-Perot fiber cavity per round trip.....	19
Figure 2. 5. The pulse train formed when seven longitudinal modes ($n = 3$) of equal amplitudes are mode locked [32].....	23
Figure 2. 6. Diagram of pulse shortening process through nonlinear polarization evolution (NPE).	28
Figure 3. 1. The NPE module in an all-fiber laser cavity [38]. PD-ISO: polarization-dependent isolator. PC: polarization controller.....	30
Figure 4. 1. The simplified energy-level diagram and cross-relaxation of thulium ³⁺ (Tm ³⁺) ion in silica glass fiber.	40
Figure 4. 2. The transition cross section of (a) holmium-doped silica fiber and (b) Tm-doped silica fiber [82–84].....	41
Figure 4. 3. The calculated and fitted transmission curve of the polarization-dependent isolator (PDI).	42
Figure 4. 4. The measured transmission curve of the 5:95 coupler.	43
Figure 4. 5. The NPE-based structure formed by polarization controller, single-mode fiber. PDI: polarization-dependent isolator.	45
Figure 4. 6. The simulated NPE-induced transmissions with different length of single-mode fiber.....	47
Figure 4. 7. The working principle of bidirectional pumping of Tm-doped fiber. (a), (b), (c), (d) is the situation of population inversion, absorption and emission at different segments of Tm-doped fiber.	49
Figure 4. 8. The experimental setup on the measurement of amplified stimulated emission (ASE) spectra. LD: laser diode.	50
Figure 4. 9. (a) The ASE spectra by bidirectional, backward, and forward pumping under the same pumping power level. (b) The original and revised ASE spectrum. The revised one is with considering the wavelength-dependent loss of PDI and coupler.	50
Figure 4. 10. Schematic illustration of the effects of different pumping methods and spectral filters on the potential tunable range. The shaded areas describe the potential tunable ranges of each scheme.	51

Figure 4. 11. The experimental setup of the widely tunable multi-wavelength Tm-doped mode-locked all-fiber laser. SMF: single-mode fiber.	52
Figure 5. 1. Tunable single-wavelength lasing emissions from 1839 to 1978 nm, from Tm-doped mode-locked all-fiber lasers enabled by nonlinear polarization evolution (NPE).	54
Figure 5. 2. (a) The pulse train, (b) RF spectrum, (c) pulse width, and (d) beam profile of Tm-doped mode-lock all-fiber lasers enabled by NPE.	56
Figure 5. 3. The output power at different emission wavelength of Tm-doped mode-locked all-fiber lasers enabled by NPE.	56
Figure 5. 4. The calculated NPE-induced transmission on different values of (a) θ_1 and (b) B_m	58
Figure 6. 1. Tunable dual-wavelength lasing emissions from 1864 to 1916 nm, from Tm-doped mode-locked all-fiber lasers enabled by NPE.	62
Figure 6. 2. (a) Tunable tri-wavelength lasing emissions from 1863 to 1912 nm and (b) tunable four-wavelength lasing emission from 1860 to 1915 nm, from Tm-doped mode-locked all-fiber lasers enabled by NPE.	63
Figure 6. 3 Switchable dual-wavelength operation with wavelength at (a) 1864/1874 nm and (b) 1875/1886 nm, from Tm-doped mode-locked all-fiber lasers enabled by NPE.	65
Figure 6. 4. Switchable tri-wavelength operation with wavelength at 1863/1874/1885 nm, from Tm-doped mode-locked all-fiber lasers enabled by NPE.	66
Figure 6. 5. Switchable tri-wavelength operation with wavelength at 1863/1874/1885 nm, from Tm-doped mode-locked all-fiber lasers enabled by NPE. The coupler is used as input and output port simultaneously which causes much loss.	67
Figure 6. 6. The spectra of quasi-five-wavelength Q-switched mode locking from Tm-doped mode-locked all-fiber lasers enabled by NPE.	68
Figure 6. 7. The pulse train under different time scales of quasi-five-wavelength Q-switched mode locking, from Tm-doped mode-locked all-fiber lasers enabled by NPE.	69
Figure 7. 1. The soliton spectrum with center wavelength at 1884 nm, from Tm-doped mode-locked all-fiber lasers enabled by NPE.	72
Figure 7. 2. The soliton spectra of Tm-doped mode-locked all-fiber lasers enabled by NPE, measured with different pump strengths, and with center wavelength at (a) 1932 nm and (b) 1945 nm.	73
Figure 7. 3. The dips on the spectra of ASE and soliton which are due to the water absorption. Each dip of ASE and soliton is at the same position.	74
Figure 7. 4. The spectra of noise-like pulses with different polarization states, from Tm-doped mode-locked all-fiber lasers enabled by NPE.	75
Figure 7. 5. The pulse train of noise-like pulses from Tm-doped mode-locked all-fiber lasers enabled by NPE. (a) and (b) are measured with one polarization state but with different time scales, (c) and (d) are measured with the other polarization state but with different time scales.	76

List of Tables

Table 4. 1. The rotation angle versus wavelength of the Faraday rotator inside the polarization-dependent isolator	42
Table 4. 2. The list of different values of modal birefringence with different radius curvatures.	46
Table 4. 3. The list of parameters and equipments used in the measurement.	52
Table 5. 1. The list of parameters used in calculating the separation of peaks in the NPE-induced transmission equation	58
Table 7. 1. The calculated $\Delta\omega$ and the corresponding wavelength of the peak sidebands with $m = 1, 2, 3, 4$. The center wavelength is $1884.05nm$	72

Summary

All-fiber lasers have attracted tremendous research interests due to the advantages of minimum alignment requirement, high energy efficiency, low maintenance, low sensitivity and wavelength independent to the temperature. The all-fiber lasers with wavelength-tunable operation and multi-wavelength emission are of much interest because the emission wavelength can be tuned within a broad spectral range and multiple lasing wavelength can be emit simultaneously, which is useful for applications in spectroscopy, wavelength division multiplexing communication, optical signal processing, optical instrument and system diagnostics, etc. Furthermore, if this kind of laser is with pulsed output and high pulse energy, it will become an irreplaceable light source for time-domain and high-intensity applications.

Now the operating wavelength of most tunable multi-wavelength all-fiber pulsed lasers are in the 1 μm and 1.5 μm regime and a few in 2 μm regime, in which thulium-(Tm-) or holmium-doped fiber is used as the gain medium. Since 2 μm regime is the eye-safe regime, lasers operating at this regime is particular important for medical and military applications.

There are various methods that can realize tunable operation and multi-wavelength emission in fiber laser. The basic principle is to form an artificial spectral filter with a tunable center wavelength, which acts as a wavelength selection element to enable the tunable operation. And this filter is with multiple maximums of equal amplitude in the spectral domain, to enable the multi-wavelength emission. This filter can be formed by multimode fiber, fiber taper, photonics crystal fiber, fiber Bragg grating, Fabry-Perot filter, nonlinear polarization evolution (NPE) technique, nonlinear amplified loop mirror technique, etc. NPE is chose because its potential tunable range covers the whole emission spectrum, rather than a specific range, and the number of emission wavelength is easily controlled by the length of birefringent fiber inside the cavity, without additional cost on the cavity complexity.

Tm-doped fiber is chosen to be the gain medium because it has broad emission spectra, the eye-safe emission regime, commercially available pumping diode, and high pumping efficiency. Bidirectional pumping method is used to broaden the gain bandwidth. NPE is used to enable mode locking, tunable operation and multi-wavelength emission. The broadband transmissions of other optical components inside

the cavity such as isolator and coupler are also studied in order to identify their effects on the bandwidth of the net gain (saturated gain minus cavity loss).

We have developed a widely tunable multi-wavelength Tm-doped mode-locked all-fiber laser. The main characteristics of this laser are the single-wavelength tunable operation, multi-wavelength tunable operation, and multi-wavelength switchable operation. The tunable range of single-wavelength mode locking is 136 nm (from 1842 to 1978 nm). The tunable range of dual-, tri-, and four-wavelength mode locking is 52 nm (from 1864 to 1916 nm), 49 nm (from 1863 to 1912 nm), and 55 nm (from 1860 to 1915 nm), respectively. The tunable ranges above are the widest in such kind of laser, to the best of our knowledge. For the multi-wavelength switchable operation, we can achieve the full binary control, which is firstly reported in such kind of laser. This could act as an optical binary system, which has potential applications in optical signal processing, optical switching devices and optical communication.

Other phenomena are also observed with this setup, including the quasi-five-wavelength Q-switched mode locking, the peaks and dips in the soliton sidebands, and the noise-like pulses.

The demonstrated laser is with a compact structure, with easy operation by adjusting the polarization controllers to realize the tunable operation and multi-wavelength emission, and offers a solution in optical communications, spectroscopy, and time-resolved applications.

Chapter 1

Introduction

This thesis discusses on a Thulium-doped (Tm-doped) mode-locked all-fiber laser with tunable operation and multi-wavelength emission. Nonlinear polarization evolution is used to enable the mode locking, tunable operation and multi-wavelength emission. The developed laser is with the widest tunable range and with the first demonstration of full-binary control in a switchable manner, in such kind of laser.

This chapter talks about the background and motivation on all-fiber lasers, tunable multi-wavelength fiber lasers with mode-locked operation, and Tm-doped fiber lasers. This chapter also talks on the challenges to achieve widely tunable operation and multi-wavelength emission with an all-fiber cavity structure. Then our objective is presented, and the organization of this thesis is described.

1.1 Background and Motivation

All-fiber lasers have attracted tremendous research interests due to the advantages of minimum alignment requirement, high energy efficiency, low maintenance, low sensitivity and wavelength independent to the temperature.

Fiber lasers with wavelength-tunable operation are of much interest because the emission wavelength can be tuned within a broad spectral range, which is useful for applications in spectroscopy, optical communication, optical instrument and system diagnostics, etc. For an example, there are many absorption bands of gases locating between 1 to 2 μm as shown in figure 1.1 [1]. The 1 to 2 μm are the emitting wavelength regime of most fiber lasers. Since these gases are the main compositions of the Earth's atmosphere, the fiber laser can be a light source to detect the gases to know more about the condition of the Earth's atmosphere. With a tunable light source, the wavelength can be tuned to match a gas absorption line to give a high spectral

power density, and it can detect at multiple points in the spectral domain to get more features on the absorption spectrum [2].

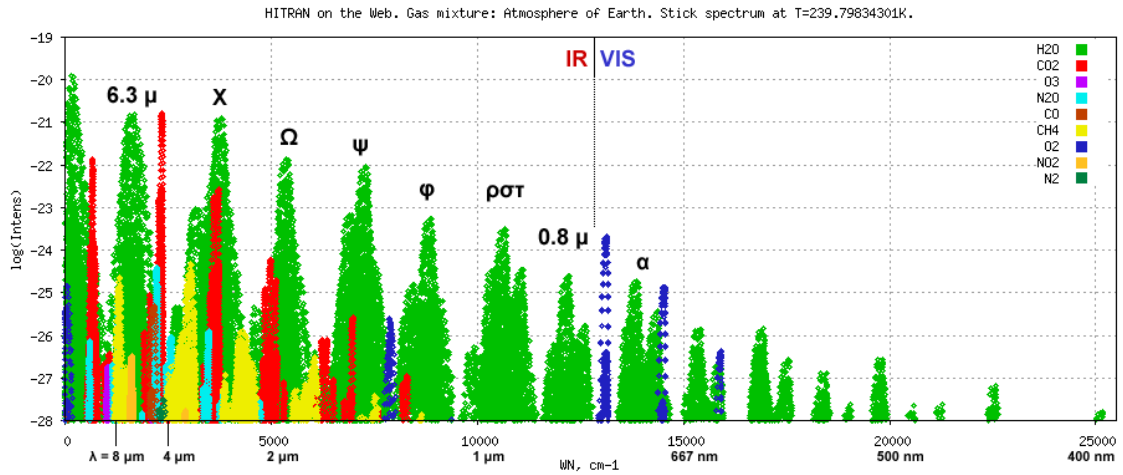


Figure 1. 1. Synthetic stick absorption spectrum of a simple gas mixture corresponding to the Earth's atmosphere composition based on HITRAN data created using HITRAN on the Web system. Green color: water vapor, WN: wavenumber (caution: lower wavelengths on the right, higher on the left). Water vapor concentration for this gas mixture is 0.4% [1].

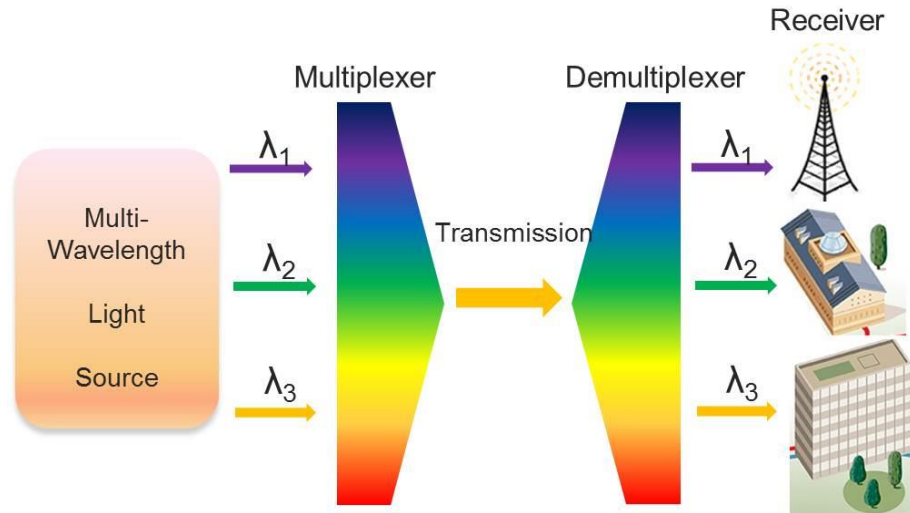


Figure 1. 2. The scheme of telecommunication with the multi-wavelength light source.

Besides, the fiber lasers with multi-wavelength emission are also widely used in fiber-optic test and measurement of wavelength division multiplexing components, optical signal processing, optical sensing, microwave photonics and precision spectroscopy [3,4]. For instance, if a multi-wavelength fiber laser is used as the light source in the telecommunication in figure 1.2, the system capacity is increased by transmitting signals in large numbers of channels and each channel works at different wavelengths. The fiber laser can be with moderate output powers to support the long-

distance transmission. Another example is to use a multi-wavelength laser source to inspect the surface profile [5]. The laser with different wavelengths carries different information. The information were combined and analyzed together by the computer to get the more precise result of the sample.

Comparing with continuous wave (CW) lasers, mode-locked lasers are irreplaceable light sources for time-domain and high-intensity applications. Examples are the sensitivity measurement of the absorption rate rather than the magnitude [6], the non-linear spectroscopy and multiphoton microscopy, which require a high-intensity beam to stimulate the nonlinear phenomena [7], and time-resolved photoluminescence and measurements [8,9].

Fiber lasers usually works at 1, 1.5 and 2 μm , depending on the kind of gain fibers used. 2 μm regime is important because firstly it is the eye-safe regime, which is mostly used in medical and military applications. Secondly it is a good candidate to increase the capacity of fiber-optic communication system, by expanding the operation wavelength from current 1.5 μm to 2 μm . Thirdly the absorption of some materials is larger at 2 μm than that in 1 and 1.5 μm . With larger absorption we can do the sensing and material processing in industry such as wetting and cutting much easier. If Tm- or holmium- (Ho-) doped fiber is used as the gain medium, the emitting wavelength of the fiber lasers will be near 2 μm . However the tunable multi-wavelength mode-locked fiber lasers are mostly reported in the 1 μm and 1.5 μm regime and a few near 2 μm regime [10–21]. The tunable range of 2 μm mode-locked all-fiber lasers is limited to 50 nm [22]. The limited tunable range significantly restricts their applications in biological and medical imaging. The number of emission wavelength from 2 μm mode-locked all-fiber lasers was only two, which was achieved by adjusting the polarization controllers [23]. It limits the further expansion of numbers of channels over large wavelength span, which are used to increase the transmission capacity in a 2 μm fiber-optic communication system. No switchable operation, especially the switchable full binary control, from a multi-wavelength mode-locked all-fiber laser near the 2 μm regime has been reported so far, which limits the application of optical signal processing.

Therefore, developing a mode-locked all-fiber laser near the 2 μm regime with widely tunable range and multi-wavelength emission is of much importance for various applications. For examples it enables a number of channels over large wavelength span to increase the transmission capacity in telecommunications [24], it

can enable both multi-species detection and the detection at different wavelengths simultaneously for some unstable species in gas spectroscopy [25], and it can convey more signals, enlarge the measurement range and help to build a compact system structure in sensor multiplexing [26]. Furthermore, the integration of tunable operation and multi-wavelength emission into one laser setup is convenient and cost-effective. When it is required, only one laser setup is used instead of multiple lasers with different emission wavelengths.

1.2 Challenges and Objective

The challenges are:

To achieve the widely tunable operation, we should find a suitable gain medium and a pumping method to achieve a wide gain bandwidth, design a module in the cavity to form the spectral filter with center wavelength tunable, and manage the cavity loss to reduce the laser threshold over the broadband emission spectrum.

To achieve the multi-wavelength emission, we should adopt a spectral filter with periodically varying amplitude and with equal amplitude maximums. This filter breaks the homogeneously broadening of ions in gain medium, to enable stable multi-wavelength operation.

To achieve a laser with all-fiber cavity structure, working near 2 μm regime, and with pulsed output, we should choose the proper all-fiber optical components, the gain fibers, and the technique to enable mode locking.

To reach all the requirements above simultaneously, we should investigate many different approaches, propose the most suitable one, and then experimentally realize it.

We aim to develop a mode-locked all-fiber laser working near the 2 μm regime, with wavelength-tunable operation and multi-wavelength emission. The tunable range of single-wavelength mode locking will challenge the state-of-art, which was 50 nm from a Tm-doped mode-locked all-fiber laser [22]. The wavelength-tunable operation in that setup was realized by stretching the fiber taper. The number of emission wavelength is more than two, which is the state-of-art from a Ho-doped fiber laser mode-locked by carbon nanotube saturable absorber [23]. The dual-wavelength emission in that setup was realized by adjusting the polarization controllers. However the paper did not give a detailed explanation on the mechanisms for the dual-wavelength emission. The multi-wavelength mode locking will be tunable and

switchable, and the switchable operation covers the full binary control, for the potential applications in optical signal processing, optical switching devices and optical communication. The experimental results will be analyzed and explained systematically.

1.3 Thesis organization

This thesis is divided into 8 chapters. Chapter 1 introduces the background, motivation, challenges and objectives for this project. Chapter 2 lists the basic theories we used in this project, including how the optical pulses propagates in single-mode fiber and a gain fiber, and how to achieve passively mode locking by nonlinear polarization evolution technique. Chapter 3 reviews the methods to achieve tunable operation and multi-wavelength emission in fiber lasers. Chapter 4 described how we designed the experimental setups. We considered the energy level, absorption and emission of Tm-doped fiber before choosing it as the gain medium. We analyzed and tested the effect on gain bandwidth with different pumping methods. We measured the transmission of optical components inside the cavity. We proposed the structure units for tunable multi-wavelength laser emission, and the cavity structure to realize the experimental objectives. Chapter 5 is the experimental results and the explanation on widely tunable single-wavelength mode-locked laser. Chapter 6 is the experimental results and analysis on tunable and switchable multi-wavelength mode-locked laser. Chapter 7 shows the extended results and discussions on peak and dip sidebands of solitons, and the observation of noise-like pulses. Chapter 8 concludes this thesis and gives the future works on tunable multi-wavelength mode-locked all-fiber laser.

Chapter 2

Theory on Passively Mode-Locked Fiber Laser

This chapter introduces the theories used in designing and analyzing the experiment. It firstly describes the pulse propagation in single-mode fiber, including the pulse propagation equation, the chromatic dispersion, and the soliton. Secondly it discusses the gain fiber, including three-, four- and quasi-three- level system, the gain coefficient and amplification factor, and the pulse propagation equation in gain fiber. Lastly it illustrates the technique we used to achieve passively mode locking, including the fiber cavity structure, the principle of mode locking, and the nonlinear polarization evolution.

2.1 Pulse Propagation in Single-Mode Fiber

2.1.1 Pulse Propagation Equation in Single-Mode Fiber

The propagation of picosecond pulses in single-mode fiber can be described by nonlinear Schrödinger (NLS) equation

$$\frac{\partial A}{\partial z} + \beta_1 \frac{\partial A}{\partial t} + \frac{i\beta_2}{2} \frac{\partial^2 A}{\partial t^2} + \frac{\alpha}{2} A = i\gamma(\omega_0) |A|^2 A. \quad (2.1.1)$$

This equation is deducted from Maxwell's equations. $A(z, t)$ is the slowly varying pulse envelope, β_1 and β_2 are the dispersion items, which will be described in section 2.1.2, α is fiber loss which is given by

$$P_T = P_0 \exp(-\alpha L), \quad (2.1.2)$$

P_0 and P_T are the launched power at fiber input and the transmitted power. L is the fiber length. $\gamma(\omega_0)$ is fiber nonlinearity which is defined as

$$\gamma(\omega_0) = \frac{n_2(\omega_0)\omega_0}{cA_{eff}}, \quad (2.1.3)$$

$n_2(\omega_0)$ is the nonlinear refractive index. It takes the value of $2.73 \times 10^{-20} \text{ m}^2/\text{W}$ when measured at $1.06 \mu\text{m}$ [27]. ω_0 is the angular frequency at the input wavelength with $\omega_0 = 2\pi c/\lambda_0$, c is the speed of light in vacuum, A_{eff} is the effective mode area. In the fundamental mode and Gaussian modal distribution, $A_{\text{eff}} = \pi w^2$. w can be calculated through

$$w/a \approx 0.65 + 1.619V^{-3/2} + 2.879V^{-6}, \quad (2.1.4)$$

$$V = k_0 a (n_l^2 - n_c^2)^{1/2}, \quad (2.1.5)$$

$$k_0 = 2\pi/\lambda_c, \quad (2.1.6)$$

where a is the core radius, n_l is the cladding refractive index, n_c is the core refractive index, and λ_c is the cut-off wavelength.

When introducing the retarded frame by making the transformation

$$T = t - z/v_g = t - \beta_1 z, \quad (2.1.7)$$

equation (2.1.1) becomes

$$\frac{\partial A}{\partial z} + \frac{i\beta_2}{2} \frac{\partial^2 A}{\partial T^2} + \frac{\alpha}{2} A = i\gamma(\omega_0) |A|^2 A. \quad (2.1.8)$$

Split-step Fourier method is used to solve this equation. Equation (2.1.8) is rewritten to

$$\frac{\partial A}{\partial z} = (\hat{D} + \hat{N})A, \quad (2.1.9)$$

$$\hat{D} = -\frac{i\beta_2}{2} \frac{\partial^2}{\partial T^2} - \frac{\alpha}{2}, \quad (2.1.10)$$

$$\hat{N} = i\gamma |A|^2. \quad (2.1.11)$$

The split-step Fourier method assumes that the fiber length is divided into a large number of segments of width h , over the small h , the fiber dispersion and nonlinearity act independently. When pulses propagate from z to $z+h$, it takes two steps. In one step, only the dispersion takes effect, and in the other step, only the nonlinearity takes effect. Mathematically,

$$A(z+h, T) \approx \exp(h\hat{D}) \exp(h\hat{N}) A(z, T). \quad (2.1.12)$$

$\exp(h\hat{D})$ can be evaluated in the Fourier domain by replacing the operator $\partial/\partial T$ to $-i\omega$. As $\hat{D}(-i\omega)$ is just a number in the frequency domain, the evaluation of equation (2.1.12) is straightforward.

2.1.2 Chromatic Dispersion

The chromatic dispersion is a phenomenon that the phase velocity or group velocity of light depend on the optical frequency when the light propagates in an optical medium. Most often the chromatic dispersion refers to the bulk material dispersion. The refractive index of the material changes with the optical frequency, which is related to the resonance frequency of the medium when the medium absorbs the electromagnetic radiation through oscillations of bound electrons. The refractive index can be approximated by the Sellmeier equation when it is far from medium resonances

$$n^2(\omega) = 1 + \sum_{j=1}^m \frac{B_j \omega_j^2}{\omega_j^2 - \omega^2}, \quad (2.1.13)$$

where ω_j is the resonance angular frequency, B_j is the strength of j th resonance. The value of ω_j and B_j depend on the material constituents. They can be found through the fittings of measured dispersion curves. For bulk-fused silica, with $m=3$, $B_1=0.6961663$, $B_2=0.4079426$, $B_3=0.8974794$, $\lambda_1=0.0684043\mu m$, $\lambda_2=0.1162414\mu m$, and $\lambda_3=9.89616\mu m$ [28].

Mathematically, the dispersion can be explained by expanding the phase constant β in a Taylor series about the central frequency ω_0

$$\beta(\omega) = n(\omega) \frac{\omega}{c} = \beta_0 + \beta_1(\omega - \omega_0) + \frac{1}{2} \beta_2(\omega - \omega_0)^2 + \dots, \quad (2.1.14)$$

where

$$\beta(\omega) = \left(\frac{d^m \beta}{d\omega^m} \right)_{\omega=\omega_0} \quad (m=0,1,2,\dots). \quad (2.1.15)$$

β_1 and β_2 can be derived by

$$\beta_1 = \frac{1}{v_g} = \frac{n_g}{c} = \frac{1}{c} \left(n + \omega \frac{dn}{d\omega} \right), \quad (2.1.16)$$

$$\beta_2 = \frac{1}{c} \left(2 \frac{dn}{d\omega} + \omega \frac{d^2n}{d\omega^2} \right), \quad (2.1.17)$$

where n_g is the group index and v_g is the group velocity. The group velocity can be found by $(\beta_1)^{-1} = c/n_g$. The dispersion of group velocity can be represented by β_2 , which is responsible for pulse broadening. β_2 is called as the group-velocity dispersion (GVD). The dispersion parameter D is also used to describe the change of dispersion versus wavelength. The relationship of D and β_2 is

$$D = \frac{d\beta_1}{d\lambda} = -\frac{2\pi c}{\lambda^2} \beta_2 = -\frac{\lambda}{c} \frac{d^2n}{d\lambda^2}. \quad (2.1.18)$$

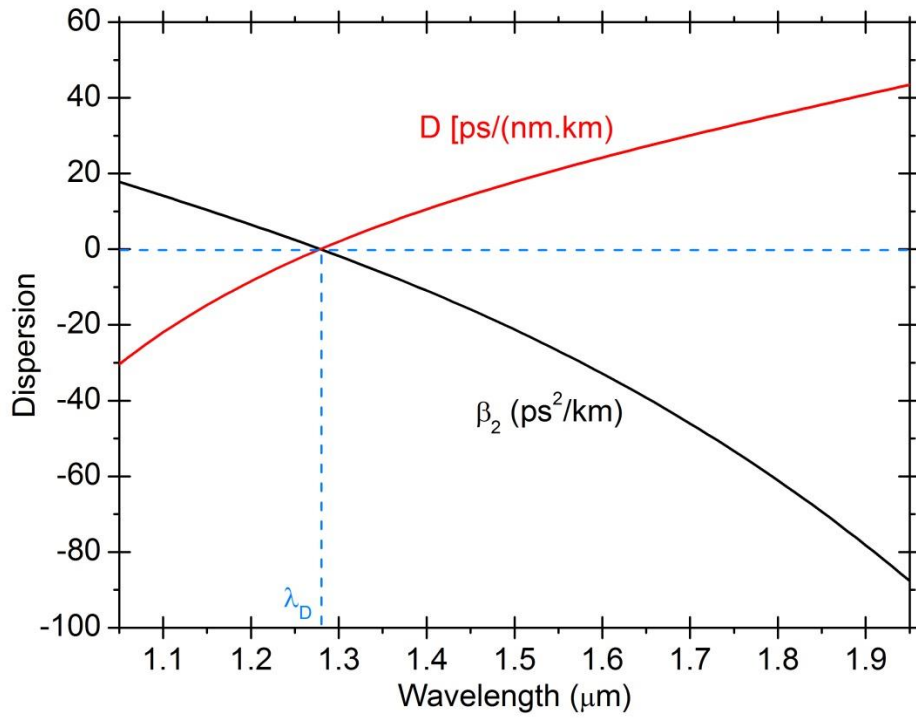


Figure 2. 1. The dispersion and group-velocity dispersion of fused silica.

Figure 2.1 shows how β_2 and D vary with wavelength λ for fused silica. When D or β_2 equals to zero, the corresponding wavelength is the zero-dispersion wavelength λ_D . When the input wavelength is within a few nanometers of λ_D , or the input pulse is ultrashort, the effect of high-order dispersion ($\beta_3, \beta_4, \beta_5, \dots$) should be taken into consideration in the analysis of pulse propagation. In the normal dispersion regime ($\beta_2 > 0$), the red-shifted (low-frequency) components of an optical pulse

travels faster than the blue-shifted (high-frequency) components of the same pulse. By contrast the opposite occurs in the anomalous dispersion regime ($\beta_2 < 0$). In the anomalous dispersion regime, the dispersion and nonlinear effect can achieve the balance to support the propagation of optical solitons, which will be discussed in the following part.

2.1.3 Optical Soliton

Fundamental soliton is an optical pulse whose temporal and spectral shapes remain unchanged during propagating a lossless medium. It results from the balance between dispersive and nonlinear effects. In order to work out the solution of fundamental soliton, we begin with NLS equation (2.1.8) by setting the fiber loss α to 0, we get

$$\frac{\partial A}{\partial z} + \frac{i\beta_2}{2} \frac{\partial^2 A}{\partial T^2} = i\gamma(\omega_0)|A|^2 A. \quad (2.1.19)$$

We introduce three dimensionless variables to normalize equation (2.1.19)

$$U = \frac{A}{\sqrt{P_0}}, \xi = \frac{z}{L_D}, \tau = \frac{T}{T_0}, \quad (2.1.20)$$

and write it in the form

$$i \frac{\partial U}{\partial \xi} = \text{sgn}(\beta_2) \frac{1}{2} \frac{\partial^2 U}{\partial \tau^2} - N^2 |U|^2 U, \quad (2.1.21)$$

where P_0 is the peak power, T_0 is the pulse width. Here the pulse width $T_0 = 0.567 \times T_{FWHM}$, T_{FWHM} is the pulse width at full width at half maximum. N is expressed

$$N^2 = \frac{L_D}{L_{NL}} = \frac{\gamma P_0 T_0^2}{|\beta_2|}. \quad (2.1.22)$$

$L_D = T_0^2 / |\beta_2|$ is the dispersion length, $L_{NL} = 1/\gamma P_0$ is the nonlinear length. Here we choose $\text{sgn}(\beta_2) = -1$ as the soliton is formed in anomalous dispersion regime. By introducing

$$u = NU = \sqrt{\gamma L_D} A, \quad (2.1.23)$$

equation (2.1.21) becomes

$$i \frac{\partial u}{\partial \xi} + \frac{1}{2} \frac{\partial^2 u}{\partial \tau^2} + |u|^2 u = 0, \quad (2.1.24)$$

which takes the standard form of NLS equation.

By solving the NLS with boundary conditions that the fundamental soliton maintains its shape during propagation, or by inverse scattering method, the solution is

$$u(\xi, \tau) = \text{sech}(\tau) \exp(i\xi/2). \quad (2.1.25)$$

The solution indicates that the fundamental soliton is a hyperbolic-secant pulse, with pulse width T_0 and peak power P_0 satisfied the condition $N = 1$.

If the input pulse width T_0 and peak P_0 power do not meet the condition $N = 1$, a fundamental soliton can still be formed in the range $0.5 < N < 1.5$ so that the values of T_0 and P_0 vary in a wide range.

N defines the soliton order. Higher-order solitons ($N \geq 2$) are described by the general solution of equation (2.1.24) where inverse scattering method is used. They evolve periodically in both temporal and spectral domain during propagation, with the period

$$z_0 = \frac{\pi}{2} L_D = \frac{\pi}{2} \frac{T_0^2}{|\beta_2|}. \quad (2.1.26)$$

Soliton can still exist in a lossy fiber by changing the fiber dispersion, or amplifying the soliton periodically. With the presence of fiber loss the soliton pulse energy decreases, leading to the decrease of nonlinear effect. Since soliton results from the balance of dispersive and nonlinear effect, the fiber dispersion needs to be reduced or the soliton pulse energy needs to be restored by an amplifier to maintain the soliton character. Dispersion-decreasing fiber is developed to compensate the reduced soliton pulse energy by fiber loss. And when amplifying the soliton, the parameters of soliton change. The soliton needs to readjust the parameters to the input value by shedding away a part of its energy as dispersive waves. The shed energy is a continuum radiation, and it forms discrete sidebands in the soliton spectrum. The sidebands are called Kelly sidebands, which is a typical feature of soliton [29].

2.2 Pulse Propagation in Gain Fiber

2.2.1 Three-, Four-, and Quasi-Three- Level System

In the thermal equilibrium, the number of particles at two adjacent non-degenerated energy levels follows the Boltzmann distribution. The population at lower energy level

is always higher. Optical pump sources are used to excite the particles at lower energy level to the higher level, to achieve the population inversion, which is a necessary condition for laser emission. A laser-active atom or ion at the excited state will spontaneously decay into a lower energy level after some time, releasing energy in the form of a photon. The released photon will trigger more photon emissions to cause the stimulate emission. The transition process happens in the gain medium of a laser or laser amplifier. There are three basic transition schemes which divide the gain medium into three types: three-, four- and quasi-three- system.

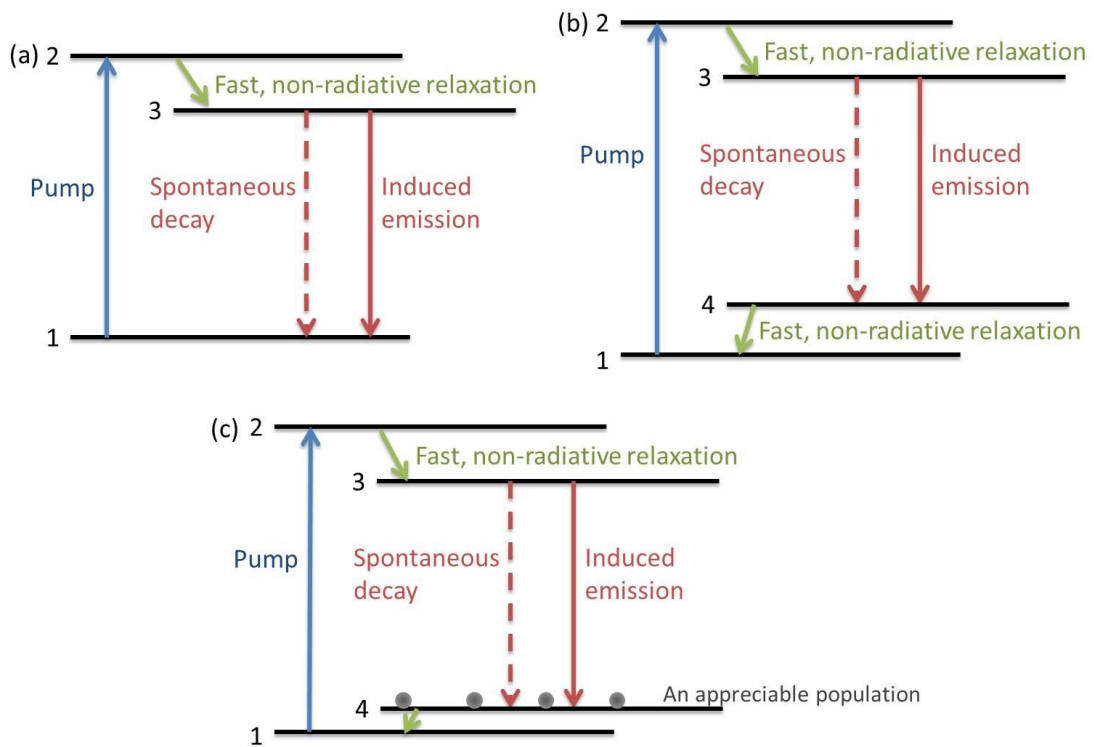


Figure 2. 2. The energy level diagrams of (a) three-level system, (b) four-level system, and (c) quasi-three-level system.

Figure 2.2 is the energy level diagrams of different laser systems. In the three-level system, the population inversion is achieved by pumping the atoms in the ground level 1 to the excited level 2. The atoms at excited level 2 go through a fast and non-radiative relaxation to energy level 3, and then spontaneously decay to the ground level 1 by releasing photons.

The ground level 1 is always populated, thus it causes reabsorption of the amplified light if the absorption cross section at the laser wavelength is non-zero. It also requires a pump with higher intensity to achieve the population inversion. These factors

increase the laser threshold. An example of a three-level laser gain medium is ruby ($\text{Cr}^{3+}:\text{Al}_2\text{O}_3$).

In the four-level system, the laser transition does not end on the ground level, which is the main difference from the three-level system. The laser transition ends on an upper level 4 above the ground level 1, then atoms at energy level 4 return to the ground level 1 by a rapid, non-radiative relaxation. Population inversion happens at energy level 3 and 4, where energy level 4 is always depopulated. The condition to achieve population inversion is less strict, compared with the condition in three-level system.

If reabsorption is considered, atoms at ground level 1 have a chance to absorb the amplified light but atoms at energy level 4 do not as energy level 4 is always depopulated. However reabsorption is less likely to be happened. It is supposed that the atoms at ground level 1 reabsorb the amplified light, and they are excited to an upper energy level. This upper energy level does not exist. Therefore the reabsorption is avoided in the four-level system.

Achieving the population inversion easily and no reabsorption make the laser threshold of four-level system lower than three-level system's. The commonly four-level laser gain medium is Nd:YAG except those operated on the ground-state transition around 0.9–0.95 μm .

The quasi-three-level system is a kind of intermediate situation where the lower laser level 4 is so close to the ground level 1 that an appreciable population in energy level 4 occurs in thermal equilibrium at the operating temperature.

The reabsorption happens in the quasi-three-level system. When atoms at energy level 4 and the unpumped atoms at the ground level 1 absorb the amplified light, they will be excited to stark levels of energy level 3. Due to the loss induced by reabsorption, a pump with higher intensity is required to reach the laser threshold.

What is more, the emission wavelength of a laser cavity depends on the cavity loss. If the laser cavity is with higher loss, higher pumping intensity is adopted. Less unpumped atoms are left so the reabsorption is reduced. Since reabsorption is strong at short wavelength, the reduced reabsorption enables laser emits at shorter wavelength. Beside a high-intensity pump, a reduced doping concentration also results in higher excitation level, to enable shorter wavelength at the maximum gain. However in low excitation level, the net gain at shorter wavelength is reduced due to the strong reabsorption at shorter wavelength. Examples of quasi-three-level laser gain media are

all ytterbium-doped gain media, thulium-doped media for 2- μm emission, and erbium-doped media for 1.5 or 1.6- μm emission.

2.2.2 Gain Coefficient and Amplification Factor

Due to the transitions of atoms between different energy levels in the gain media as described in part 2.2.1, the media transfer part of its energy to the emitted light. This results in an increase in optical power. Gain is used to measure the ability of a laser gain medium to increase optical power quantitatively. In the simple quasi two-level system, the gain coefficient can be expressed

$$G = \sigma_e N_2 - \sigma_a N_1, \quad (2.2.1)$$

where N_1 and N_2 are populations of lower and excited states, σ_a and σ_e are effective absorption and emission cross-sections. The absorption and emission cross section are used to quantitatively describe the likelihood of absorption and stimulated emission behavior over a certain wavelength range, which can be obtained from absorption spectra and fluorescence spectra, respectively. In the case of non-pumped medium, the gain coefficient is negative.

The gain coefficient in a gain medium with homogeneously broadened is

$$g(\omega) = \frac{g_0}{1 + (\omega - \omega_a)^2 T_2^2 + P/P_s}, \quad (2.2.2)$$

where g_0 is the peak value of optical gain, ω is the angular frequency of the incident signal, ω_a is the atomic transition frequency, T_2 is the dipole relaxation time and is typically small (around 0.1 ps) for fiber amplifiers, P is the optical power of the continuous wave light being amplified. The saturation power P_s depends on dopant parameters such as the fluorescence time T_1 and the transition cross section σ . The fluorescence time T_1 varies in the range from 0.1 μs to 10 ms depending on the dopants.

The amplification factor describes how the input power is amplified by passing through a certain length of gain fiber. The relationship between amplification factor G and input/output power is $G = P_{out}/P_{in}$, where P_{in} and P_{out} is the input and output average power, respectively. G can be obtained by solving

$$\frac{dP}{dz} = g(\omega)P(z), \quad (2.2.3)$$

by setting $P(0) = P_{in}$ and $P(z) = P_{out}$, and $P(z)$ is the optical power at the position z from the input of the amplifier.

If the amplification factor maintains a fixed value for different input power, the amplifier works at unsaturated regime and the gain is unsaturated. In this case $P/P_s \ll 1$. Equation (2.2.2) becomes

$$g(\omega) = \frac{g_0}{1 + (\omega - \omega_a)^2 T_2^2}. \quad (2.2.4)$$

The $g(\omega)$ is governed by Lorentzian profile. The peak value of $g(\omega)$ is reached when signal frequency ω is the same with the atomic transition frequency ω_a . Solving equation (2.2.3) we get the amplification factor of an amplifier with the length of L is

$$G(\omega) = \exp\left[\int_0^L g(\omega) dz\right] = \exp[g(\omega)L], \quad (2.2.5)$$

If the amplification factor cannot maintain a fixed value when increasing the input power, in order to amplify the signal additional amounts of power are required. In equation (2.2.2), when $P/P_s \sim 1$, $g(\omega)$ decreases so that the amplification factor G decreases too. Therefore, the gain reduces for high input powers. This is called gain saturation. To make it simple we consider the situation when $\omega = \omega_a$. By substitute $g(\omega)$ from equation (2.2.2) into equation (2.2.3), we get

$$\frac{dP}{dz} = \frac{g_0 P}{1 + P/P_s}, \quad (2.2.6)$$

$$G = G_0 \exp\left(\frac{P_{out}}{P_s} \frac{1-G}{G}\right). \quad (2.2.7)$$

where $G_0 = \exp(g_0 L)$ is the peak value of the amplification factor.

2.2.3 Ginzburg–Landau Equation

When pulse propagates in a doped gain fiber, the effect of dopants is considered. To simplify it, the dopants are modeled as an ideal two-level atomic system. We begin with the wave equation which is deduced from Maxwell's equations:

$$\nabla^2 \mathbf{E} - \mu_0 \frac{\partial^2 \mathbf{D}}{\partial t^2} = 0, \quad (2.2.8)$$

where \mathbf{E} is the electric field vector, μ_0 is the vacuum permeability, and \mathbf{D} is the displacement vector. The Fourier transform of \mathbf{D} is related to \mathbf{E} by

$$\tilde{\mathbf{D}}(\mathbf{r}, \omega) = \varepsilon_0 \varepsilon(\omega) \tilde{\mathbf{E}}(\mathbf{r}, \omega), \quad (2.2.9)$$

where ω is the optical angular frequency, ε_0 is the vacuum permittivity, $\varepsilon(\omega)$ is a complex dielectric constant defined as [30]

$$\varepsilon(\omega) = n_f^2(\omega) + 2in_f(c/\omega)\alpha_f + \chi_a(\omega). \quad (2.2.10)$$

α_f is the fiber loss. n_f is the refractive index of the fiber, which includes the linear and nonlinear contributions

$$n_f(\omega) = n(\omega) + n_2 I. \quad (2.2.11)$$

We introduce atomic susceptibility $\chi_a(\omega)$, which governs the response of dopants, if the pulse width $T_0 \gg T_2$:

$$\chi_a(\omega) = \frac{g_p c}{\omega} \frac{(\omega - \omega_a) T_2 - i}{1 + (\omega - \omega_a)^2 T_2^2}. \quad (2.2.12)$$

where $g_p = \sigma(N_2 - N_1)$ is the peak gain, σ is the transition cross section, N_2 and N_1 are the atomic densities for the upper and lower density levels of the two-level system. ω_a is the atomic resonance angular frequency, T_2 is the dipole (polarization) relaxation time. The Fourier transform defines as

$$\tilde{\mathbf{E}}(\mathbf{r}, \omega) = \int_{-\infty}^{\infty} \mathbf{E}(\mathbf{r}, t) \exp(i\omega t) dt. \quad (2.2.13)$$

The equations above describe the propagation of electromagnetic field in any dispersive nonlinear medium. It is simplified in optical fibers due to the fiber waveguide property. The electric field vector is written as

$$\mathbf{E}(\mathbf{r}, t) = \frac{1}{2} \left\{ \hat{e} F(x, y) A(z, t) \exp[i(\beta_0 z - \omega_0 t)] + c.c. \right\}, \quad (2.2.14)$$

where \hat{e} is the polarization unit vector, $F(x, y)$ is the field distribution associated with the fundamental mode, $A(z, t)$ is the complex amplitude of the pulse envelope, β_0 is the propagation constant at the carrier frequency ω_0 , and *c.c.* stands for the complex conjugate.

Equation (2.2.8) to (2.2.14) can be used to obtain a basic propagation equation for the pulse envelope $A(z, t)$. With a similar technique in part 2.3.1 in book [31], $A(z, t)$ is found to be

$$\frac{\partial \tilde{A}}{\partial z} = i[\beta(\omega) - \beta_0] \tilde{A}, \quad (2.2.15)$$

where $\beta(\omega)$ is the propagation constant with

$$\beta(\omega) = \sqrt{\varepsilon(\omega)} \omega / c. \quad (2.2.16)$$

By substituting equation (2.2.10) into equation (2.2.16), and α_f , $n_2 I$, and $|\chi_a|$ are much smaller than n , $\beta(\omega)$ is

$$\beta(\omega) = \beta_f(\omega) + \frac{\omega}{c} n_2 I + \frac{i}{2} \alpha_f + \frac{1}{2n} \chi_a(\omega). \quad (2.2.17)$$

By writing $\beta(\omega)$ in Taylor series, we can get the propagation equation. When expanding $\beta(\omega)$ in Taylor series, although α_f and n_2 vary with frequency, they are considered as constants over the pulse bandwidth because they vary very slow. However this is not the case for $\chi_a(\omega)$. The response of dopants varies across the pulse bandwidth. The spectral components at ω_a have the maximum gain and others have smaller gain. All spectral components cannot be amplified by the same amount. This is called the gain dispersion. $\chi_a(\omega)$ is expanded in Taylor series:

$$\chi_a(\omega) = \frac{g_p}{2n(\omega_0)} \left[\frac{\delta - i}{1 + \delta^2} + \frac{1 - \delta^2 + 2i\delta}{(1 + \delta^2)^2} (\omega - \omega_0) T_2 + \frac{\delta(\delta^2 - 3) + i(1 - 3\delta^2)}{(1 + \delta^2)^3} (\omega - \omega_0)^2 T_2^2 \right]. \quad (2.2.18)$$

δ is the detuning parameter with $\delta = (\omega_0 - \omega_a) T_2$. $\beta_f(\omega) = n(\omega) \omega / c$ is the propagation constant in the undoped fiber, the Taylor expansion is

$$\beta_f(\omega) = \beta_0 + \beta_1(\omega - \omega_0) + \frac{1}{2} \beta_2(\omega - \omega_0)^2. \quad (2.2.19)$$

β_1 and β_2 are dispersion items which are described in part 2.1.2. Then we get the propagation equation:

$$\frac{\partial A}{\partial z} + \beta_1^{eff} \frac{\partial A}{\partial t} + \frac{i}{2} \beta_2^{eff} \frac{\partial^2 A}{\partial t^2} = -\frac{\alpha_f}{2} A + \frac{g_p}{2n(\omega_0)} \left[\frac{\delta - i}{1 + \delta^2} \right] + i\gamma(\omega_0) |A|^2 A, \quad (2.2.20)$$

where

$$\beta_1^{eff} = \beta_1 + \frac{g_p T_2}{2n(\omega_0)} \frac{1 - \delta^2 + 2i\delta}{(1 + \delta^2)^2}, \quad (2.2.21)$$

$$\beta_2^{eff} = \beta_2 + \frac{g_p T_2^2}{2n(\omega_0)} \frac{\delta(\delta^2 - 3) + i(1 - 3\delta^2)}{(1 + \delta^2)^3}, \quad (2.2.22)$$

2.3 Passively Mode-Locked Fiber Laser

2.3.1 Fiber Laser Cavity

The three requirements for laser emission are population inversion, stimulated emission and reaching the laser threshold. The population inversion is realized by an optical pump. With population inversion, there are a large number of atoms at the excited energy level, which are ready to be de-excited back to the lower energy level via stimulated emission process. Large photon energy density is needed to enable the stimulated emission. This can be achieved by forming a laser cavity. The laser threshold will be discussed in the next part.

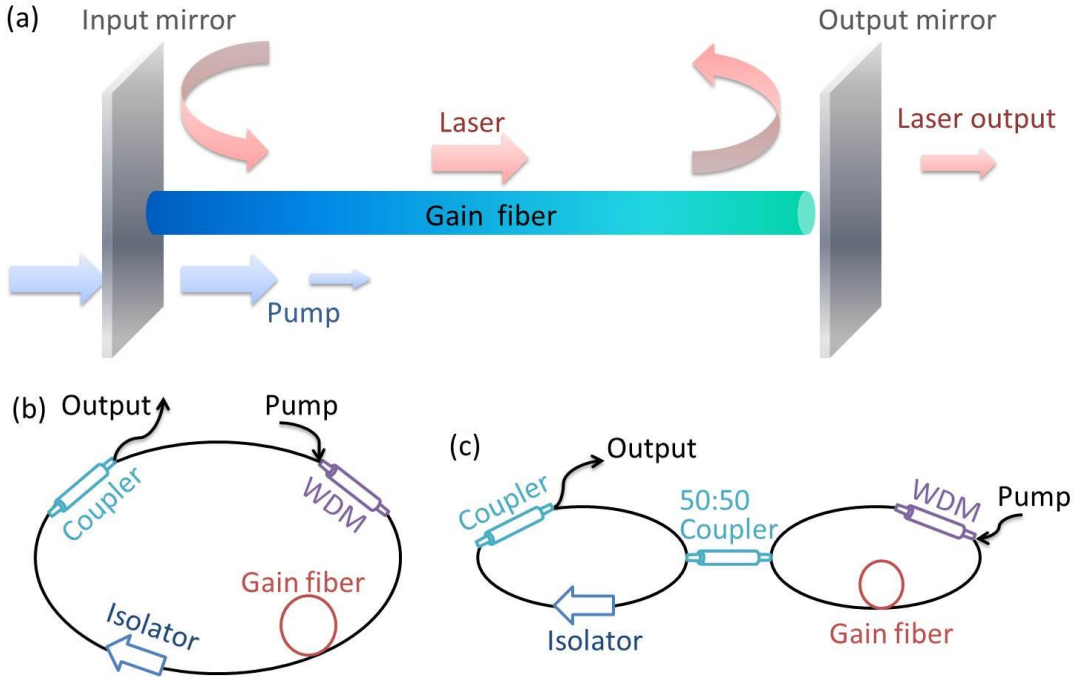


Figure 2. 3. The schematic of (a) Fabry-Perot cavity, (b) fiber ring cavity, and (c) figure-8 cavity. WDM: wavelength-division multiplexer.

Fabry-Perot (FP) cavity is the most commonly used to form a laser cavity. A gain fiber is placed in between two mirrors, as shown in figure 2.3 (a). The input mirror has

high reflection for the laser light and high transmission for the pump light. The output mirror transmits parts of the laser light and leaves most of the light circulating inside the cavity. By multiple reflections the photon density can be built up to trigger the stimulated emission. The mirrors here should be precisely aligned as a little tilt will increase the cavity loss largely. This can be solved by applying a high-reflection coating to the end of gain fibers. However this kind of coating is very sensitive to the defects of fiber end and cannot sustain the high power operation.

In a fiber-based cavity, the input mirror can be replaced by wavelength-division multiplexer (WDM) or fiber Bragg gratings (FBG), to transmit the pump light and reflect the laser light. The output mirror can be replaced by couplers or FBG. The WDM, FBG and coupler can be fabricated with fiber pigtails, which can be spliced to gain fiber and other fiber-based components, to form the all-fiber cavity, to avoid the alignment issue with a cavity containing free-space components. By adding saturable absorbers, the cavity can realize the mode-locked operation.

The fiber laser can be also a ring cavity and a figure-8 cavity as shown in figure 2.3 (b) and (c). The use of isolator is to keep the propagation of laser light unidirectional. By adding polarization controllers and using polarization-dependent isolator, the ring cavity can support the nonlinear polarization evolution, thus to realize the mode-locked operation without saturable absorbers. By adding polarization controllers, the figure-8 cavity can have a high transmission under high power operation and a low transmission under low power operation, which acts as a saturable absorber, to realize the mode locking.

2.3.2 Laser Threshold

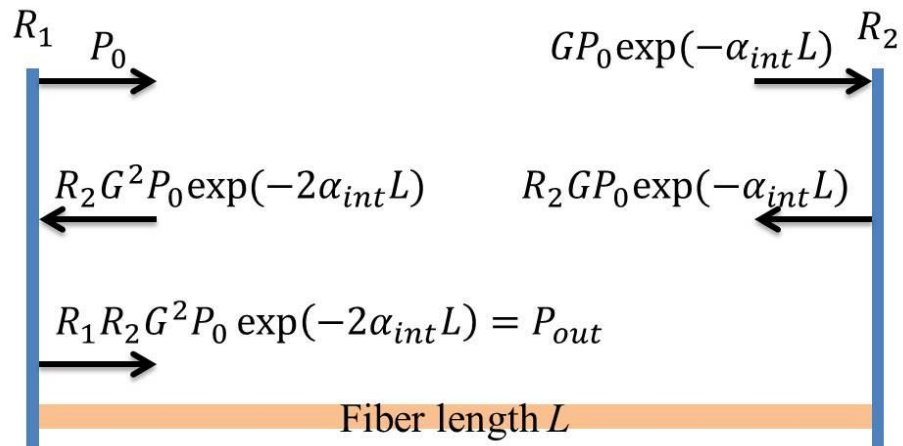


Figure 2. 4. The power change in a Fabry-Perot fiber cavity per round trip.

When the pump power reaches a certain threshold, the pump power can be converted to laser power. Laser threshold is the pump absorption power which can make optical gain balance the optical loss during each round trip. If we consider a Fabry-Perot cavity formed by a fiber with length L and two mirrors with reflection of R_1 and R_2 in the fiber end as shown in figure 2.4, the round trip gain G_{round} should be larger than 1 so that there will be net amplification and laser oscillations will grow. Then the laser threshold condition is

$$G_{round} = P_{out}/P_{in} = G^2 R_1 R_2 \exp(-2\alpha_{int} L) = 1, \quad (2.3.1)$$

where α_{int} is the internal losses within the cavity and G is the single-pass amplification factor with

$$G = \exp\left[\int_0^L g(z) dz\right] \quad g(z) = \sigma_s [N_2(z) - N_1(z)], \quad (2.3.2)$$

where σ_s is transition cross section and N_1 and N_2 are the dopant densities in the two energy states participating in the stimulated-emission process. Substituting equation (2.3.2) into (2.3.1) the laser threshold condition becomes

$$\frac{1}{L} \int_0^L g(z) dz = -\ln(R_1 R_2)/2L + \alpha_{int} \equiv \alpha_{cav}, \quad (2.3.3)$$

where α_{cav} is the total cavity loss.

In a four-level energy system, the dopant densities in the upper energy level can be calculated by the rate equation below [32]:

$$\frac{\partial N_2}{\partial t} = W_p N_t - W_s N_2 - \frac{N_2}{T_1}, \quad (2.3.4)$$

Where N_t is the total ion density, T_1 is the fluorescence time, W_p and W_s are the transition rates for the pump and signal, respectively. They are expressed as:

$$W_p = \frac{\Gamma_p \sigma_p P_p}{a_p h \nu_p} \quad W_s = \frac{\Gamma_s \sigma_s P_s}{a_s h \nu_s}, \quad (2.3.5)$$

where Γ_p is the overlap factor representing the fraction of pump power P_p within the doped region of the fiber, σ_p is the transition cross section at the pump frequency ν_p , and a_p is the mode area of the pump inside the fiber. Γ_s , P_s , σ_s , ν_s , and a_s are defined similarly for the signal. The steady-state solution of equation (2.3.4) is

$$N_2 = \frac{\left(\frac{P_p}{P_p^{sat}}\right) N_t}{1 + P_s/P_s^{sat}}, \quad (2.3.6)$$

where P_p^{sat} and P_s^{sat} are the saturation pump power and saturation signal power, respectively, given by

$$P_p^{sat} = \frac{a_p h \nu_p}{\Gamma_p \sigma_p T_1} \quad P_s^{sat} = \frac{a_s h \nu_s}{\Gamma_s \sigma_s T_1}. \quad (2.3.7)$$

The pump power decreases exponentially along the light propagation direction with $P_p(z) = P_p(0) \exp(-\alpha_p z)$. Near the laser threshold the gain saturation effect can be neglected due to $P_s/P_s^{sat} \ll 1$. Referring to equation (2.3.3), we can get the required pump power to reach the laser threshold:

$$P_p(0) = \frac{\alpha_{cav} L}{1 - \exp(-\alpha_p L)} \left(\frac{\alpha_p}{\alpha_s} \right) P_p^{sat}, \quad (2.3.8)$$

where $\alpha_p = \sigma_p N_t$ and $\alpha_s = \sigma_s N_t$ are the absorption coefficients at the pump and signal wavelengths, respectively. The laser threshold can be express by the absorbed pump power

$$P_{th} = P_{abs} = P_p(0) [1 - \exp(-\alpha_p L)]. \quad (2.3.9)$$

2.3.3 Mode Locking

Mode locking refers to the process that makes different longitudinal modes oscillating with a definite phase relation and equal or comparable amplitudes. We consider $(2n+1)$ longitudinal modes oscillating with the same amplitude E_0 . We assume the phase difference between the adjacent longitudinal modes is a constant φ , the total electric field $E(t)$ of the electromagnetic wave at any given point in the output beam is

$$E(t) = \sum_{-n}^{+n} E_0 \exp\{j[(\omega_0 + l\Delta\omega)t + l\varphi]\}, \quad (2.3.10)$$

where ω_0 is the angular frequency of the central mode, $\Delta\omega$ is the angular frequency difference between two adjacent longitudinal modes, and the value of the phase for the center mode is taken to be zero. The total electric field $E(t)$ of the electromagnetic wave can be rewritten as

$$E(t) = A(t) \exp(j\omega_0 t), \quad (2.3.11)$$

where

$$A(t) = \sum_{l=-n}^{+n} E_0 \exp[jl(\Delta\omega t + \varphi)]. \quad (2.3.12)$$

From equation (2.3.11) and (2.3.12), we know that $E(t)$ can be represented in terms of a sinusoidal carrier wave at center angular frequency ω_0 , with the time-dependent amplitude $A(t)$. To calculate $A(t)$, we make the transformation $\Delta\omega t' = \Delta\omega t + \varphi$, equation (2.3.12) becomes

$$A(t') = \sum_{l=-n}^{+n} E_0 \exp[jl(\Delta\omega t')]. \quad (2.3.13)$$

The summation of $A(t')$ is

$$A(t') = E_0 \frac{\sin[(2n+1)\Delta\omega t'/2]}{\sin(\Delta\omega t'/2)}. \quad (2.3.14)$$

Figure 2.5 is the pulse train formed when seven longitudinal modes ($n=3$) of equal amplitudes are mode locked [32]. From equation (2.3.14), if all the longitudinal modes oscillate independently without a fixed phase difference, the longitudinal modes will not have the interference, the pulse train will not be formed. With the fixed phase difference between adjacent longitudinal modes, the longitudinal modes have constructive interference to produce a pulse train. The pulses are evenly spaced by a time

$$\tau_p = 2\pi/\Delta\omega = 1/\Delta\nu, \quad (2.3.15)$$

where $\Delta\nu$ is the frequency separation between two adjacent longitudinal modes. From equation (2.3.14) we also can easily calculate the pulse width $\Delta\tau_p$ at half maximum of $A^2(t')$:

$$\Delta\tau_p \cong 2\pi/(2n+1)\Delta\omega = 1/\Delta\nu_L, \quad (2.3.16)$$

where $\Delta\nu_L = (2n+1)\Delta\omega/2\pi$ is the total bandwidth of all phase-locked longitudinal modes.

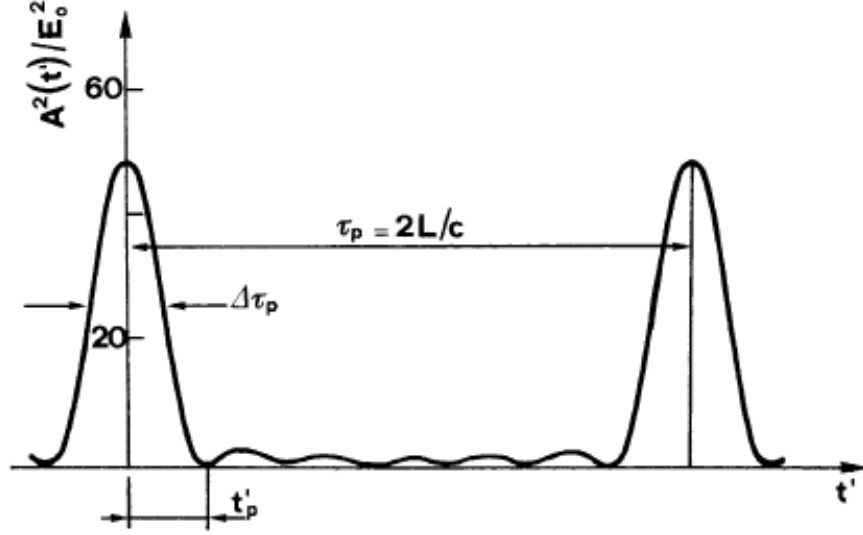


Figure 2. 5. The pulse train formed when seven longitudinal modes ($n = 3$) of equal amplitudes are mode locked [32].

2.3.4 Passive Mode Locking Enabled by Nonlinear Polarization Evolution

We will describe how mode locking is achieved in time domain as it becomes complicated in frequency domain where we should consider a very large number of longitudinal modes [33]. Mode locking is a resonant phenomenon. By adopting coherence between the phases of different longitudinal modes, pulsed radiation can be produced. A pulse is initiated from the radiation circulating in the laser cavity. The pulse becomes shorter on every pass through the resonator by modulation, meanwhile the spectrum of the pulse becomes wider. The shortening process continues until the pulse broadening process by GVD happens, and the spectrum narrowing processes happens such as finite bandwidth of the gain [34]. Depending on the kinds of modulation, mode locking can be divided into two kinds: active mode locking and passive mode locking. In active mode locking the modulation element is driven by external sources while passive mode locking is not. Passive mode locking exploits nonlinear effects such as saturation absorption or nonlinear refractive index change of a certain material.

Nonlinear polarization evolution is a technique to realize the mode locking. It sharpens the pulse through an optical fiber and a polarizer. The nonlinear birefringence of the optical fiber induces the nonlinear refractive index change depending on the intensity in two polarization directions. For a polarized pulsed light which has an incident angle with the fiber axis, when propagating through the optical fiber, the

different parts of the pulse in the time domain changes the polarization state differently depending on the intensity. Then after a polarizer, the different parts of the pulse are with different transmissions. By setting the polarization direction of the polarizer, the center part of the pulse with higher intensity can be transmitted meanwhile the tails of the pulse with lower intensity will be blocked. Then the pulse becomes shorter. The following two parts will discuss the how the nonlinear birefringence works, and how it induces the polarization-dependent loss during pulse shaping process.

2.3.4.1 Fiber Birefringence

The fiber birefringence can be divided into linear and nonlinear birefringence. We first discuss the linear birefringence. Ideally, a single-mode fiber is with cylindrical symmetry, it can maintain the two degenerate modes that are polarized in two orthogonal directions. The mode excited at x direction will not couple into y direction. However in real fibers, the random variation in the core shape and stress-induced anisotropy along the fiber length break the cylindrical symmetry, resulting in a mix of two modes at x and y directions. That is, the mode-propagation constant β in x and y directions becomes slightly different for the modes polarized in these two directions. This induces the modal birefringence, and the strength of modal birefringence is

$$B_m = \frac{|\beta_x - \beta_y|}{k_0} = |n_x - n_y|, \quad (2.3.17)$$

where $k_0 = 2\pi/\lambda_0$ is the propagation constant, n_x and n_y are the modal refractive index in x and y directions, respectively. It is the built-in variation that makes the fibers exhibit nearly constant birefringence along the entire length. For a given value of B_m , the two modes exchange their powers in a periodic way. The period L_B is

$$L_B = \frac{2\pi}{|\beta_x - \beta_y|} = \frac{\lambda}{B_m}. \quad (2.3.18)$$

After propagating an effective fiber length L_{eff} , where $L_{eff} = [1 - \exp(-\alpha L)]/\alpha$ by considering the fiber loss α , the relative linear phase shift $\Delta\phi_L$ is

$$\Delta\phi_L = 2\pi L_{eff} B_m / \lambda. \quad (2.3.19)$$

In some applications we expect the polarization state of light is not changed during propagation. The polarization-maintaining fiber is developed to keep the polarization state of light when the light incident along the x or y direction of the fiber. The design

and fabrication of polarization-maintaining fiber are different from commonly used single-mode fiber, by intentionally introducing large amount of birefringence. Therefore a small and random change in fiber birefringence will not change the polarization state of light.

For the nonlinear birefringence, it arises when nonlinear effects become important under a sufficient intense optical field. The value of the effective refractive index in x and y directions will change in such an optical field depending on the optical intensity, which is a nonlinear process. The nonlinear contributions to the refractive index are

$$\Delta n_x = n_2 \left(|E_x|^2 + \frac{2}{3} |E_y|^2 \right), \quad (2.3.20)$$

$$\Delta n_y = n_2 \left(|E_y|^2 + \frac{2}{3} |E_x|^2 \right), \quad (2.3.21)$$

where n_2 is the nonlinear refractive index defined in part 2.1.1, E_x and E_y are the complex amplitudes of the polarization components of the field oscillating at the carrier frequency ω_0 . On the right-hand side of equation (2.3.20) and (2.3.21), the first term is responsible for self-phase modulation and the second term is responsible for cross-phase modulation. There is a nonlinear coupling between two polarization components E_x and E_y . The nonlinear contributions Δn_x and Δn_y are not equal so that they cause nonlinear birefringence whose strength depends on the intensity and polarization state of the incident light. The nonlinear birefringence rotates the polarization direction of the elliptically polarized light, which is known as the nonlinear polarization rotation. When the light propagates through the optical fiber, the polarization state continues to rotate. Thus nonlinear polarization evolution is used broadly.

The Δn_x and Δn_y are deduced by substituting the electric field

$$\mathbf{E}(\mathbf{r}, t) = \frac{1}{2} (\hat{x}E_x + \hat{y}E_y) \exp(-i\omega_0 t) + c.c. , \quad (2.3.22)$$

into the relation between the induced nonlinear polarization \mathbf{P}_{NL} and the electric field

$$\mathbf{P}_{NL}(\mathbf{r}, t) = \varepsilon_0 \chi^{(3)} : \mathbf{E}(\mathbf{r}, t) \mathbf{E}(\mathbf{r}, t) \mathbf{E}(\mathbf{r}, t), \quad (2.3.23)$$

where ε_0 is the vacuum permittivity and $\chi^{(3)}$ is the 3rd order susceptibility.

The nonlinear birefringence will cause the relative nonlinear phase shift. To get the relative nonlinear phase shift we firstly consider a linear birefringent fiber, i.e. the

fiber has two principal axes and if linearly polarized light propagates along either axis the polarization of light remains linearly. The slowly varying amplitude A_x and A_y satisfy the following coupled NLS equations:

$$\frac{\partial A_x}{\partial z} + \beta_{1x} \frac{\partial A_x}{\partial t} + \frac{i\beta_2}{2} \frac{\partial^2 A_x}{\partial t^2} + \frac{\alpha}{2} A_x = i\gamma \left(|A_x|^2 + \frac{2}{3} |A_y|^2 \right) A_x + \frac{i\gamma}{3} A_x^* A_y^2 \exp(-2i\Delta\beta z), \quad (2.3.24)$$

$$\frac{\partial A_y}{\partial z} + \beta_{1y} \frac{\partial A_y}{\partial t} + \frac{i\beta_2}{2} \frac{\partial^2 A_y}{\partial t^2} + \frac{\alpha}{2} A_y = i\gamma \left(|A_y|^2 + \frac{2}{3} |A_x|^2 \right) A_y + \frac{i\gamma}{3} A_y^* A_x^2 \exp(-2i\Delta\beta z), \quad (2.3.25)$$

where

$$\Delta\beta = \beta_{0x} - \beta_{0y} = (2\pi/\lambda) B_m = 2\pi/L_B, \quad (2.3.26)$$

is related to the linear birefringence, $A_{j(j=x,y)}(z,t)$ is the slowly varying amplitude, α is the fiber loss, and γ is the fiber nonlinearity. The last items in equation (2.3.24) and (2.3.25) are related to coherent coupling between the two polarization components and will result in degenerate four-wave mixing depending on the phase matching condition. When fiber length $L \gg L_B$, the last items usually change sign to make the average contribution zero. The typical value of L_B is $\sim 1\text{cm}$ for highly birefringent fiber and $\sim 1\text{m}$ for low birefringent fiber.

However in practice, fiber is twisted to become an elliptically birefringent fiber. The twist results from a twisted preform during fiber drawing, or applying controlled twist to a fiber when we use the polarization controllers [35]. The twist induces shear strain or a deformation of the core, so that the coupling of modes is changed. In a highly and elliptically birefringent fiber, the coupled equations become:

$$\frac{\partial A_x}{\partial z} + \beta_{1x} \frac{\partial A_x}{\partial t} + \frac{i\beta_2}{2} \frac{\partial^2 A_x}{\partial t^2} + \frac{\alpha}{2} A_x = i\gamma \left(|A_x|^2 + B |A_y|^2 \right) A_x, \quad (2.3.27)$$

$$\frac{\partial A_y}{\partial z} + \beta_{1y} \frac{\partial A_y}{\partial t} + \frac{i\beta_2}{2} \frac{\partial^2 A_y}{\partial t^2} + \frac{\alpha}{2} A_y = i\gamma \left(|A_y|^2 + B |A_x|^2 \right) A_y, \quad (2.3.28)$$

where

$$B = \frac{2 + 2\sin^2 \theta}{2 + \cos^2 \theta}. \quad (2.3.29)$$

is the coupling parameter, depending on the elliptical angle θ . For the linearly birefringent fiber, $\theta = 0$, $B = \frac{2}{3}$. The equations (2.3.27) and (2.3.28) reduced to equations (2.3.24) and (2.3.25), respectively.

When deal with continuous wave, or pulsed wave with fiber length L is much shorter than the dispersion length $L_D = T_0^2 / |\beta_2|$ and walk-off length $L_w = T_0 / |\Delta\beta|$, where T_0 is the pulse width, the coupled equation can be further simplified into:

$$\frac{dA_x}{dz} + \frac{\alpha}{2} A_x = i\gamma \left(|A_x|^2 + B|A_y|^2 \right) A_x, \quad (2.3.30)$$

$$\frac{dA_y}{dz} + \frac{\alpha}{2} A_y = i\gamma \left(|A_y|^2 + B|A_x|^2 \right) A_y. \quad (2.3.31)$$

The equations are solved using

$$A_x = \sqrt{P_x} e^{-\alpha z/2} e^{i\phi_x}, \quad A_y = \sqrt{P_y} e^{-\alpha z/2} e^{i\phi_y}, \quad (2.3.32)$$

where P_x , P_y , ϕ_x , ϕ_y are the power and phase for the two polarization components.

P_x and P_y do not change with z , but ϕ_x and ϕ_y change with z :

$$\frac{d\phi_x}{dz} = \gamma e^{-\alpha z} (P_x + BP_y), \quad \frac{d\phi_y}{dz} = \gamma e^{-\alpha z} (P_y + BP_x). \quad (2.3.33)$$

The solution for equation (2.3.33) is:

$$\phi_x = \gamma (P_x + BP_y) L_{eff}, \quad \phi_y = \gamma (P_y + BP_x) L_{eff}, \quad (2.3.34)$$

which is the nonlinear phase shift of the two polarization components. The relative nonlinear phase difference is

$$\Delta\phi_{NL} \equiv \phi_x - \phi_y = \gamma L_{eff} (1-B) (P_x - P_y). \quad (2.3.35)$$

If $B = 1$, no relative phase shift exists. If $B \neq 1$ and the incident light is launched with $P_x \neq P_y$, relative phase shift exists. Consider a linearly birefringent fiber which $B = 2/3$, and a linearly polarized light with power P_0 is launched with polarization angle θ between the slow axis, the relative phase shift is

$$\Delta\phi_{NL} = (\gamma P_0 L_{eff} / 3) \cos(2\theta). \quad (2.3.36)$$

2.3.4.2 Pulse shaping by nonlinear polarization evolution

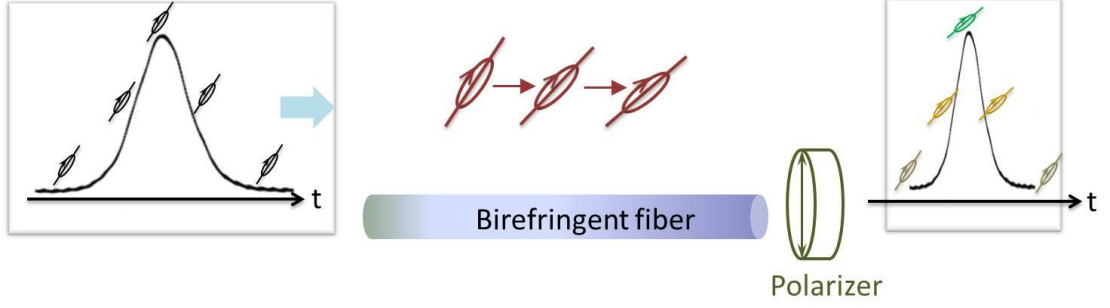


Figure 2. 6. Diagram of pulse shortening process through nonlinear polarization evolution (NPE).

For the qualitative description as shown in figure 2.6, we consider a pulse with elliptical polarization state. The ellipse can be resolved into right- and left- hand circular polarization components of different intensities [36]. These two components accumulate different nonlinear phase shifts related to the intensity, and the polarization ellipse rotates meanwhile keeps its elliptical shape and handedness. The polarization ellipse rotates more at the pulse peak than the pulse wings. At the output of the fiber, the polarizer orients the pulse so that the peak of the pulse passes through while the wings are blocked.

For the quantitative description, we neglect the dispersion effect and consider that the light incident to the optical fiber with an angle θ to the fiber axis (x axis), and the relative nonlinear phase shift between the two polarization components after propagating through the fiber are given by equation (2.3.36).

$$A_x = \sqrt{P_0} \cos \theta \exp(i\Delta\phi_{NL}), \quad A_y = \sqrt{P_0} \sin \theta. \quad (2.3.37)$$

where $\Delta\phi_{NL}$ is the relative nonlinear phase shift. We consider a simple case that the polarizer is with the angle of $(\pi/2 + \theta)$ to the x axis. After the polarizer the total transmission $A(t)$ is [37]:

$$A(t) = A_y \cos \theta - A_x \sin \theta = \sqrt{P_0} \sin \theta \cos \theta [1 - \exp(i\Delta\phi_{NL})]. \quad (2.3.38)$$

With equation (2.3.36), the transmission is:

$$T_p(\theta) = |A(t)|^2 / P_0 = \sin^2 \left[(\gamma P_0 L_{eff} / 6) \cos(2\theta) \right] \sin^2(2\theta). \quad (2.3.39)$$

For a given θ , the transmission is related the peak power P_0 . The transmission is the maximum at the pulse center and the transmission goes down at the pulse tails due

to the reduced peak power. Thus the pulse is shortened after propagating an optical fiber and a polarizer.

Chapter 3

Literature Review

This chapter reviews different techniques to achieve tunable operation and multi-wavelength emission in a fiber laser. These techniques are nonlinear polarization evolution (NPE), nonlinear amplifier loop mirror (NALM), gratings, fiber tapers, Fabry-Perot (FP) interferometers, some special fibers, etc. The related researchers' works are described as examples in each part.

3.1 Nonlinear Polarization Evolution Based Technique

The principle of NPE on tunable operation and multi-wavelength emission is to form a spectral filter with periodically varying amplitude, and with multiple maximums of equal amplitude in the spectral domain. The tunable operation is realized when the maximum shifts, or when the laser emits at different maximums. The multi-wavelength emission is enabled when laser emits at multiple maximums simultaneously.

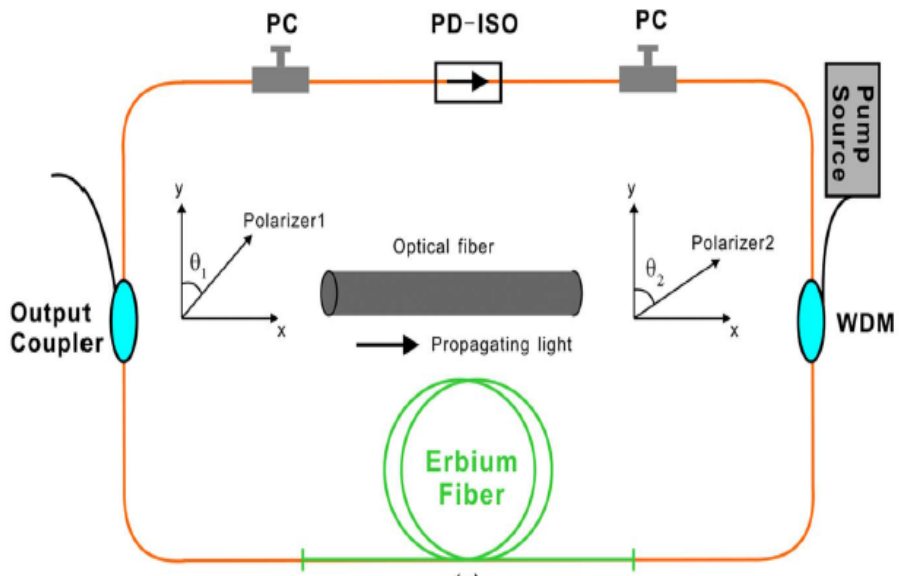


Figure 3. 1. The NPE module in an all-fiber laser cavity [38]. PD-ISO: polarization-dependent isolator. PC: polarization controller.

One example of NPE module in an all-fiber laser cavity is shown in figure 3.1 [38]. The NPE module contains one polarization-dependent isolator sandwiched by two polarization controllers (PCs). The polarization-dependent isolator includes two polarizers and one Faraday rotator. When a free-space module is built, the isolator is replaced by two polarizers at the start and the end, and one free-space isolator. The PCs are replaced by wave plates. Both PCs and wave plates are to change the polarization state of the light.

For the tunable operation, Endo *et al.* reported a tunable erbium-doped (Er-doped) mode-locked fiber laser with the tunable range from 1.54 to 1.6 μm in 1996. The cavity contains free-space component, which is used to achieve NPE effect. The cavity is with dispersion management so that the output pulse is ultrashort, with duration of 270 to 345 fs [39]. In Nelson's work [40], the tunable range is as wide as 104 nm, from 1798 to 1902 nm, with a thulium-doped (Tm-doped) fiber and an NPE cavity structure. It keeps the widest tunable range for mode-locked fiber laser for the time being, although some free-space components were used in the cavity.

For the multi-wavelength emission, the experimental results vary with different setups. Pan *et al.* reported a multi-wavelength Er-doped mode-locked all-fiber laser [41]. The mode locking was by an active intensity modulator driven by a synthesized microwave generator. NPE effect is responsible for the dual- and five-wavelength mode locking. The NPE also suppress the supermode noise to make the laser emission stable. The wavelength also can be smoothly tunable by managing the cavity dispersion through a piece of dispersion compensation fiber. Huang *et al.* achieved tri-wavelength emission in an ytterbium-doped (Yb-doped) fiber laser, which is the largest number of emission wavelength from mode-locked all-fiber laser in the 1 μm regime [15]. The tri-wavelength emission from this setup can be switchable, but switchable state cannot achieve the three-bit binary control. They added a graphene-oxide saturable absorber to further support the mode-locked state, and they also got the wavelength-tunable range of 16.4 nm. Sova *et al.* achieved a tunable dual-wavelength continuous wave (CW) all-fiber laser [42]. The spacing of the two emitted waves can be tunable too. They used multi-segment polarization maintaining fiber and polarizers to form a Lyot filter. As the separation of the transmission peaks of Lyot filter is inversely proportional to cavity effective length, they rotated each segment of polarization maintaining fiber to change the effective length of the cavity, thus to change the wavelength spacing of the emitted waves. Zhao *et al.* realized the

switchable operation of a dual-wavelength mode-locked all-fiber laser in the 1.5 μm regime, and switchable operation could achieve the two-bit full binary control [43]. The mode-locked state was assisted by a saturable absorber made of single-wall carbon nanotube.

Increasing the length or the modal birefringence of the fiber between two polarizers in the NPE module will increase the number of emission wavelength. The dependence of NPE-induced transmission modulation on the length or the modal birefringence of the fiber will be discussed in part 4.4. Zhang *et al.* realized 25-wavelength CW lasing in an erbium-doped (Er-doped) fiber laser by adding 11 m polarization maintaining fiber into the NPE module [44]. The modal birefringence of polarization maintaining fiber is hundreds times larger than the single-mode fiber. Feng *et al.* realized 28-wavelength CW lasing in an Er-doped fiber laser by adding the single-mode fiber as long as 1.2 km into the NPE module [45]. They also tried to reduce the cavity loss by using the 10% output coupler, to lower the threshold of multi-wavelength emission.

Although some of the works were with NPE structure, they failed to realize mode-locked lasing. The NPE-induced transmission modulation in these works is usually with narrow channel spacing and narrow spectral bandwidth. The narrow spectral bandwidth is hard to support mode-locked operation. Luo *et al.* added a semiconductor saturable absorber mirror to relax the mode-locked condition and reduced the length of polarization maintaining fiber into 1.6 m. to realize the seven-wavelength emission [11]. Then this group increased the length of polarization maintaining fiber into 7.4 m, to realize the 11-wavelength emission, which is the largest number of emission wavelength from mode-locked all-fiber laser in the 1.5 μm regime [46].

3.2 Nonlinear Amplifier Loop Mirror Based Technique

In a NALM based laser cavity, the incident light is divided into two counter-propagating optical paths with different intensity. The two counter-propagating lights have different nonlinear phase shift due to the different intensity, and the nonlinear phase shift will affect the reflectivity of NALM [47]. The reflectivity of NALM can be expressed as [48]:

$$R = 2\alpha G(1-k)k[1 + \cos(\phi_{NL} + \phi_{Bias})], \quad (3.2.1)$$

$$\phi_{NL} = \frac{2\pi n_2}{\lambda A_{eff}} P_{in} (1-k-Gk) \frac{[1 - \exp(-\alpha L)]}{\alpha}, \quad (3.2.2)$$

where α is the fiber loss, G is the gain of the gain fiber, k is the split ratio of the NALM formed coupler, ϕ_{Bias} is the phase bias in the NALM, ϕ_{NL} is the nonlinear phase shift, n_2 is the nonlinear refractive index, λ is the wavelength of the propagating wave, A_{eff} is the effective mode area, and P_{in} is the power of the light.

The nonlinear phase shift changes with the wavelength so that the reflectivity of NALM changes with the wavelength too. A spectral filter will be formed to support the wavelength-tunable operation and multi-wavelength emission.

Near the 2 μm regime, Jin *et al.* achieved the tri-wavelength mode-locked all-fiber laser based on NALM [49]. The tri-wavelength mode locking can be tunable with 30 nm, from 1935 to 1965 nm, and can be switchable by adjusting PCs. Liu *et al.* reported a dual-wavelength fiber laser in a NALM cavity [50]. The tuning of the spacing of two emitting waves were assisted by FBGs. Up to 42-wavelength lasing was realized in a thulium-doped (Tm-doped) fiber laser by NALM [48].

3.3 Grating Based Technique

For the tunable operation, the shift of the wavelength is achieved when temperature, strain and/or pressure are applied to the grating. Fiber Bragg grating (FBG) is commonly used. The shift of the wavelength in FBG can be expressed [51]:

$$\Delta\lambda = 2n\Lambda \left\{ \varepsilon - \varepsilon \frac{n^2}{2} [P_{12} - \nu(P_{11} + P_{12})] + \left[\alpha + \frac{\left(\frac{dn}{dT} \right)}{n} \right] \Delta T \right\}, \quad (3.3.1)$$

where n is the effective refractive index of the fiber core, Λ is the period of fiber, ε is the applied strain, $P_{i,j}$ (i, j is integer) is the Pockel's (piezo) coefficients of the stress-optic tensor, ν is the Poisson's ratio, α is the thermal expansion coefficient of the silica fiber with a typical value of $0.015 \text{ nm}/^\circ\text{C}$, and ΔT is the temperature change in degree Celsius.

For tunable operation, the tunable range can be larger than 20 nm in a FBG based Er-doped all-fiber laser mode-locked by carbon nanotube based saturable absorber [52]. Besides wavelength-tunable operation, the pulse width also can be tuned by FBGs, reported by Liu's group [52]. The grating based tunable laser can reach as wide as 160 nm, in a CW mode in 2014, from 1920 to 2082 nm [53]. And it is

amplified by master oscillator power amplifier system to reach more than 100 W of the average output power.

For multi-wavelength emission, multiple gratings are integrated into the laser cavity. Liu *et al.* made a tri-wavelength all-fiber laser system in 1.5 μm regime by three FBGs with different central wavelengths, mode-locked by carbon nanotube based saturable absorber [54]. This is the largest number of emission wavelength in a FBG based mode-locked all-fiber laser. For each emitting waves, the wavelength can be tuned too, with a tunable range of 6 nm.

Long-period fiber grating, which has the similar function with FBG, was used to achieve the wavelength-tunable operation too. Anzueto-Sanchez *et al.* used the long-period fiber grating in an Er-doped fiber ring laser to get 38 nm for the tunable range, from 1527 to 1565 nm [55]. Lim *et al.* fabricated the long-period fiber grating with a photonic crystal fiber (PCF) [56]. The response wavelength induced by such grating can be tunable by mechanical pressure, which can be used in a tunable fiber laser setup.

3.4 Fiber Taper Based Technique

When the fiber is tapered the light is no longer guided by fiber core only but also propagates along the fiber cladding. More than one mode is excited in the tapered region and interference happens between these modes. The interference can be either constructive or deconstructive, resulting in a transmission maximum and minimum at different wavelengths, to form a periodical spectral filter [57]. By stretching the taper, its spectral response will be shifted and the transmission of the formed filter will be changed too.

With the fiber taper, Fang *et al.* achieved wavelength-tunable range of more than 50 nm in a Tm-doped all-fiber laser, mode-locked by a carbon nanotube saturable absorber [22]. The tunable range is the widest in a mode-locked all-fiber laser near the 2 μm regime.

If the fiber taper is with low modulation depth, graphene solution is deposited on the tapered region to increase the modulation depth. Tri-wavelength and four-wavelength mode-locked all-fiber laser was demonstrated in 1035 nm and 1533 nm, respectively with such a graphene-deposited tapered fiber [58,59].

However the stretching of the fiber taper should be within the elastic region otherwise the fiber taper will be broken. To further increase the tunable range without damaging the fiber taper, cascading several tapers might be the solution.

3.5 Fabry-Perot Interferometer Based Technique

The FP interferometer can transmit light as a function of wavelength. It forms a filter as a function of wavelength and the filter is with periodicity. The separation of transmission maximum $\Delta\lambda$ in the spectral domain is expressed below [60]:

$$\Delta\lambda = \frac{\lambda^2}{2nL}, \quad (3.7.1)$$

where λ is the central wavelength of the nearest transmission peak, L is the distance between two reflecting surface inside the FP interferometer, n is the refractive index of the medium inside the FP interferometer.

The FP interferometer can support both tunable single-wavelength and multi-wavelength lasing. The length of FP interferometer can be changed by stretching or pressing the device, or the reflected wavelength can be changed by applying voltage. The wavelength separation of the transmission function is changed accordingly referring to equation (3.7.1), thus the emission wavelength and the numbers of emission wavelength are changed too.

Park *et al.* used a tunable FP interferometer module to realize the single-wavelength tunable operation with the tunable range of more than 30 nm in a Er-doped fiber ring laser [61]. Tian *et al.* used a FP interferometer to induce the periodic loss in the frequency domain to enable the five-wavelength emission in a Er-doped fiber ring laser [62].

FP interferometers can be made in different platforms, such as in a microstructured fiber or micro-fiber [63], micro-electro-mechanical system [64], semiconductor modulator [65], etc.

The FP module also can be integrated with the sample to be detected. Marshall *et al.* put the gas sample into the FP module [25]. By tuning the FP, the state of multi-wavelength emission is changed, and the absorption spectra of the gas sample under different states of the laser source are collected. Thus they could get the results more accurately.

3.6 Special Fibers Based Technique

Mach-Zehnder interferometer can be formed when PCF is spliced with two segments of single-mode fibers at the two ends. The core and cladding of PCF act as two arms of the interferometer. When the light is incident from the single-mode fiber into the

PCF, the fundamental mode will be partially coupled into the cladding. The core mode and cladding mode accumulate phase difference when they propagate along PCF and then they are recoupled together at the other splicing point of PCF and single-mode fiber. A spectral filter will be formed in this case, and the wavelength response will be changed in the refractive index or optical-path length of PCF changes.

By changing the curvature radius in the Mach–Zehnder interferometer, Sierra-Hernandez *et al.* was able to get the single-, dual-, and tri-wavelength emissions and the wavelength tunable operation from 1526 to 1550 nm in a fiber ring laser [66]. Soltanian *et al.* achieved the dual-wavelength emission in a Tm-doped fiber ring laser and the dual-wavelength emission is stable over a long time [67].

Multimode fiber also can work as a band-pass filter. When light is incident from a single-mode fiber into the multimode fiber, multiple modes which are supported by the multimode fiber are excited. The modes have interference between each other when they propagate along the multimode fiber, resulting in a transmission response function in the frequency domain.

The peak in the spectral transmission is fixed with a certain length of multimode fiber. In order to change the effective length of multimode fiber, Antonio-Lopez *et al.* inserted the index matching liquid into a tube and connected the tube with multimode fiber [68]. They added the tube and multimode fiber into the fiber laser ring cavity together and by pushing the multimode fiber forward or backward to the tube, the effective length of multimode fiber is changed. Thus the lasing wavelength is tunable. With this method, Castillo-Guzman *et al.* achieved the wavelength-tunable range of 60 nm, from 1549 to 1609 nm in a ring fiber laser [69]. The center wavelength of the band-pass filter, which depends on the length of multimode fiber, is fixed. In order to achieve tunability, some mechanisms are designed to change the effective length of multimode fiber. Zhao *et al.* reported tri-wavelength emission in a fiber ring laser with a multimode fiber near 2 μm regime [70]. The number of emission wavelengths was changed by PCs and the spacing of emission wavelengths could be tuned by inserting different length of multimode fiber into the cavity.

3.7 Other Techniques in Tunable Multi-Wavelength Fiber Lasers

Four-wave mixing effect is introduced to stabilize the multi-wavelength emission in a laser setup. Sometimes the multi-wavelength is lasing but different wavelengths are with different power levels, which make the laser unstable. To stabilize it, four-wave

mixing effect is induced by a piece of long fiber, such as highly nonlinear PCFs or dispersion-shifted fiber. Due to four-wave mixing effect, energy transfers from the higher power wave to the lower power waves to achieve the balance between multiple emission waves. Most of the lasers with four-wave mixing effect work in the CW mode due to the narrow spectral bandwidth. The four-wave mixing effect can be combined in different laser structures. Liu *et al.* used 51 m highly nonlinear PCF in a FBG based laser to achieve stable tri-wavelength emission [12]. By setting the FBGs, the separation of the emitted waves can match the four-wave mixing effect. Tran *et al.* used 1 km dispersion-shifted fiber to trigger the four-wave mixing effect to stabilize four-wavelength lasing in a FBG based laser [71]. Furthermore, the four-wave mixing can even realize the number of emission wavelength more than the number of FBGs. Han *et al.* used 1 km dispersion-shifted fiber to enable the four-wave mixing effect to achieve as much as 12 lasing wavelengths with only 8 FBGs [72]. The four-wave mixing effect also works well with NPE and NALM based laser cavity. Wang *et al.* used a 400 m single-mode fiber in a NPE laser cavity to realize six-wavelength emission near 2 μm regime [14]. Han *et al.* used 1 km dispersion-shifted fiber in a NALM laser cavity to achieve up to 17 lasing wavelengths [73].

For the tunable operation, Shubochkun *et al.* controlled the temperature of the coupler to control the optical output coupling, further to control the transmission spectra [74]. The transmission spectra determined the lasing wavelength. This group could get a continuous temperature tuning over 43 nm range for a Tm-doped all-fiber laser. Chamorovskiy *et al.* achieved the wavelength-tunable range of 70 nm, from 2030 to 2100 nm, by only adjusting the polarization controller (PC) in a holmium-doped (Ho-doped) fiber laser [23]. This laser was based on a linear cavity, and mode-locked by a carbon nanotube saturable absorber. Zhang *et al.* demonstrated the Er-doped fiber laser tunable by PCs in both normal dispersion and anomalous dispersion regime [75]. The mode locking was enabled by graphene and the tunable range is 30 nm, from 1570 to 1600 nm. Fedotov *et al.* also realized the wavelength-tunable operation with tunable range of 5 nm by only adjusting PCs in a Yb-doped fiber laser [76]. The spectral bandwidth and pulse width was observed to be tunable too with this setup. This laser was a ring cavity, and mode-locked by a carbon nanotube saturable absorber.

For the multi-wavelength lasing, Jun *et al.* generated more than 8 wavelength channels with the help of a phase modulator in 2011 [77]. The phase modulator was

driven by voltage, worked at a low frequency with large modulation amplitude. It enables mode locking, creates different optical path length when different voltages are applied. The modulation on cavity length suppresses the buildup of the predominant cavity mode thus allows multi-wavelength operation. The use of all-fiber phase modulator also helps to build an all-fiber laser cavity. Zhang *et al.* obtained the dual- and tri- wavelength dissipative soliton by the artificial birefringence filter to disturb the homogenous gain in an Er-doped fiber laser [16]. Zhao *et al.* realized the switchable dual-wavelength mode-locked state around 1550 nm by inserting a tunable attenuator in the cavity to change the intracavity loss [43]. Chamorovskiy *et al.* demonstrated the dual-wavelength soliton pulse in Ho-doped fiber laser by adjusting the polarization controller (PC) in the cavity [23]. Wang *et al.* used the cascaded filter structure, which is formed by cascading a Mach-Zehnder interferometer and a Sagnac ring, to construct a 2 μm switchable dual-wavelength fiber laser operating [78]. Feng *et al.* combined two kinds of interferometer, the FP interferometer and Mach-Zehnder interferometer, to achieve the switchable tri-wavelength lasing in an Er-doped fiber laser [79].

Chapter 4

The Configuration of Experimental Setup

This chapter gives the details on the configuration of the experimental setup. Thulium-doped (Tm-doped) fibers are chosen as our gain fiber. Its energy level, absorption and emission spectrum are analyzed. Since the proposed laser is working on a wide spectral range, the broadband transmission of isolators and couplers are analyzed. To construct a compact cavity structure, nonlinear polarization evolution (NPE) technique is employed to enable the mode locking, multi-wavelength emission and tunable operation simultaneously. Lastly the schemes for multi-wavelength emission, tunable operation, the overall cavity structure are studied and presented.

4.1 The Energy Level, Absorption and Emission of Thulium-Doped Fibers

Tm-doped fibers and holmium-doped (Ho-doped) fibers are of much interest for building the fiber laser systems since they provide the laser emission near 2 μm , which locate in the eye-safe regime. It is called “eye-safe” since light in this wavelength regime are almost absorbed in cornea and lens, which are the anterior portions of human eye, and never reach retina, which is the significant light-sensitive layer. It is noted that high power laser light may also cause thermal damage to human eyes. To figure out eye-safety level laser beam divergence and laser beam quality should also be taken into consideration besides power level. Lasers operating in eye-safe regime will find various applications in military, industry, and biomedicine.

Compared with Ho-doped fiber, Tm-doped fiber is chosen in our experiment. Firstly it has lower propagation loss. The emission wavelength of Tm-doped fiber is at shorter wavelength than that of Ho-doped fiber, it has lower propagation loss as the propagation loss increase largely in silica fiber when operation wavelength is larger than 2 μm . Secondly Tm-doped fiber can be pumped directly by 793 nm laser diode, but for Ho-doped fiber, there is lack of available pump laser diode to directly pump it to make it emitted near 2 μm [80]. Thirdly the pump efficiency is higher with Tm-

doped fiber because of cross relaxation process. Fourthly the emission cross section of Tm-doped fiber is wider than that of Ho-doped fiber. Tm-doped fiber is more promising to build a widely tunable laser. The reasons are discussed in detail in following paragraphs.

The left part of figure 4.1 shows the simplified energy-level diagram of Tm^{3+} ion in silica glass fiber. The atoms at ground level $^3\text{H}_6$ are excited to energy level $^3\text{H}_4$ by 793 nm laser pumping. The excited atoms relax to energy level $^3\text{F}_4$ by non-radiative relaxation or releasing photons at 1487 nm. The atoms at energy level $^3\text{F}_4$ return to the ground level by releasing photons at 1800nm [80]. The photons with 1487 nm are usually absorbed by adjacent and unpopulated atoms at the ground level. This is the cross relaxation as shown in figure 4.1. Then these atoms are excited to energy level $^3\text{F}_4$ to make it further populated. The excitation process yields two excited ions for each absorbed pump photon, which is highly efficient. With cross relaxation process the pump to laser efficiency can be >60% [81].

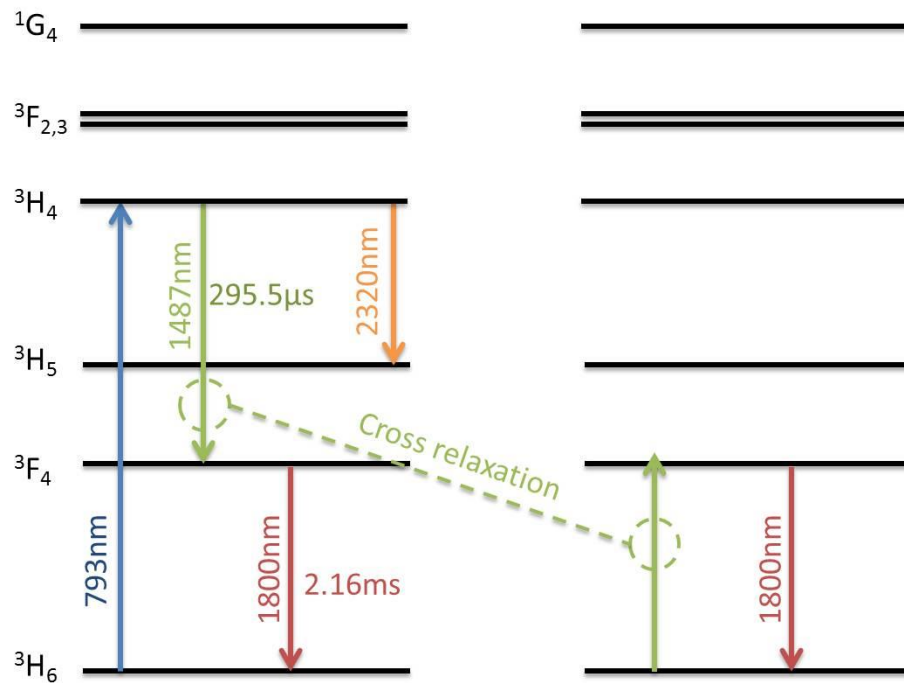


Figure 4. 1. The simplified energy-level diagram and cross-relaxation of thulium³⁺ (Tm^{3+}) ion in silica glass fiber.

Figure 4.2 shows the measured transition cross sections, including absorption and emission cross section of Ho-doped and Tm-doped fiber [82–84], which emit at the eye-safe regime. For each kind of fiber, the transition cross section varies a little with different dopants and different doping concentrations. The emission bandwidths of

Tm-doped are wider than Ho-doped fiber. A wider emission bandwidth will result in a wider gain bandwidth, which is important for building a widely tunable laser.

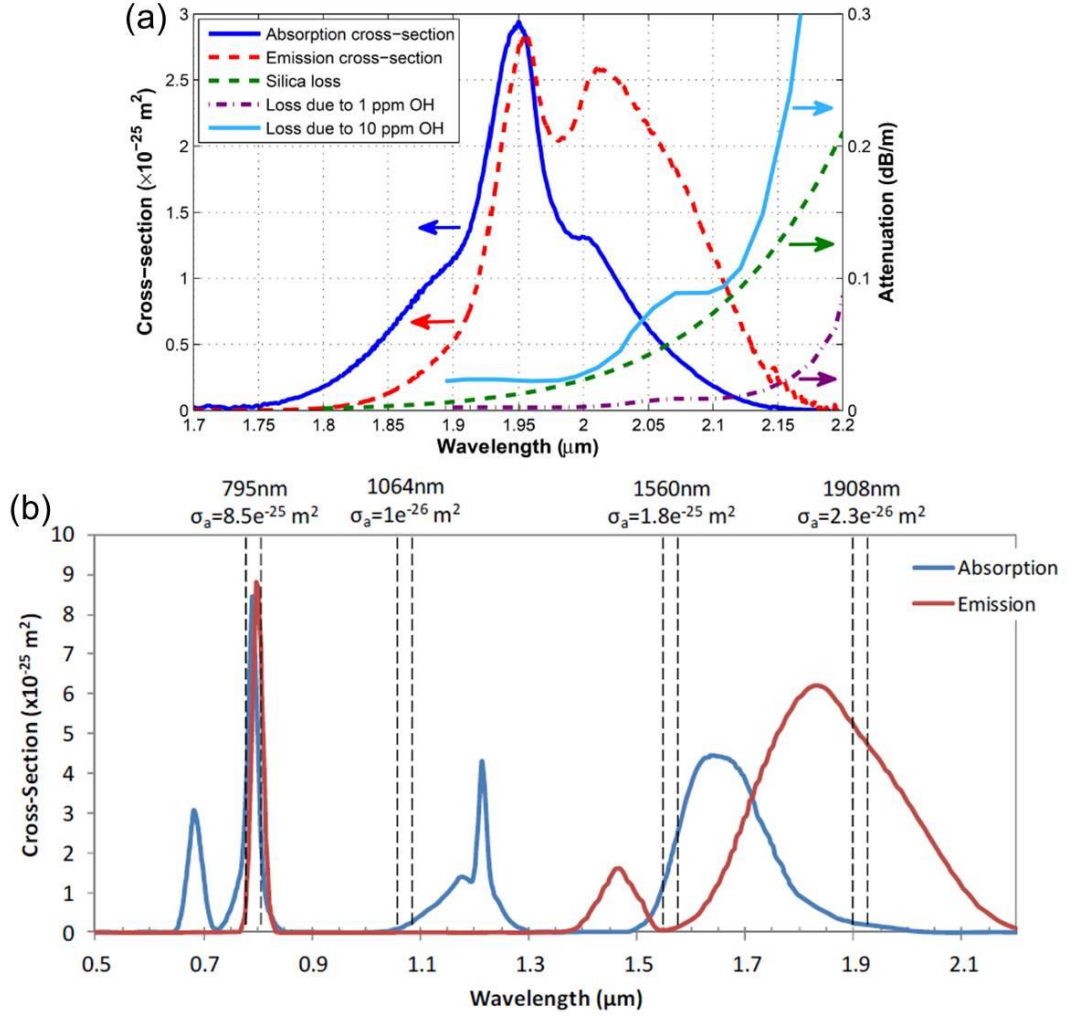


Figure 4. 2. The transition cross section of (a) holmium-doped silica fiber and (b) Tm-doped silica fiber [82–84].

4.2 The Transmission of Polarization-Dependent Isolator

The working wavelength of the polarization-dependent isolator (PDI) is 2000 nm, and the loss of this PDI at 2000 nm is the minimum. However the proposed laser is working on a wide spectral range. The transmission of PDI over a wide spectral range is studied.

The working principle of PDI is Faraday rotation. It includes one Faraday rotator sandwiched by two polarizers. The angle between the two polarizers is usually set to 45° . When light passes through the input polarizer, the polarization direction of the light is the same with the polarization direction of input polarizer. Then the light

passes through Faraday rotator, the polarization direction of the light rotates due to the magneto-optic effect. The rotation angle β is

$$\beta = VBL, \quad (4.2.1)$$

where V is the Verdet constant of the material, B is the magnetic flux density (in the direction of propagation), and L is the length of the rotator medium. By choosing the proper V , B , and L , to make the rotation angle equal to 45° , then the light will pass through the output polarizer, the angle of which is 45° to the input polarizer without further loss. The Verdet constant is wavelength-dependent. The rotation angle with different wavelength is given by table 4.1. The data is from Advanced Fiber Resources, the manufacturer of this PDI.

Table 4. 1. The rotation angle versus wavelength of the Faraday rotator inside the polarization-dependent isolator

Wavelength (nm)	1850	1950	2000
Rotation angle (°)	50.5	46.85	45

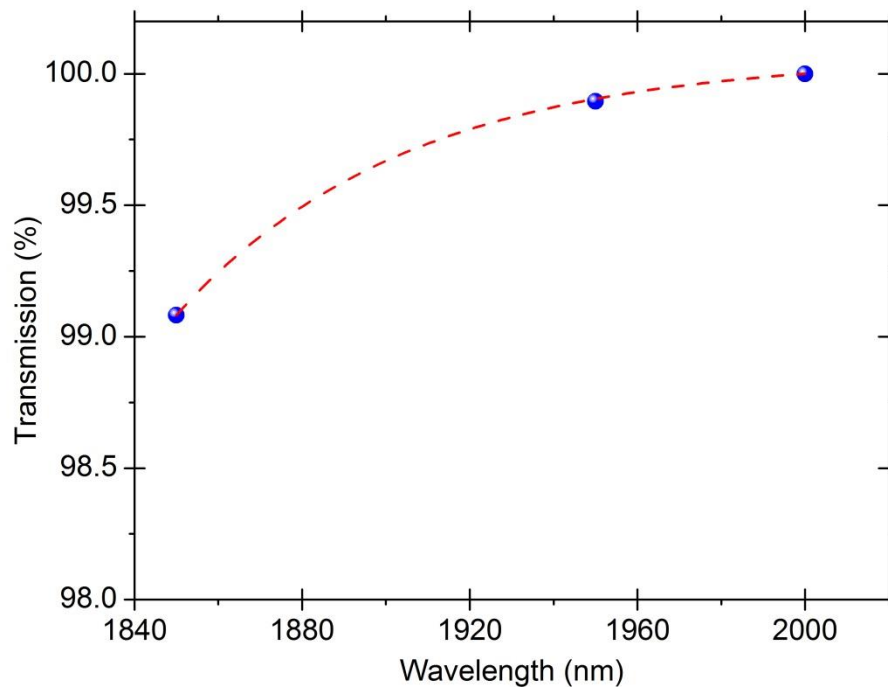


Figure 4. 3. The calculated and fitted transmission curve of the polarization-dependent isolator (PDI).

If the light is not rotated by 45° by Faraday rotator, it will have the loss when it propagates through the output polarizer. The transmission of the PDI becomes

$$T = \cos^2(\theta - 45^\circ), \quad (4.2.2)$$

where θ is the rotation angle of Faraday rotator. Figure 4.3 is the calculated and fitted transmission curve of the PDI in the wavelength range of 1850 to 2000 nm. The minimum transmission is 99.08% and the maximum is 100%, showing that the variation of PDI transmission is very small over the wide spectral range.

4.3 The Transmission of Coupler

The working wavelength of 5:95 coupler is 1900 nm. The transmission of couplers over a wide spectral range is measured with a broadband laser light source. The broadband light source is home-made with fiber pigtail. The spectrum from the light source is measured first by an optical spectrum analyzer (OSA). The input fiber of coupler is spliced to the output of the light source. The splice makes the fiber connection loss neglected. The output end of the coupler with 95% output ratio is connected to the OSA to measure the spectrum. The measurement result is shown in figure 4.4. The two spectra are close to each other so that the transmission of coupler varies little over the wide spectral range.

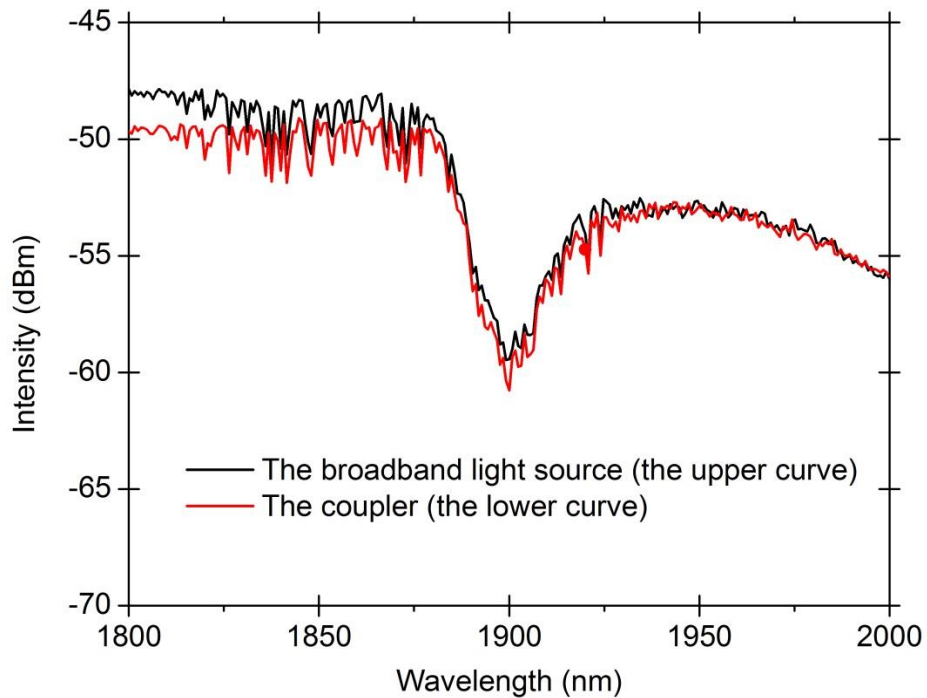


Figure 4. 4. The measured transmission curve of the 5:95 coupler.

4.4 The Scheme for Multi-Wavelength Emission

There are many methods to enable the multi-wavelength emission in a mode-locked fiber laser. We want to integrate the module of mode-locked enablement, tunable operation and multi-wavelength emission into one laser setup meanwhile keeps the system compact, NPE is chosen.

The NPE-induced transmission modulation induces a spectral filter, which is responsible for the multi-wavelength emission [85–87]. Equation (2.3.39) is re-deduced to see how the spectral filter is like and how it enables multi-wavelength emission.

We consider more factors for the NPE-induced transmission equation, such as the linear phase shift, nonlinear phase shift, and the polarizer with the angle of θ_2 to the x axis. The slowly varying amplitude $A(z, t)$ can be expressed in two polarization components when the pulsed light is incident with angle of θ_1 to the x axis of the optical fiber:

$$A_{x0} = \sqrt{P_o} \cos \theta_1, \quad (4.4.1)$$

$$A_{y0} = \sqrt{P_o} \sin \theta_1. \quad (4.4.2)$$

After propagation the fiber with length L and we assume the fiber loss is zero, the two polarization components becomes:

$$A_{x1} = \sqrt{P_o} \cos \theta_1 \exp(i\Delta\phi_L + i\Delta\phi_{NL}), \quad (4.4.3)$$

$$A_{y1} = \sqrt{P_o} \sin \theta_1. \quad (4.4.4)$$

where $\Delta\phi_L$ and $\Delta\phi_{NL}$ are the linear and nonlinear phase shift, respectively with the definition in equation (2.3.19) and (2.3.36).

The pulsed light passes through the polarizer, and the two polarization components become:

$$A_{x2} = A_{x1} \cos \theta_2 = \sqrt{P_o} \cos \theta_1 \cos \theta_2 \exp(i\Delta\phi_L + i\Delta\phi_{NL}), \quad (4.4.5)$$

$$A_{y2} = A_{y1} \sin \theta_2 = \sqrt{P_o} \sin \theta_1 \sin \theta_2. \quad (4.4.6)$$

Then we get the transmission function:

$$T = \frac{|A_{x2} + A_{y2}|^2}{|A_{x0} + A_{y0}|^2} = \frac{P_o \left| \left[\cos \theta_1 \cos \theta_2 \exp(i\Delta\phi_L + i\Delta\phi_{NL}) + \sin \theta_1 \sin \theta_2 \right]^2 \right|}{P_o |\cos \theta_1 + \sin \theta_1|^2}, \quad (4.4.7)$$

$$T = \cos^2 \theta_1 \cos^2 \theta_2 + \sin^2 \theta_1 \sin^2 \theta_2 + \frac{1}{2} \sin(2\theta_1) \sin(2\theta_2) \cos(\Delta\phi_L + \Delta\phi_{NL}). \quad (4.4.8)$$

The NPE-induced transmission can be treated as function of wavelength since the variable λ is included in the linear and nonlinear phase shift. The NPE-induced transmission introduces a spectral filter with multiple peaks to make laser emitted at the multiple peaks simultaneously. Therefore the multi-wavelength emission is realized. The more peaks from the spectral filter located within the laser emission range, the more numbers of potential emission wavelength we will get. The number of peaks is determined by the modal birefringence and fiber length when other parameters are fixed.

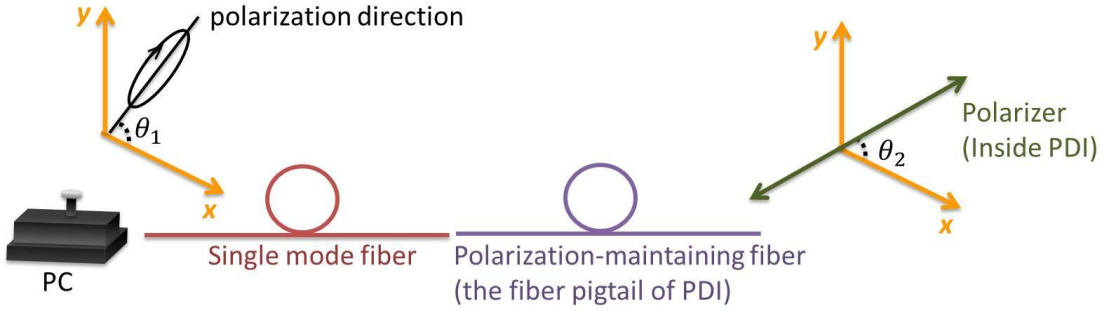


Figure 4. 5. The NPE-based structure formed by polarization controller, single-mode fiber.

PDI: polarization-dependent isolator.

We refer to the corresponding NPE-based structure as shown in figure 4.5. It includes polarization controller (PC) which controls the polarization direction of the incident light, single-mode fiber, 0.6 m polarization-maintaining fiber which is the fiber pigtail of PDI, and one polarizer inside the PDI. We concern the modal birefringence and fiber length in the NPE-based structure. The modal birefringence can be tuned within a certain range, and the fiber length includes the length of both polarization-maintaining fiber and single-mode fiber. We will firstly figure out the roughly tunable range of modal birefringence, and then calculate how long of the single-mode fiber should be used in order to increase the number of peaks within a certain laser emission range, as the length of polarization-maintaining fiber is fixed.

We calculate the bending-induced birefringence in single-mode fibers. The bending-induced birefringence is essentially a stress effect. Squeezing PCs will bend the fiber inside PCs. The bent fiber will build up the lateral and compressive stress under the conditions of “large” deformations. This pressure will cause the birefringence.

The difference of the mode-propagation constant $\Delta\beta$ in x and y directions becomes [88,89]:

$$\Delta\beta = |\beta_x - \beta_y| = 0.25k_0n^3(p_{11} - p_{12})(1+\nu)\left(\frac{1}{R}\right)^2 r^2, \quad (4.4.9)$$

The modal birefringence B_m is:

$$B_m = \frac{|\beta_x - \beta_y|}{k_0} = 0.25n^3(p_{11} - p_{12})(1+\nu)\left(\frac{1}{R}\right)^2 r^2, \quad (4.4.10)$$

where $k_0 = 2\pi/\lambda_0$ is the propagation constant, n is the refractive index of the material, p_{ij} is the strain-optical coefficients, ν is the Poisson's ratio, R is the radius curvature when bending the fiber, and r is the outer radius of the fiber.

In fused silica, $n = 1.46$, $\nu = 0.17$. $p_{11} - p_{12} = -0.15$, the negative sign here indicates the fast axis of the bending birefringence coincides with the radius curvature. In our single-mode fiber, $r = 62.5\mu m$. Table 4.2 is the list of different values of modal birefringence with different radius curvatures.

Table 4. 2. The list of different values of modal birefringence with different radius curvatures.

Radius curvature (cm)	Modal birefringence
0.6	14.82×10^{-6}
0.8	8.33×10^{-6}
1	5.33×10^{-6}
2	1.33×10^{-6}

Since only a small parts of the fiber are pressed by PCs where the modal birefringence changes, we take an estimated and average value of $\sim 10^{-6}$ for the whole length of fiber in the later simulation.

We begin to calculate how long of single-mode fiber we need to use. We firstly revise the linear and nonlinear phase shift in equation (4.4.8) to include the contributions of single-mode fiber and polarization-maintaining fiber since the pulsed light propagates through both fibers. The linear and nonlinear phase shift become:

$$\Delta\phi_L = \Delta\phi_{L,SMF} + \Delta\phi_{L,PMF} = \frac{2\pi}{\lambda} (L_{SMF} B_{m,SMF} + L_{PMF} B_{m,PMF}), \quad (4.4.11)$$

$$\Delta\phi_{NL} = \Delta\phi_{NL,SMF} + \Delta\phi_{NL,PMF} = [\gamma P_0 (L_{SMF} + L_{PMF})/3] \cos(2\theta_1), \quad (4.4.12)$$

where L_{SMF} and L_{PMF} are the fiber length of single-mode fiber and polarization-maintaining fiber, respectively, $B_{m,SMF}$ and $B_{m,PMF}$ are the modal birefringence of single-mode fiber and polarization-maintaining fiber, respectively.

We roughly simulated how the NPE-induced transmission can form a spectral filter, by choosing $\theta_1 = \pi/4$, $\theta_2 = \pi/6$, $P_0 = 3mW$, $n_2 = 2.7 \times 10^{-20} m^2/W$. γ is calculated by the equation below, which is another expression of equation (2.1.3).

$$\gamma = 2\pi n_2 / \lambda A_{eff}. \quad (4.4.11)$$

The mode-field effective area is $A_{eff} = \pi \times (5\mu m)^2 = 78.54\mu m^2$. The fiber pigtail of PDI is PM1550 fiber from Corning. The modal birefringence of PM1550 is $B_{m,PMF} = 0.4 \times 10^{-3}$ and the length of PM1550 is 0.6 m [90].

Figure 4.6 shows different NPE-induced transmissions with 10 m, 40 m, 70 m and 100 m single-mode fiber. In order to increase the number of emission wavelength, a long haul of single-mode fiber is required to increase the number of peaks in the spectral filter within a certain laser emission range. However if too long fiber is used, too much transmission loss will be induced so that the mode-locked threshold will be affected. Therefore we choose to use 70 m single-mode fiber in the cavity to realize the mutli-wavelength emission.

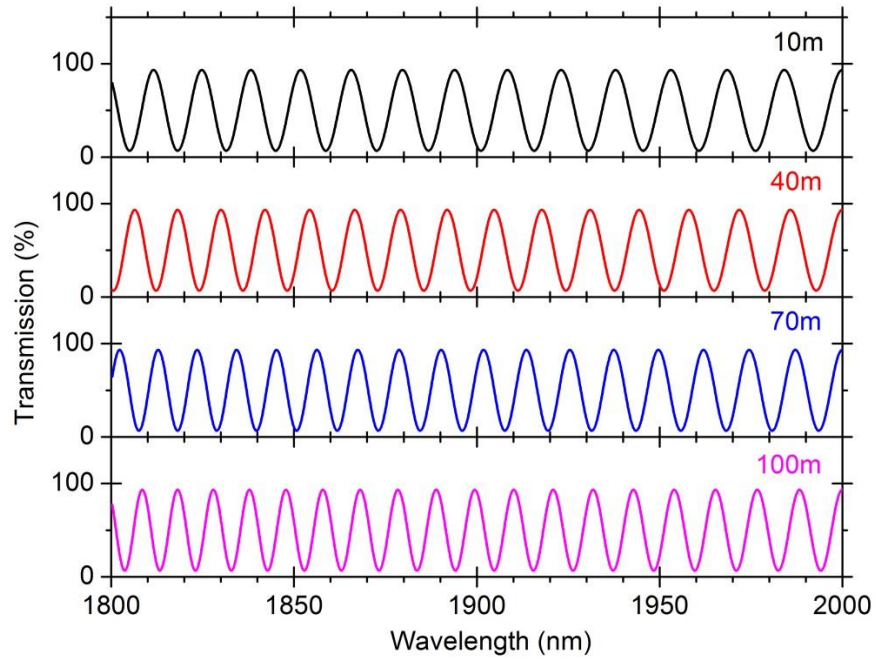


Figure 4. 6. The simulated NPE-induced transmissions with different length of single-mode fiber.

4.5 The Scheme for Tunable Operation

To obtain a wide tunable range, the following three aspects are most important. The first is to broaden the gain bandwidth so that there is a potential wide range for wavelength tuning. The second is to form an artificial spectral filter with a tunable center wavelength, which acts as a wavelength selection element. The third is to reduce the cavity loss to lower the laser threshold. Thus the laser at shorter or longer wavelength where the gain is smaller can emit, to have a broad emission wavelength range.

In order to have a broad bandwidth of gain, the bidirectional pumping is proposed. The working principle is illustrated in figure 4.7. Along the signal propagation direction, the Tm-doped fiber is divided into four segments: (a), (b), (c), and (d). The pump light is gradually absorbed along the fiber. Most of the pump light is absorbed by fiber segment near the pump, and a little pump light is left to be absorbed by fiber segment away from the pump. Therefore at the fiber segment near the pump, such as segment (a) and (d), almost all the atoms at the ground level absorb the pump light and get excited. At the fiber segment away from the pump, such as segment (b) and (c), a few atoms still remain unpumped at the ground level. With forward pumping, at segment (a) the atoms transition will result in the emission of signal light with wavelength range of 1.6 to 2 μm . The signal light propagates towards segment (b). The signal light in the short-wavelength range is absorbed at segment (b) by a few atoms which are unpumped at ground level and are populated at the near-ground level in thermal equilibrium at the operating temperature, because the absorption spectrum of these atoms has overlap with the emission spectrum of the signal light in the wavelength range of 1.6 to 1.9 μm . Thus the final emitting light is in the long-wavelength range. However with backward pumping, the signal light propagates towards the fiber segment which is with high excited level, with most of atoms at the ground level excited, as shown in segment (d). There is less reabsorption so that the final emitting light is in short-wavelength range. By combining forward and backward pumping, the emitting light will cover both short-wavelength and long-wavelength range, which is a broad emission wavelength range.

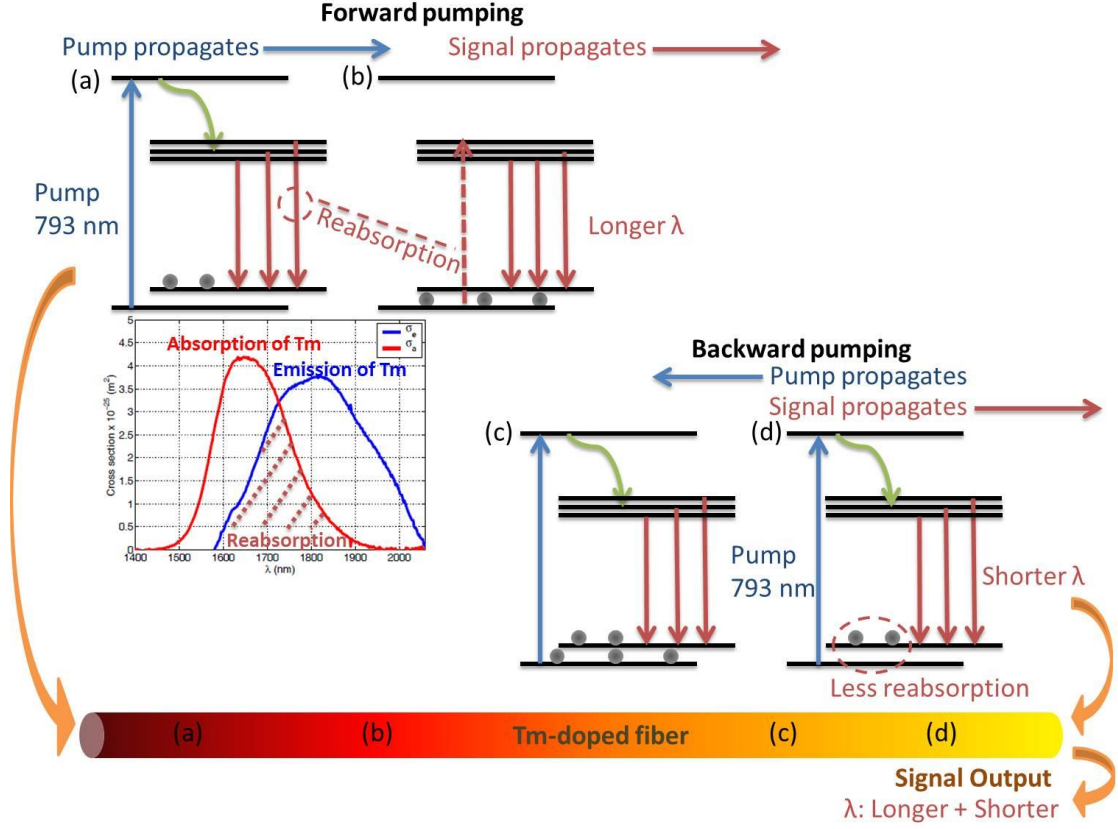


Figure 4. 7. The working principle of bidirectional pumping of Tm-doped fiber. (a), (b), (c), (d) is the situation of population inversion, absorption and emission at different segments of Tm-doped fiber.

The amplified stimulated emission (ASE) spectra, which are the estimation of gain, were measured with backward, forward and bidirectional pumping under the same pump power level. Figure 4.8 shows the experimental setup on the measurement of ASE spectra. The 793-nm light from laser diode (LD) was pumped into the Tm-doped fiber by wavelength-division multiplexer (WDM). The fibers at point A and B were angle cleaved to avoid Fresnel reflection. The fiber at point A was connected to optical spectrum analyzer (OSA) to measure the ASE spectrum. When measuring the forward ASE, LD1 was off and the power of LD2 was set to 150 mW. When measuring the backward ASE, LD2 was off and the power of LD1 was set to 150 mW. When measuring the bidirectional pump effect, the total power of LD1 and LD2 was set to 150 mW. As shown in figure 4.9 (a), the spectral bandwidth of bidirectional pumping was the widest. Figure 4.9 (b) shows the revised ASE spectrum with considering the wavelength-dependent loss of PDI and coupler. We can see that the wavelength-dependent loss of the two components takes minor effects on the bandwidth variance of the net gain (saturated gain minus cavity loss) spectrum.

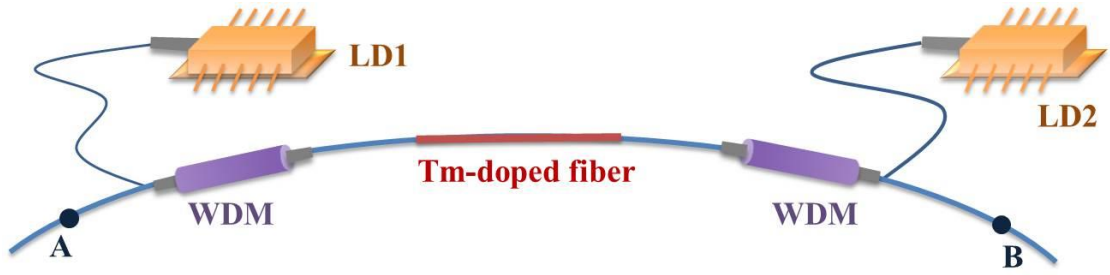


Figure 4. 8. The experimental setup on the measurement of amplified stimulated emission (ASE) spectra. LD: laser diode.

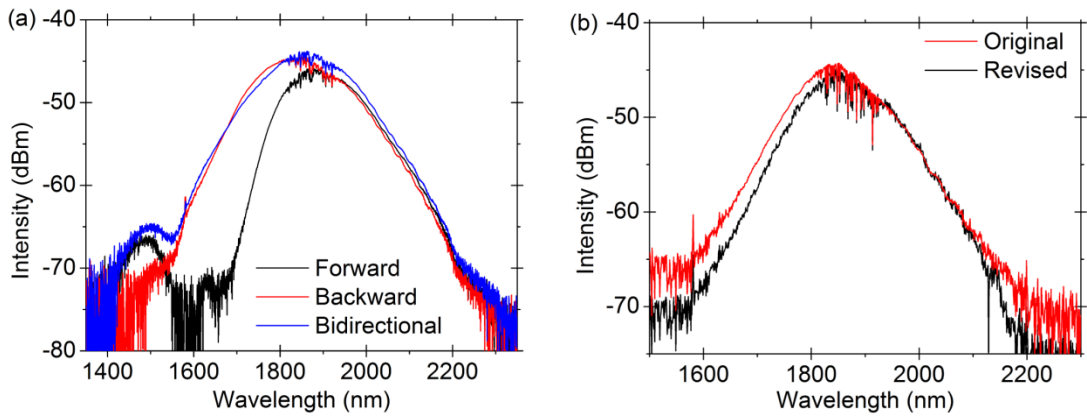


Figure 4. 9. (a) The ASE spectra by bidirectional, backward, and forward pumping under the same pumping power level. (b) The original and revised ASE spectrum. The revised one is with considering the wavelength-dependent loss of PDI and coupler.

For the artificial spectral filter, it can be formed by multimode fiber, fiber taper, photonics crystal fiber, fiber Bragg grating, Fabry-Perot filter, NPE technique, or nonlinear amplified loop mirror (NALM) technique. Except NPE and NALM, the tunability of other components is due to the center-wavelength shifting of these spectral filters. The shifting is achieved by applying tension or stress to the component, which is limited by the variation of the physical structures. Up to now, the tunable range is several tens of nanometers. For NPE and NALM, the tunability is due to the periodic spectral filters stemmed from the NPE or NALM effect, which takes effects on the whole emission spectrum, not within a specific range. The factors related to gain should be considered on NALM effect. The wavelength tuning by NPE effect is easily achieved by changing the polarization state of the light inside the cavity, and the mechanism of tunable operation is explained in part 5.1.2. Theoretically the tuning range can be as wide as the spectral range that above laser threshold. NPE-induced spectral filter is chosen.

The combination of bidirectional pumping and NPE will increase the potential tunable range. The process is illustrated in figure 4.10.

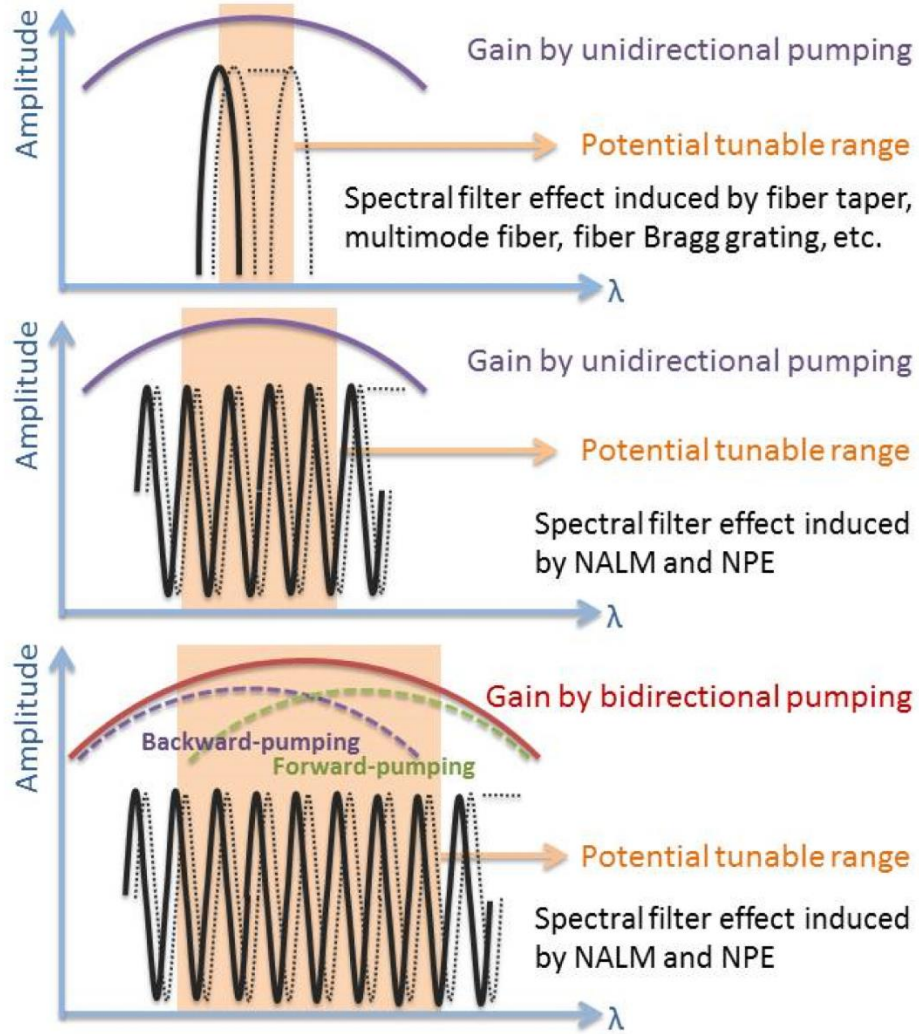


Figure 4. 10. Schematic illustration of the effects of different pumping methods and spectral filters on the potential tunable range. The shaded areas describe the potential tunable ranges of each scheme.

4.6 The Experimental Setup

Figure 4.11 shows the experimental setup of tunable multi-wavelength Tm-doped mode-locked all-fiber laser. A 1.5 m Tm-doped fiber (core/cladding diameter: 9/125 μm , Nufern) was bidirectional pumped by two single-mode LDs with center wavelength at 793 nm. The reason of choosing 793 nm as pumping wavelength was that it had higher pump to laser efficiency due to cross relaxation process. The maximum output powers of the two LDs were 170 mW and 200 mW, respectively. The 793 nm pump light was coupled into the laser cavity by two WDMs, and a part of

the light inside the cavity was outputted through one coupler. We used two couplers with different coupling ratio (40:60, 5:95), to change the cavity loss thus to change the bandwidth of net gain. A 70 m single mode silica fiber (SMF28e, Corning) and the 0.6 m polarization maintaining fiber pigtails of the PDI were used as the birefringent fiber. The components from point A to B, including single-mode fiber, two PCs and one PDI, are responsible for NPE effect, which is described in figure 4.5. We use two PCs here is to control the polarization states more precisely. NPE effect enables the mode locking and forms a spectral filter for tunable operation and multi-wavelength laser emission.

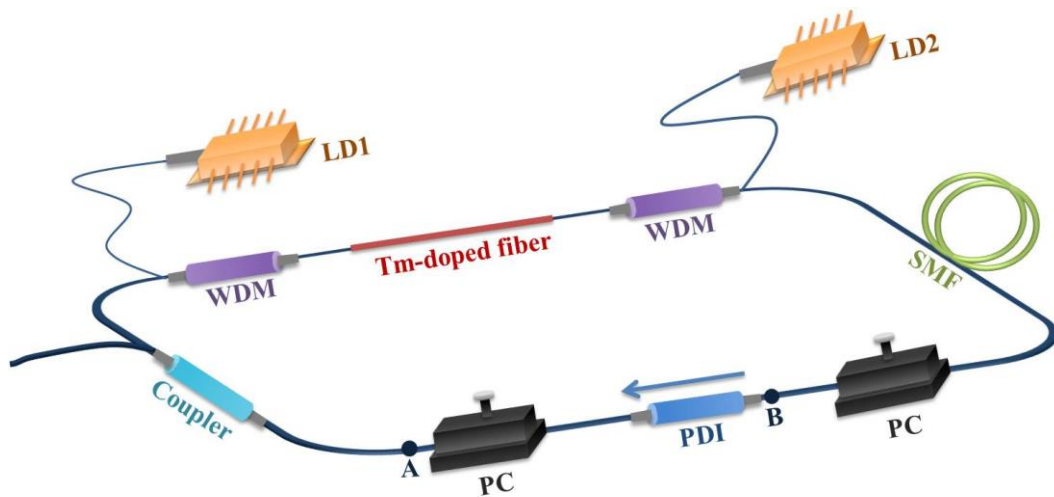


Figure 4. 11. The experimental setup of the widely tunable multi-wavelength Tm-doped mode-locked all-fiber laser. SMF: single-mode fiber.

Table 4. 3. The list of parameters and equipments used in the measurement.

Parameters	Equipments	Manufacturers of the equipments
Output spectra	Optical spectrum analyzer	Yokogawa
Pulse trains	Digital oscilloscope	Agilent
	12 GHz photon detector	Newport
RF spectra	Signal source analyzer	Rohde & Schwarz
	12 GHz photon detector	Newport
Pulse width	Autocorrelator	Femtochrome Research, Inc.
Beam profile	CCD camera beam profiler	Thorlabs

The dispersion of Tm-doped fiber and single-mode fiber at 1900 nm were ~ -71 and -67 ps²/km, respectively. With 1.5 m Tm-doped fiber and 78.5 m single-mode fiber

including the fiber pigtail of the components, the net cavity dispersion was $\sim -5.37 \text{ ps}^2$.

Table 4.3 is the list of parameters and equipments used in the measurement.

Chapter 5

Tunable Single-Wavelength Mode Locking

The first result we get is the tunable single-wavelength mode locking. This chapter shows the experimental results, and discusses the mechanism of tunable operation.

5.1 The Experimental Results

The mode-locked laser emission is enabled by nonlinear polarization evolution (NPE) effects and it appears when the pump power reaches 330 mW with 40:60 coupler. The output pulses are solitons with typical Kelly sidebands (the peak sidebands) [29]. The dips on the spectra are due to the water absorption [91]. By adjusting the polarization controllers (PCs) above the threshold power, such as rotating or squeezing, the emission wavelength can be tuned. The tunable range is 107 nm, from 1839 to 1946 nm.

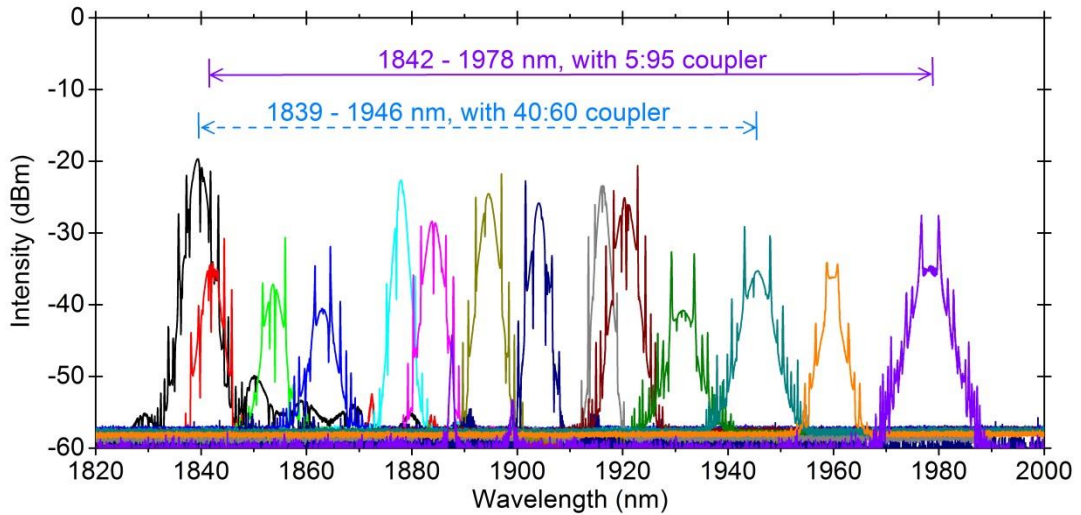


Figure 5. 1. Tunable single-wavelength lasing emissions from 1839 to 1978 nm, from Tm-doped mode-locked all-fiber lasers enabled by nonlinear polarization evolution (NPE).

The overall cavity loss should be reduced to lower the laser threshold where the gain is smaller to let laser emit at more wavelength. Here we replaced the 40:60 coupler by a 5:95 coupler to reduce the cavity loss and, thus a broadband net gain

(saturated gain minus cavity loss) will be formed to enable the broad laser emission. With 5:95 coupler, the mode-locked threshold decreases to 300 mW, meanwhile the tunable range increases to 136 nm, from 1842 to 1978 nm, as shown in figure 5.1.

The mode locking usually works in the multi-pulse regime above the threshold, where one pulse contains many subpulses, due to the nonlinear effects in a long cavity and the loss perturbation of the optical components. The corresponding spectrum in the multi-pulse regime has more peaks in the sidebands, compared with the one in the single-pulse regime. It is noted that the tunable operation can only be achieved above the threshold power. When mode locking appears, decreasing the pump power below the threshold will not make the pulse disappeared. However when tuning the PCs at this power level, it will no longer get mode locking at any wavelength.

After the initiation of mode locking and then decreasing the pump power slightly below the threshold, the mode locking can work in the single-pulse regime. Further decreasing the pump power to 230 mW and 180 mW, for the 40:60 coupler and the 5:95 coupler cases, respectively, the mode locking disappears. This is known as power hysteresis phenomenon.

Most of the spectra in figure 5.1 were measured at single-pulse regime with different pump power below the threshold. Therefore the height of each spectrum is different.

In single-pulse regime, the repetition rate is 2.6 MHz as shown in figure 5.2 (a), corresponding to 80 m cavity length, which includes 70 m single-mode fiber, 1.5 m thulium-doped (Tm-doped) fiber and fiber pigtailed of other optical components. The RF spectrum in figure 5.2 (b) shows that the pulse has a good signal-to-noise ratio of more than 40 dB. The 3-dB bandwidth of the RF spectrum is 1.35 kHz. The pulse width is measured with 40:60 coupler as shown in figure 5.2 (c), and it fails to be measured with 5:95 coupler as the output power is too low to measure the pulse width. The output power changes with the wavelength. The output laser beam shows a symmetric Gaussian profile, as shown in figure 5.2 (d), and the beam quality is guaranteed by the adopted single-mode fiber.

When the pump power is 350 mW, with the 5:95 coupler, the laser near the center of the tunable range is with output power of ~ 1 mW, and the edge ones are with the output power of ~ 0.3 mW. With the 40:60 coupler, the laser near the center of the tunable range is with output power of ~ 3 mW, and the edge ones are with the output

power of ~ 1 mW. The output power at different emission wavelength is shown in figure 5.3.

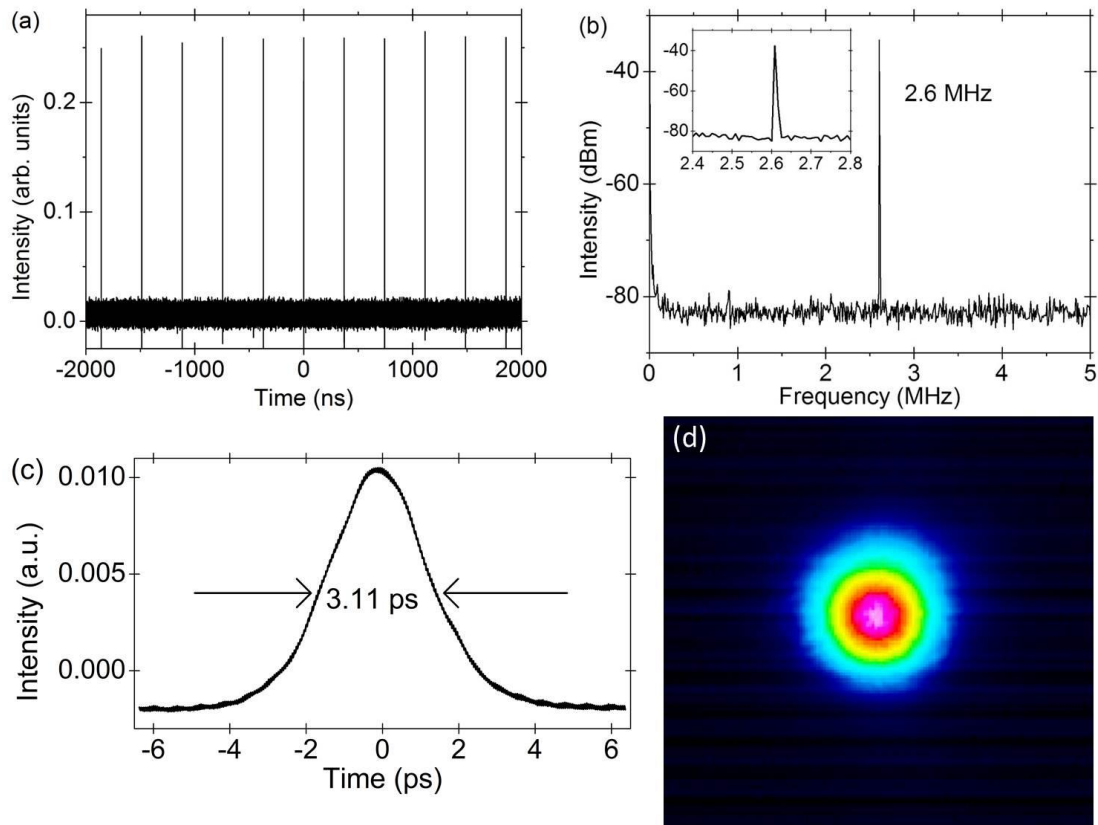


Figure 5. 2. (a) The pulse train , (b) RF spectrum, (c) pulse width, and (d) beam profile of Tm-doped mode-lock all-fiber lasers enabled by NPE.

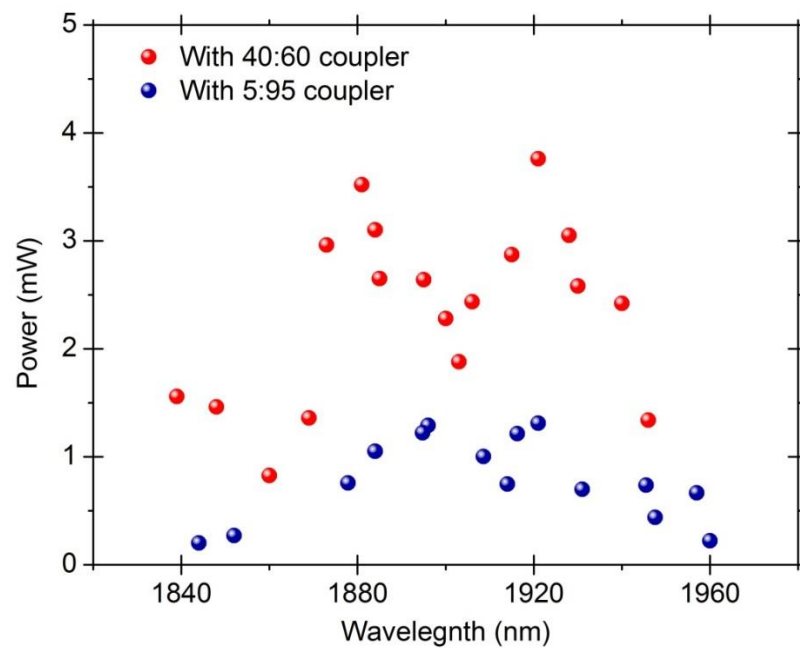


Figure 5. 3. The output power at different emission wavelength of Tm-doped mode-locked all-fiber lasers enabled by NPE.

5.2 The Mechanisms

We refer to the NPE-induced transmission equation (4.4.8) and the simulated NPE-induced transmission curve in figure (4.6). The mechanism for tunable operation is two-folded.

Firstly, the cavity net gain is modulated periodically. The modulation is induced by NPE effect obtaining multiple peaks. Laser emits at the peak position of the net gain. With different cavity polarization states, laser tends to emit at one of the peak positions. Thus when tuning the PCs the cavity polarization states are changed, as well as at which peaks that laser tends to emit, so that the output wavelength of the laser is tuned. In this case, the tunable resolution equals to the separation of peaks in the NPE-induced transmission curve. The calculation process of the separation of peaks is as follows:

The separation of peaks is related to the items containing the wavelength λ in equation (4.4.8). The item is $\cos(\Delta\varphi_L + \Delta\varphi_{NL})$ and the separation of adjacent peaks $\Delta\lambda$ satisfies:

$$\Delta(\Delta\varphi_L + \Delta\varphi_{NL}) = 2\pi. \quad (5.1.1)$$

With equation (4.4.9), (4.4.10) and (4.4.11), we get

$$\left[2\pi \left(L_{SMF} B_{m,SMF} + L_{PMF} B_{m,PMF} \right) + \frac{2\pi n_2}{A_{eff}} P_0 \frac{L_{SMF} + L_{PMF}}{3} \cos(2\theta_1) \right] \left(\frac{1}{\lambda_1} - \frac{1}{\lambda_2} \right) = 2\pi. \quad (5.1.2)$$

We use the frequency Δf instead of $\Delta\lambda$, equation (5.1.2) becomes:

$$\Delta f = \frac{c}{\left\{ \left(L_{SMF} B_{m,SMF} + L_{PMF} B_{m,PMF} \right) + \left[\left(n_2 / A_{eff} \right) P_0 \left(L_{SMF} + L_{PMF} \right) / 3 \right] \cos(2\theta_1) \right\}}. \quad (5.1.3)$$

We choose the parameters in table 5.1 to calculate the separation of peaks in the NPE-induced transmission equation. The modal birefringence of single-mode fiber is an estimated and average value over the whole fiber length of 70 m, because parts of the fiber are pressed or twisted by PCs where the modal birefringence changes while others are not.

The separation of peaks changes with wavelength. It gets smaller at short wavelength regime and gets larger at long wavelength regime. Near 1900 nm, the separation is 8.1 to 11.7 nm when the modal birefringence of single-mode fiber is from 10^{-6} to 3×10^{-6} . Thus the tunable resolution in this case is around 8.1 to 11.7 nm.

Table 5. 1. The list of parameters used in calculating the separation of peaks in the NPE-induced transmission equation

Parameters	Description	Value
θ_1	The angle between polarization direction of incident light and x axis of the fiber	$\pi/6$
θ_2	The angle between polarization direction of polarizer and x axis of the fiber	$\pi/3$
n_2	The nonlinear refractive index	$2.7 \times 10^{-20} \text{ m}^2 / \text{W}$
P_0	The instantaneous power	3 mW
A_{eff}	The effective mode area	$\pi \times (5 \mu\text{m})^2 = 78.54 \mu\text{m}^2$
L_{PMF}	The length of polarization-maintaining fiber	0.6 m
$B_{m,\text{PMF}}$	The modal birefringence of polarization-maintaining fiber	0.4×10^{-3}
L_{SMF}	The length of single-mode fiber	70 m
$B_{m,\text{SMF}}$	The estimated and average value of modal birefringence of single-mode fiber	$10^{-6} \sim 3 \times 10^{-6}$

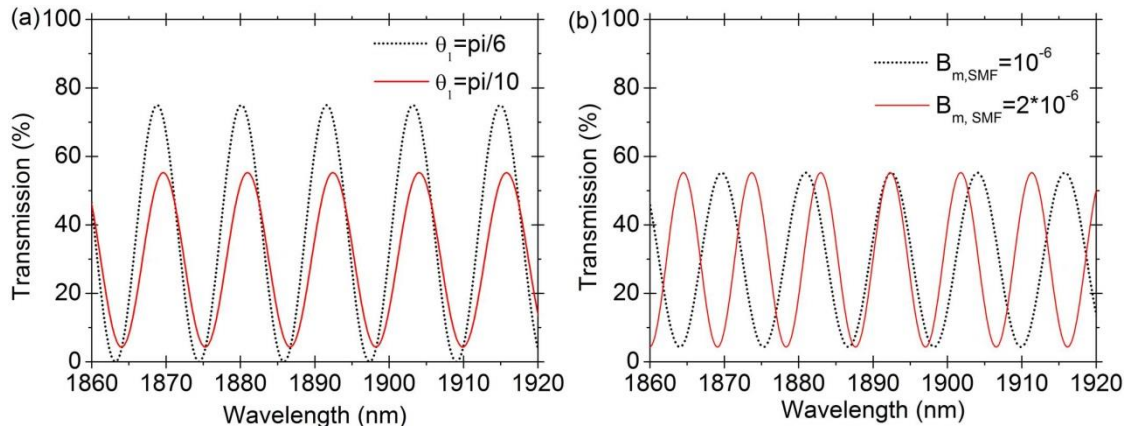


Figure 5. 4. The calculated NPE-induced transmission on different values of (a) θ_1 and (b) B_m .

Secondly, only one peak of the modulated net gain is analyzed. It can be shifted by changing the polarization angle θ_1 of the incident light and modal birefringence B_m , depending on the NPE-induced transmission equation (4.4.8). B_m is changed when fiber inside the PCs becomes deformed by rotating or squeezing PCs. Thus the peak will ideally appear continuously at any position within one period. Figure (5.4) shows

how θ_1 and B_m shift the NPE-induced transmission. The tunable resolution in this case can be as small as possible. However because of the manual tuning operation we cannot achieve ideally continuous tuning. The tunable resolution we can achieve is 0.5 nm.

Chapter 6

Multi-Wavelength Mode Locking

The second result we get is multi-wavelength mode locking. We have got dual-, tri-, four- wavelength mode locking. All of them are with wavelength-tunable operation. The dual- and tri- wavelength mode locking can be switchable, and it can realize the full binary control which is very useful in applications of optical signal processing and optical telecommunication. We also observe quasi-five-wavelength Q-switched mode locking, which is presented in this chapter together with the above phenomena. The mechanism of multi-wavelength emission is studied in this chapter too.

6.1 Tunable Multi-Wavelength Mode Locking

6.1.1 The Experimental Results

Besides the tunable single-wavelength mode locking, tunable dual-wavelength mode locking can be also achieved by tuning the polarization controllers (PCs) above the mode-locked threshold. The results are shown in figure 6.1. With 40:60 coupler, the tunable range is 34 nm, from 1852 to 1886 nm [92]. With 5:95 coupler the tunable range increase to 52 nm, from 1864 to 1916 nm [93]. The separation of two spectra is 10 to 11 nm, which agrees with the calculated separation of peaks based on the nonlinear polarization evolution (NPE) induced transmission equation. From the separation of two spectra we can also estimate the corresponding average value of modal birefringence of single mode fiber, using the method in part 5.2.

The tunable tri- and four-wavelength mode locking is only achievable with 5:95 coupler above the mode-locked threshold. As shown in figure 6.2, the tunable range is 49 nm, from 1863 to 1912 nm for tri-wavelength mode-locking, and 55 nm, from 1860 to 1915 nm for four-wavelength mode-locking, respectively.

The repetition rate of multi-wavelength mode locking is 2.6 MHz, which corresponds to the cavity length.

The multi-wavelength operation can be achieved through two steps. The first is coarse adjustment of the polarization controllers (PCs) to get the stable single-wavelength mode locking. The second step is fine adjustment of the PCs around this position to get the multi-wavelength mode locking.

The multi-wavelength mode locking usually works in the multi-pulse regime above the threshold, and when decreasing the pump power it sometimes switches to single-pulse regime, which are the same with single-wavelength mode locking. However in most cases when decreasing the pump power, the number of emission wavelength will be decreased or the mode-locked states will disappear. This is because when decreasing the pump power a little, not all the lasing peaks in the spectral domain decrease with the same power level as expected. Some peaks decrease more while some do not. If no adjustment on the power level of these peaks through PCs, the peaks decreasing more are less stable and they will be vanished soon, which results in decrease of the numbers of the emission wavelength or no mode locking any more. In this case, the PCs should be fine-tuned to make all the peaks with the same height by monitoring the optical spectral analyzer. Then we can repeat decreasing the pump power and tuning PCs, until single-pulse regime appears. When tuning PCs the separation of peaks will be changed or the peaks will be shifted a little, which is explained in part 5.2, due to the change of the modal birefringence of single-mode fiber.

6.1.2 The Mechanisms

The multi-wavelength emission is enabled when the net gain (saturated gain minus cavity loss) has multiple peaks, and the laser tends to be emitted at these multiple peaks. This multi-peak net gain is formed by the periodic modulation of cavity transmission induced by NPE effect as discussed in part 4.4. When tuning the PCs, the cavity transmission changes. At a certain state the cavity radiation at multiple wavelengths obtains the same net gain, thus optical power was equally distributed among two or three or four peaks to reduce the mutual mode competition, to enable the multi-wavelength emission. The spectra in each sub-figure in figure 5.5 and 5.6 have the same height, showing that the optical power distributes among the multiple emission wavelengths equally.

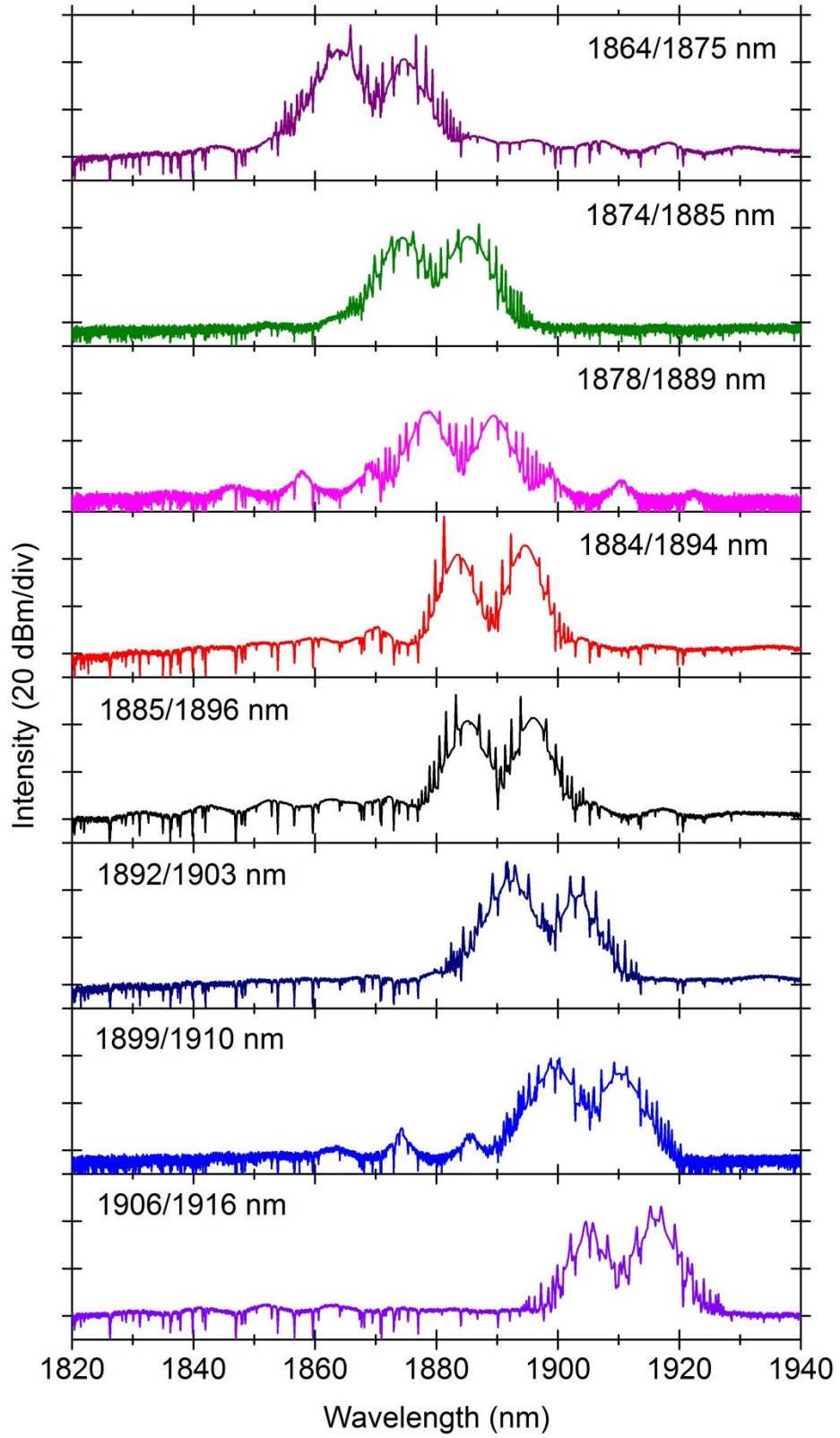


Figure 6. 1. Tunable dual-wavelength lasing emissions from 1864 to 1916 nm, from Tm-doped mode-locked all-fiber lasers enabled by NPE.

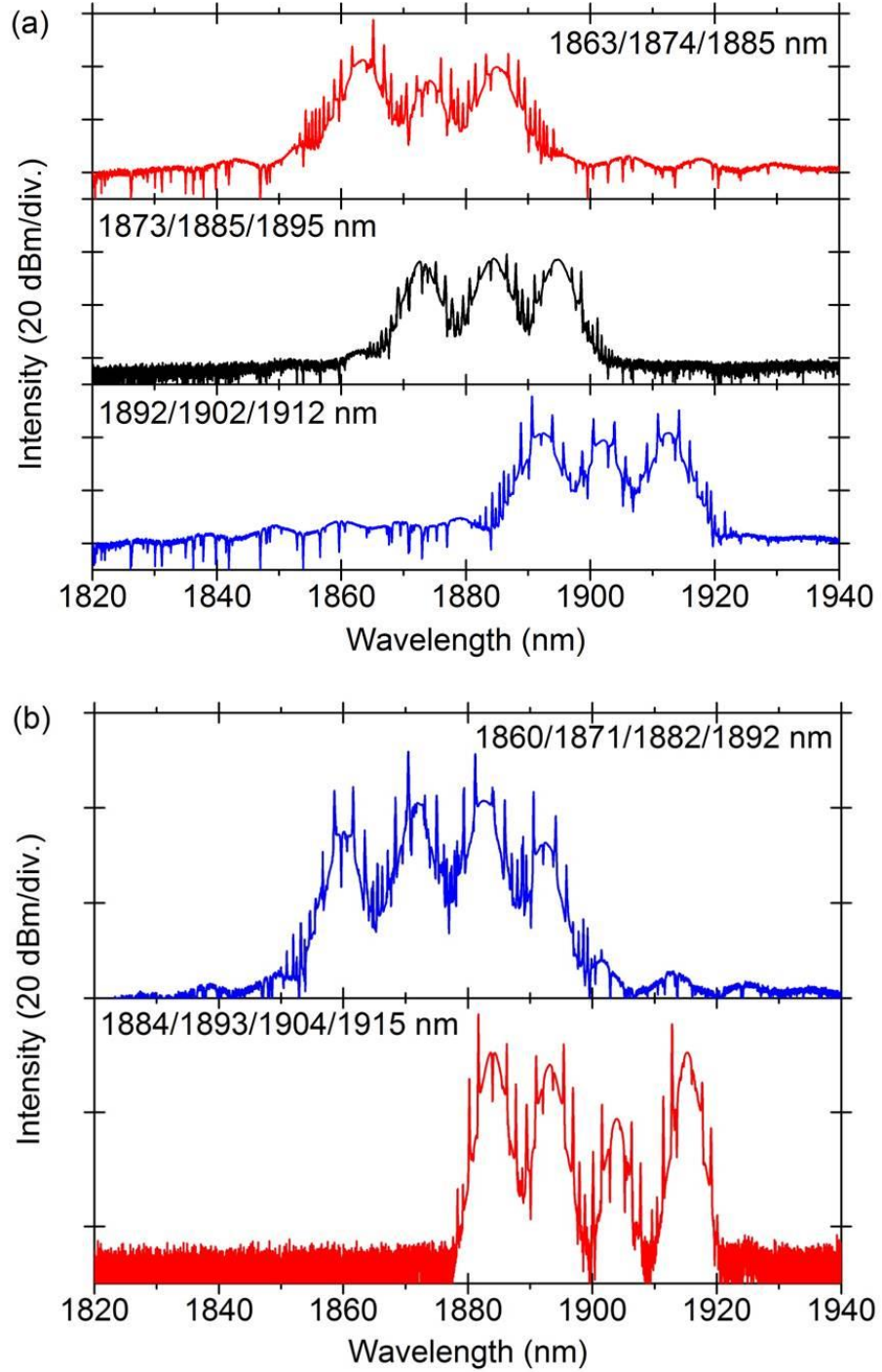


Figure 6. 2. (a) Tunable tri-wavelength lasing emissions from 1863 to 1912 nm and (b) tunable four-wavelength lasing emission from 1860 to 1915 nm, from Tm-doped mode-locked all-fiber lasers enabled by NPE.

The tunable operation is similar with the first case of tunable single-wavelength operation in part 5.2. When tuning the PCs, the cavity polarization states changes. Thus with each time of laser emission the wavelength is different. However the possibility of continuously tuning with small tunable resolution, such as the second

case of tunable single-wavelength operation, is quite low. When tuning the PCs precisely, the power distribution in the multiple peaks will change. The multi-wavelength emission condition will be disturbed and the laser will downgrade to operate at fewer numbers of emission wavelengths, before the multiple peaks can shift continuously together.

6.2 Switchable Multi-wavelength Mode Locking

Interestingly, the dual-wavelength mode locking can be switchable. Either one of the two peaks in the spectral domain can appear or both can appear when the polarization state is changed by PCs. This functions as the switchable operation. If a peak in the spectral domain is treated as a digital number “1” and no peaks means “0”, it is like a two-bit binary control with the state of “00”, “01”, “10”, “11”. Figure 6.3 shows two examples of dual-wavelength mode locking with switchable operation.

Furthermore, tri-wavelength mode locking can be switchable. The peaks in the spectral domain can appear either one-by-one or pair-by-pair when tuning PCs. This is able to cover the full three-bit binary range, as shown in figure 6.4.

In our previous setup, the coupler is used as input and output port simultaneously [94], which causes much loss. In the pair-by-pair switchable operation, the pair of 1863/1885 nm does not appear as shown in state “101” in figure 6.5. The first peak at the wavelength of 1861 nm is a CW laser emission instead of the expected soliton mode at 1863 nm. This indicates the insufficient gain at around 1863 nm to make it reach the mode-locked threshold. By adding wavelength-division multiplexer as the input port and putting the 40:60 coupler as the output port, the cavity loss is reduced so that the radiation at 1863 nm can obtain sufficient gain and reach the mode-locked threshold.

The switchable operation is of much interest as it could act as an optical binary system, which has potential applications in optical signal processing, optical switching devices and optical communication.

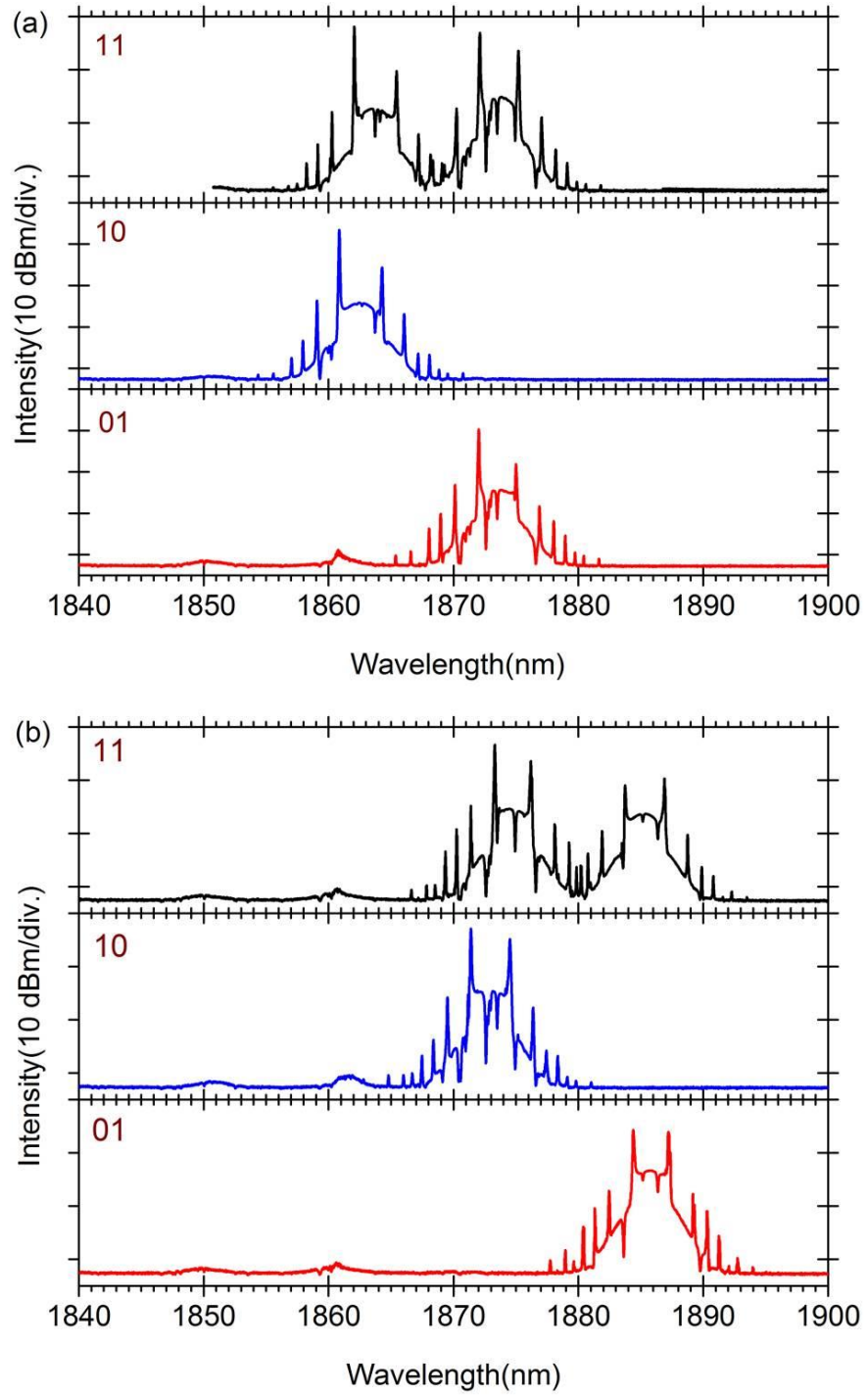


Figure 6. 3 Switchable dual-wavelength operation with wavelength at (a) 1864/1874 nm and (b) 1875/1886 nm, from Tm-doped mode-locked all-fiber lasers enabled by NPE.

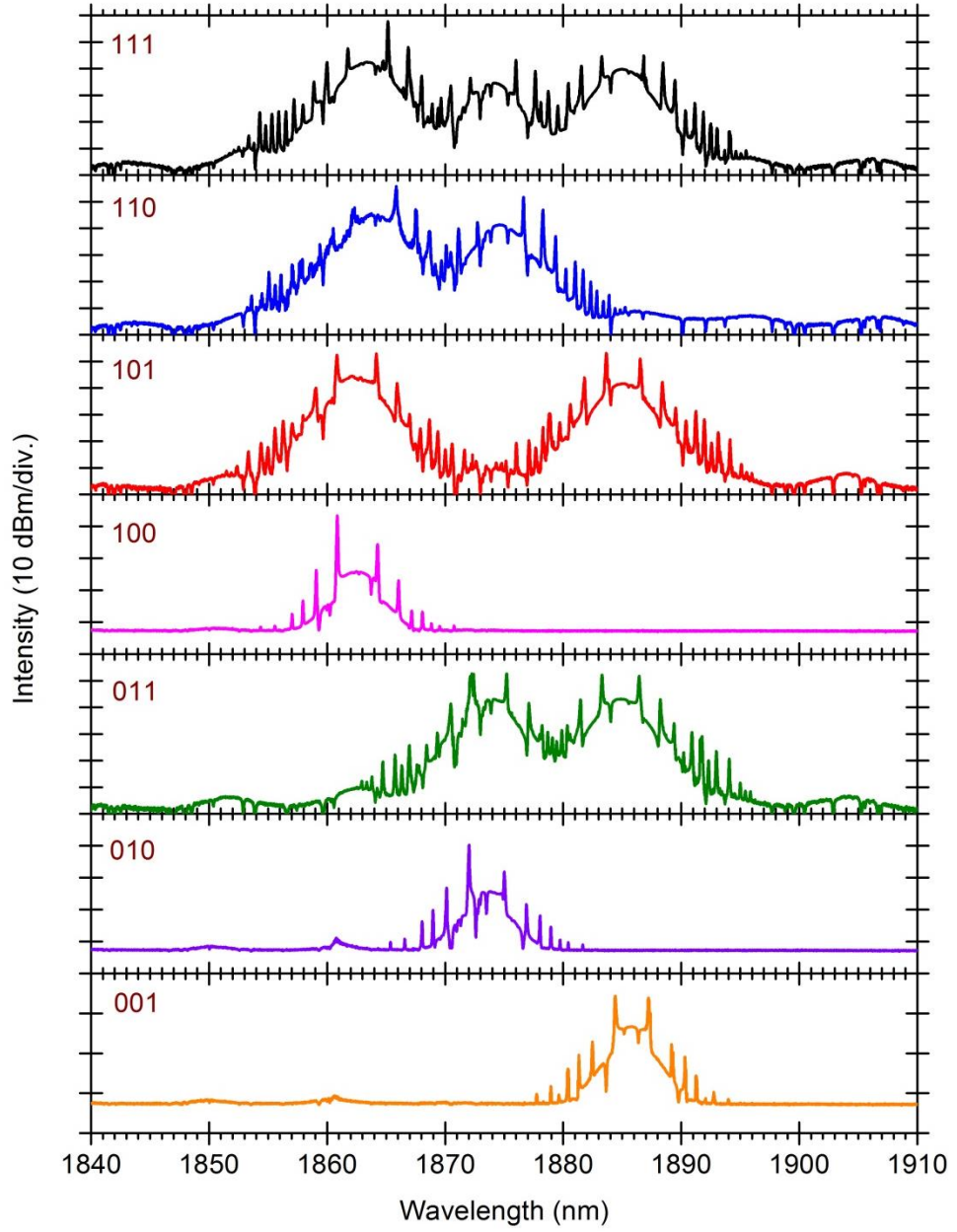


Figure 6. 4. Switchable tri-wavelength operation with wavelength at 1863/1874/1885 nm, from Tm-doped mode-locked all-fiber lasers enabled by NPE.

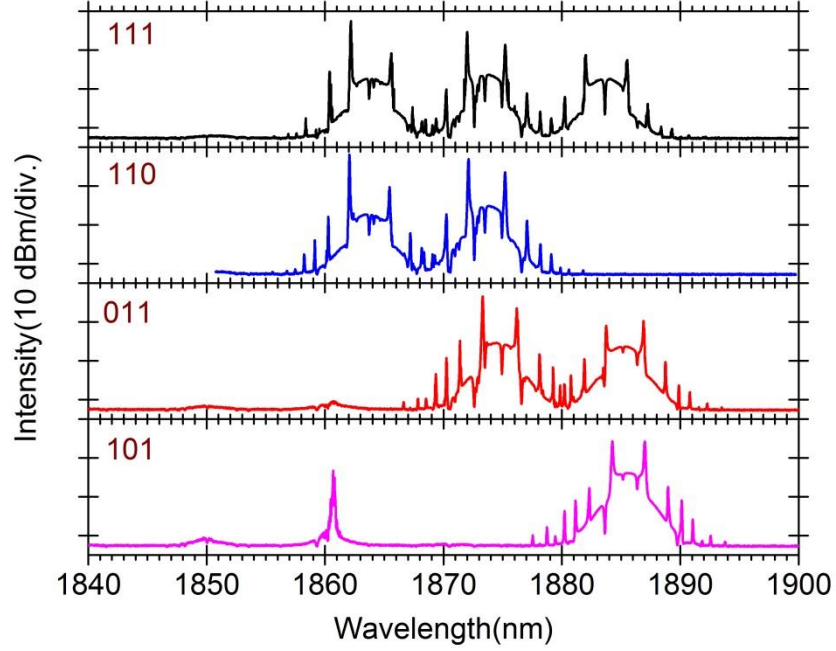


Figure 6. 5. Switchable tri-wavelength operation with wavelength at 1863/1874/1885 nm, from Tm-doped mode-locked all-fiber lasers enabled by NPE. The coupler is used as input and output port simultaneously which causes much loss.

6.3 The Quasi-Five-Wavelength Q-Switched Mode Locking

By further tuning the PCs at the maximum pump power of 370 mW, the quasi-five-wavelength laser emission can be observed, as shown in figure 6.6. The pulse train is a Q-switched envelop in a large time scale as shown in figure 6.7 (a) with repetition rate of 6.33 kHz. The width of each envelope is around 20 μ s as shown in figure 6.7 (b). Inside each envelop there are many pulses working at mode-locked state with repetition rate of 2.6 MHz corresponding to the cavity length as shown in figure 6.7 (c). Each pulse works at single-pulse regime as shown in figure 6.7 (d). The pulse train indicates that the laser is working at Q-switched mode-locked regime.

The Q-switched mode-locked regime consists of mode-locked pulses underneath a Q-switched envelope. The repetition rate of mode-locked pulses is determined by cavity length and the typical Q-switched modulations have frequencies in the kilohertz region. In order to switch the Q-switched mode-locked to the stable mode-locked state, the intracavity pulse energy E_p should satisfy the following equation for soliton mode-locked lasers [95].

$$E_{sat,L} g K^2 E_p^3 + E_p^2 > E_{sat,L} E_{sat,A} \Delta R, \quad (6.3.1)$$

where $E_{sat,L}$ is the saturation energy of the gain, g is the time-dependent round-trip power gain, $E_{sat,A}$ is the saturation energy of the absorber, ΔR is the maximum modulation depth of the absorber,

$$K = \frac{df}{dE_p}, \quad (6.3.2)$$

with $f = \Delta v(E_p)/\Delta v_g$, which is the ratio of pulse bandwidth and gain bandwidth.

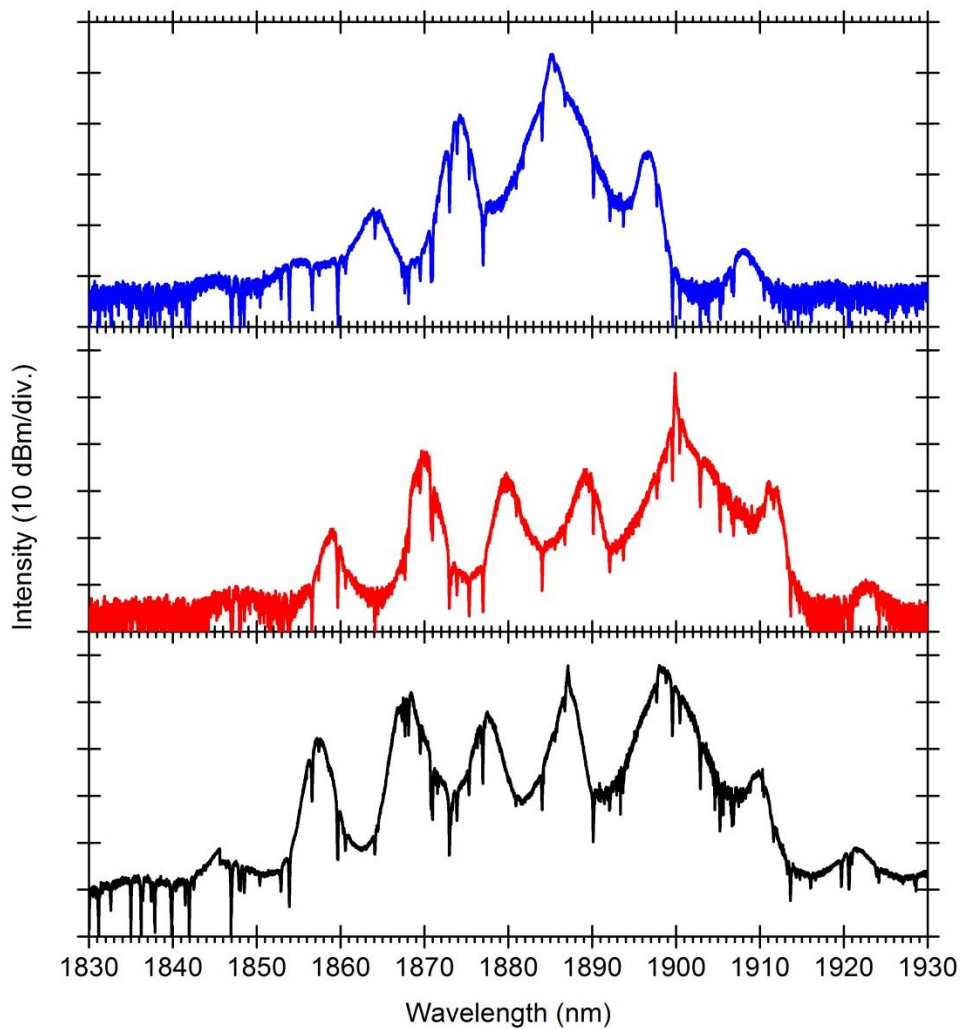


Figure 6. 6.The spectra of quasi-five-wavelength Q-switched mode locking from Tm-doped mode-locked all-fiber lasers enabled by NPE.

The formation of Q-switched mode-locked pulses is as follows: the energy of an ultrashort pulse rises slightly due to the relaxation oscillations initially. The pulse spectrum is broadened then by self-phase modulation and/or self-amplitude modulation. The broadened spectrum reduces the effective gain because of the finite gain bandwidth, which provides the negative feedback and decreases the intracavity

pulse energy. If the intracavity pulse energy is less than the energy required for the stable mode locking, the laser tends to work at Q-switched mode-locked regime.

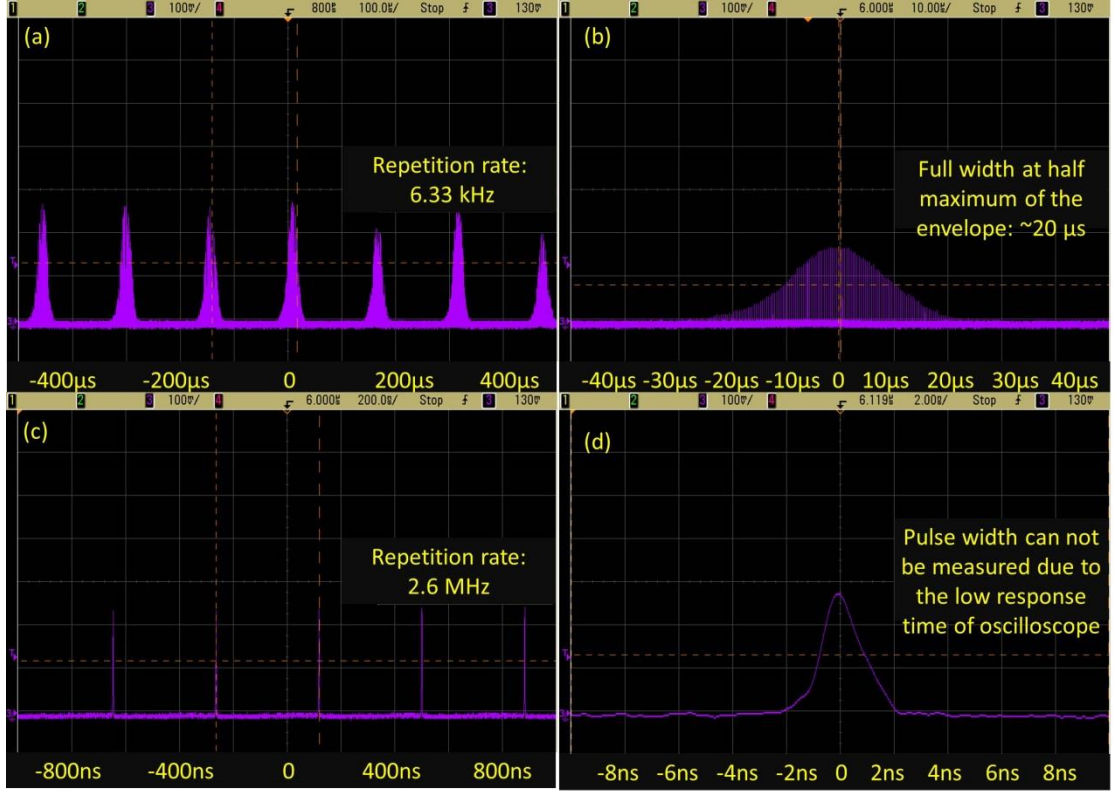


Figure 6. 7. The pulse train under different time scales of quasi-five-wavelength Q-switched mode locking, from Tm-doped mode-locked all-fiber lasers enabled by NPE.

In order to get stable mode locking with multi-wavelength emission, the intracavity pulse energy should be increased by broadening the gain bandwidth to avoid the negative feedback, by enlarging the pump power, or by reducing the cavity loss. What is more, in this case the net gain profile also should be flat, to make sure the power distributed on multiple potential lasing peaks equally. From figure 6.6 we can see the power fails to distribute equally on multiple peaks. If further increased the pump power, the lasing peak with more net gain tends to emit meanwhile other potential lasing peaks are suppressed. Thus it is hard to get the five-wavelength mode locking with such an unflat gain.

Chapter 7

The Extended Results and Discussions

This chapter discusses the extended results on the peak and dip sidebands on soliton spectrum and the noise-like pulses, the laser stability and repeatability.

7.1 Soliton Dynamics

7.1.1 The Peak Sidebands

There are two types of peak sidebands of soliton, classified by different formation mechanisms. One kind of peak sidebands is Kelly sideband. It is due to the constructive interference between dispersive waves and solitons. The position of Kelly sidebands in the spectral domain is related to the cavity dispersion, cavity length, and pulse width. It does not have a threshold characteristic. The other kind of peak sidebands is modulation instability based sidebands. It is generated due to modulation instability inside the laser cavity. It appears with a threshold effect.

We begin with the Kelly sideband. We know that soliton is a balance effect of fiber dispersion and the nonlinear effect. When soliton propagates along a lossy fiber, the soliton pulse energy reduces. The decrease of soliton pulse energy results in the decrease of nonlinearity. Thus the balance of fiber dispersion and nonlinear effect is disrupted and soliton propagation cannot be kept. In order to maintain the soliton propagation, the soliton needs to be amplified. With our ring fiber laser cavity, the soliton circulates inside the cavity, and it is amplified and experiences loss periodically. The parameters of soliton change during amplification and after amplification it is required to readjust the parameters to the input value by shedding away a part of its energy as dispersive waves. The shed energy is a continuum radiation, and it forms discrete sidebands in the soliton spectrum. Average soliton model is used to analysis the sideband generation in the present of periodical loss and gain [96,97].

The generated dispersive waves each period will interfere constructively with the solitons when the phase-matching condition is achieved at particular frequencies.

Otherwise they will interfere destructively and disappear. With phase-matching condition, the periodic perturbation which is related to the amplifier spacing or laser length Z_p with propagation constant k_p makes up the difference between the propagation constant of soliton k_s and the propagation constant of dispersive waves k_d . The phase-matching condition is expressed by [29,36]:

$$Z_p (k_s - k_d) = 2\pi m, \quad (7.1.1)$$

$$k_s = \frac{|\beta_2|}{2T_0^2}, \quad (7.1.2)$$

$$k_d = -\frac{|\beta_2|}{2} \Delta\omega^2, \quad (7.1.3)$$

where m is an integer, β_2 is the group-velocity dispersion, T_0 is the pulse width. Here the pulse width $T_0 = 0.567 \times T_{FWHM}$, T_{FWHM} is the full width at half maximum of the pulse. $\Delta\omega$ is the angular frequency offset between the peak of the soliton and the adjacent dispersive waves. $\Delta\omega$ is expressed as:

$$\Delta\omega = \pm \frac{1}{T_0} \sqrt{m \frac{8Z_0}{Z_p} - 1}, \quad (7.1.4)$$

where Z_0 is the soliton period with

$$Z_0 = \frac{\pi}{2} L_D = \frac{\pi}{2} \frac{T_0^2}{\beta_2}. \quad (7.1.5)$$

In our setup, $T_{FWHM} = 3.11ps$, $T_0 = 0.567 \times 3.11ps = 1.76ps$, $Z_p = 80m$, $\beta_2 = 67.13ps^2/km$. The calculated results are: $L_D = 46.15m$, $Z_0 = 72.49m$. With the center wavelength of $1884.05nm$ for the soliton we obtained in the experiment, the calculated $\Delta\omega$ and the corresponding wavelength of the peak sidebands with $m = 1, 2, 3, 4$ are shown in table 7.1.

The soliton spectrum with the center wavelength of $1884.05nm$ of our laser setup is shown in figure 7.1. The calculated wavelength of peak sidebands in table 7.1 matches well with the experimental result in figure 7.1.

Table 7. 1. The calculated $\Delta\omega$ and the corresponding wavelength of the peak sidebands with $m = 1, 2, 3, 4$. The center wavelength is 1884.05nm .

m	$\Delta\omega(1/ps)$	$\Delta f = \frac{\Delta\omega}{2\pi}(1/ps)$	The corresponding wavelength of the peak sidebands (nm)
1	1.42	0.23	1881.38 & 1886.73
2	2.09	0.33	1880.12 & 1888.00
3	2.59	0.41	1879.19 & 1888.94
4	3.01	0.48	1878.40 & 1889.74

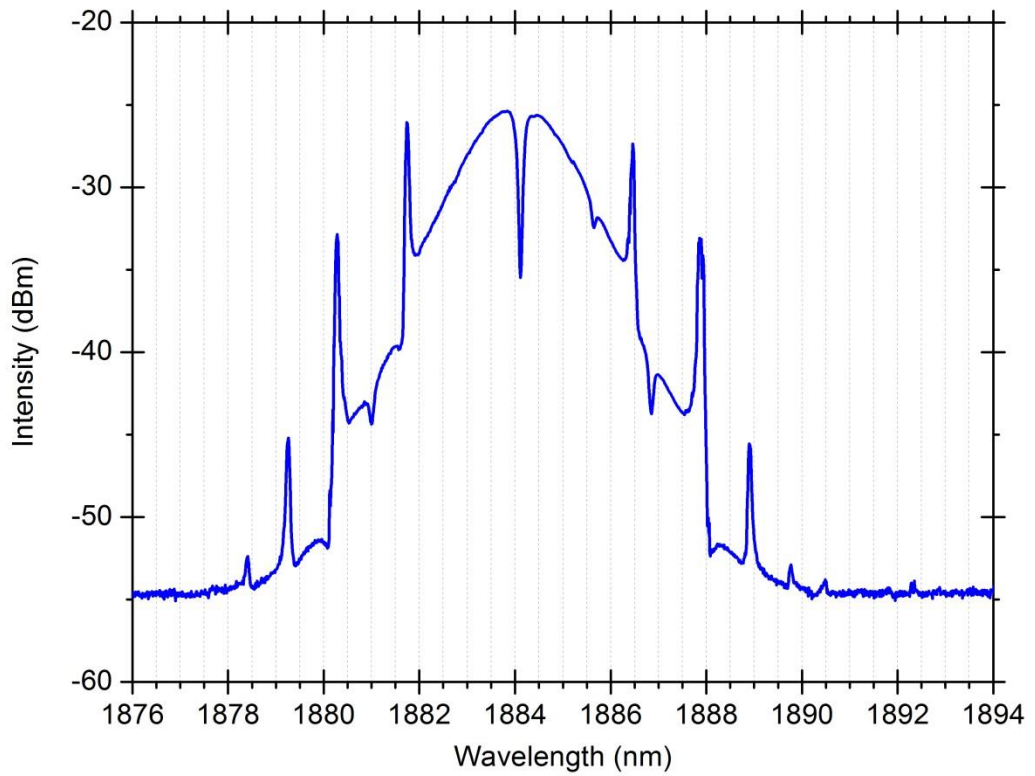


Figure 7. 1. The soliton spectrum with center wavelength at 1884 nm, from Tm-doped mode-locked all-fiber lasers enabled by NPE.

For the modulation instability based sidebands, it is generated through a parametric coupling process between dispersive waves and soliton, when the energy of a soliton reaches a certain threshold value [98]. It is a result of soliton modulation instability.

As shown in figure 7.2, when the pump power increases, some new sets of peak sidebands appear. This is the modulation instability based sidebands. Mostly these sidebands appear symmetrically on the side of the spectrum. We observed this phenomenon with solitons of different center wavelengths. For the solitons with

different center wavelengths, the threshold pump power of the modulation instability based sidebands is different too. In addition, the process of generating modulation instability based sidebands is reversible. When decreasing the pump power, the modulation instability based sidebands is removed from the spectrum and when increasing the pump power the sidebands appears again.

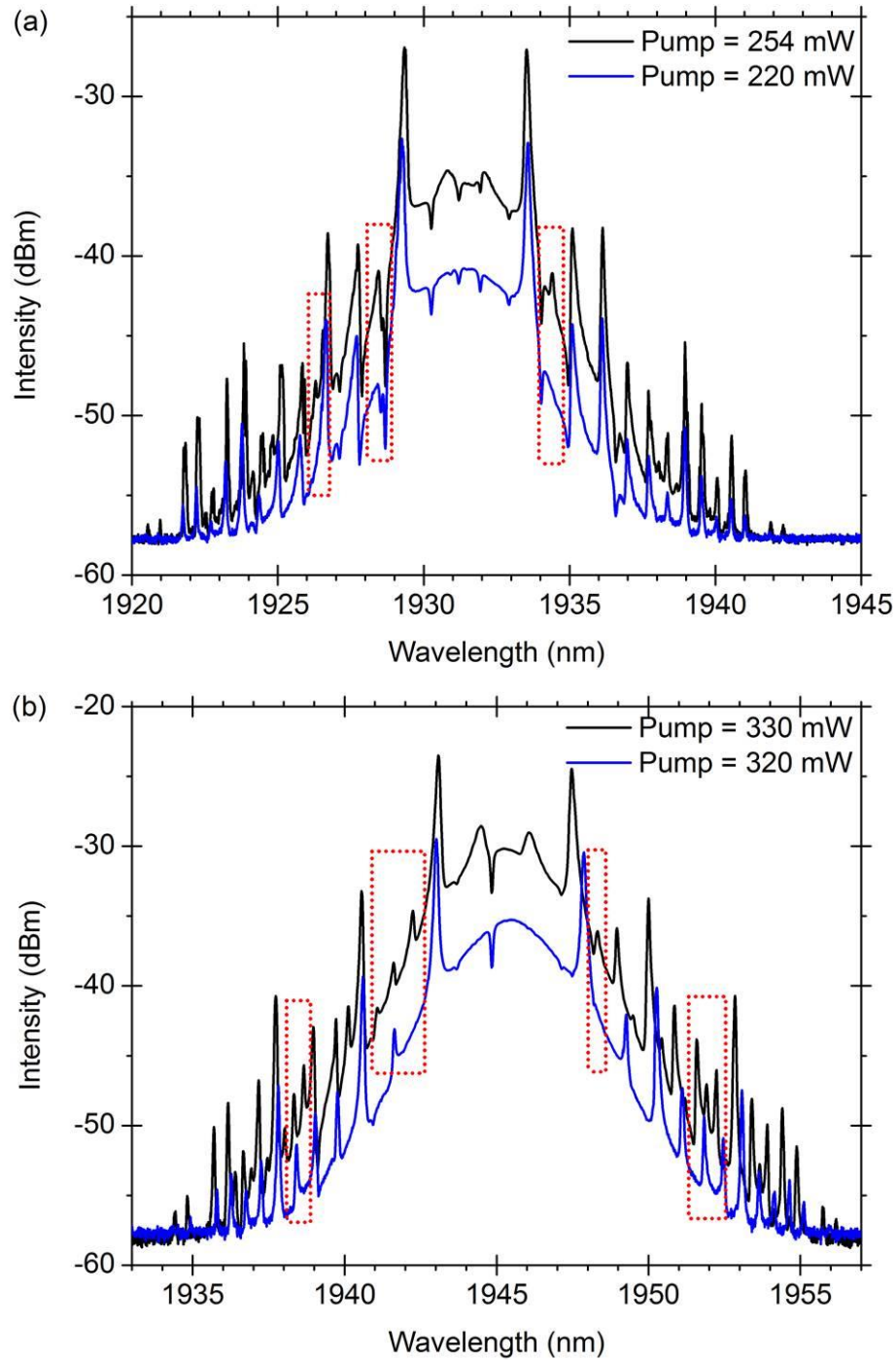


Figure 7. 2. The soliton spectra of Tm-doped mode-locked all-fiber lasers enabled by NPE, measured with different pump strengths, and with center wavelength at (a) 1932 nm and (b) 1945 nm.

7.1.2 The Dip Sidebands

The dips in the sidebands are due to the water absorption in atmospheric air, which spectral regime is located from 1.8 to 1.95 μm . Both amplified stimulated emission (ASE) and soliton show the dips at their spectra, and each dip of ASE and soliton is at the same positions, as shown in figure 7.3. For a clear illustration, the strength of ASE is reduced by 10 dBm in order to make it un-overlapped with the soliton spectra. The dip sidebands of soliton will not change the position when tuning the polarization controllers or changing the pump power. The more spectral dips due to water absorption can be referred to the high-resolution transmission molecular absorption (HITRAN) database [99].

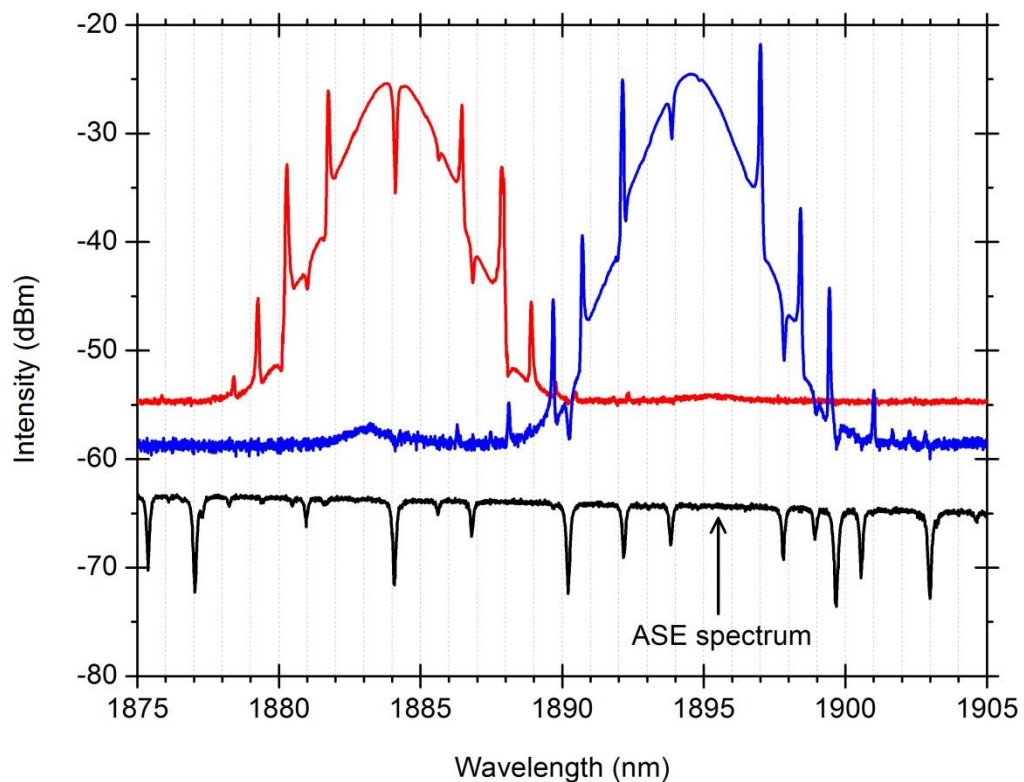


Figure 7. 3. The dips on the spectra of ASE and soliton which are due to the water absorption. Each dip of ASE and soliton is at the same position.

7.2 The Observation of Noise-Like Pulses

With the highest pump power at 370 mW and tuning the polarization controllers (PCs), we were able to get the noise-like pulses. The noise-like pulses have some characteristics. In the spectral domain, the noise-like pulses have a broad and smooth spectrum, compared with the peaks in the sidebands of a soliton spectrum [100]. In the

time domain, it works at multi-pulse regime. There are hundreds or thousands subpulses in one pulse envelope and the pulse width and peak power of subpulses are varying randomly [101–103].

Figure 7.4 shows the spectra of noise-like pulses with different polarization states. When tuning the PCs, the bandwidth and center wavelength of noise-like pulse is changed. Here we can get two spectra with bandwidth of around 60 nm and 40 nm, respectively.

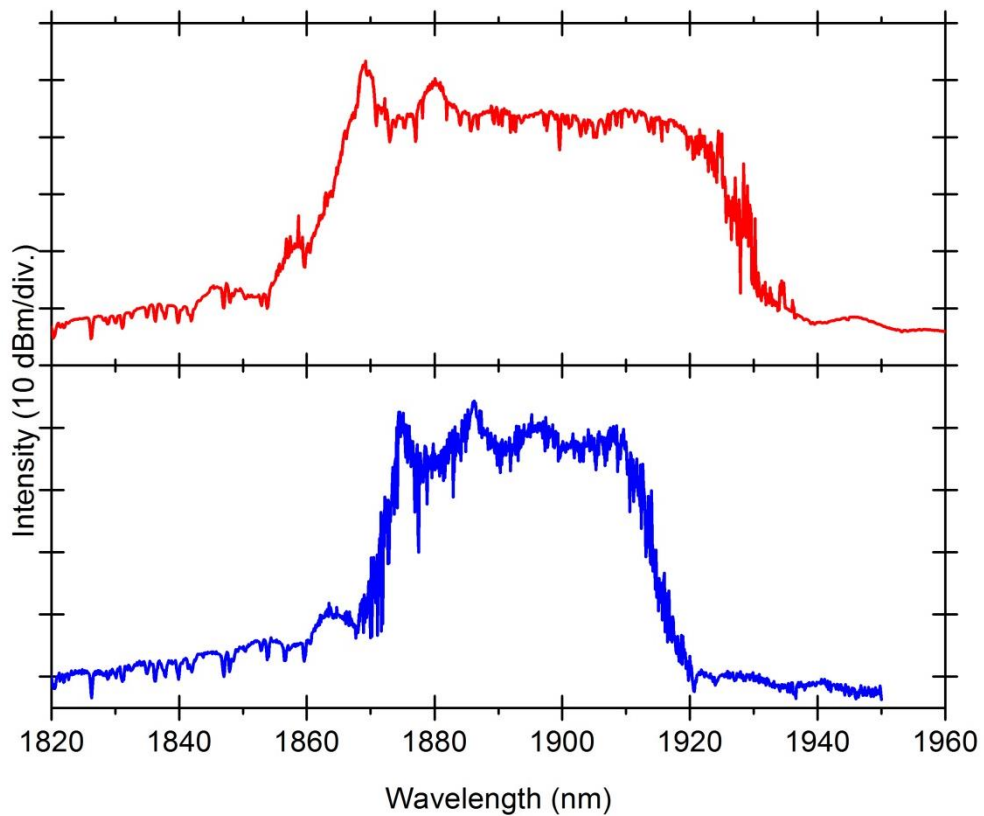


Figure 7. 4. The spectra of noise-like pulses with different polarization states, from Tm-doped mode-locked all-fiber lasers enabled by NPE.

The repetition rate of noise-like pulses is 2.6 MHz, the same with that of single-pulse, which corresponds to the cavity length. We can see from the pulse train of noise-like pulses in figure 7.5 that one pulse envelope contains many subpulses, and the subpulses are with different pulse width and peak powers. The number of subpulses inside one pulse envelope also varies. In this laser setup, the pulse envelope is around 40 ns. However we cannot get the pulse width of subpulses due to the limitation of sensitivity on our oscilloscope.

The noise-like pulse is formed in a long cavity and with strong pumping [104]. The possible mechanisms are soliton collapse effect [105], the nonlinear effects such as self-phase modulation, cross-phase modulation, and Raman [106], and the fiber birefringence combined with nonlinear polarization evolution (NPE) induced cavity transmission modulation and the gain response of the fiber amplifier [107].

The noise-like pulses are with higher pulse energy and have potential applications in supercontinuum generation [108–112].

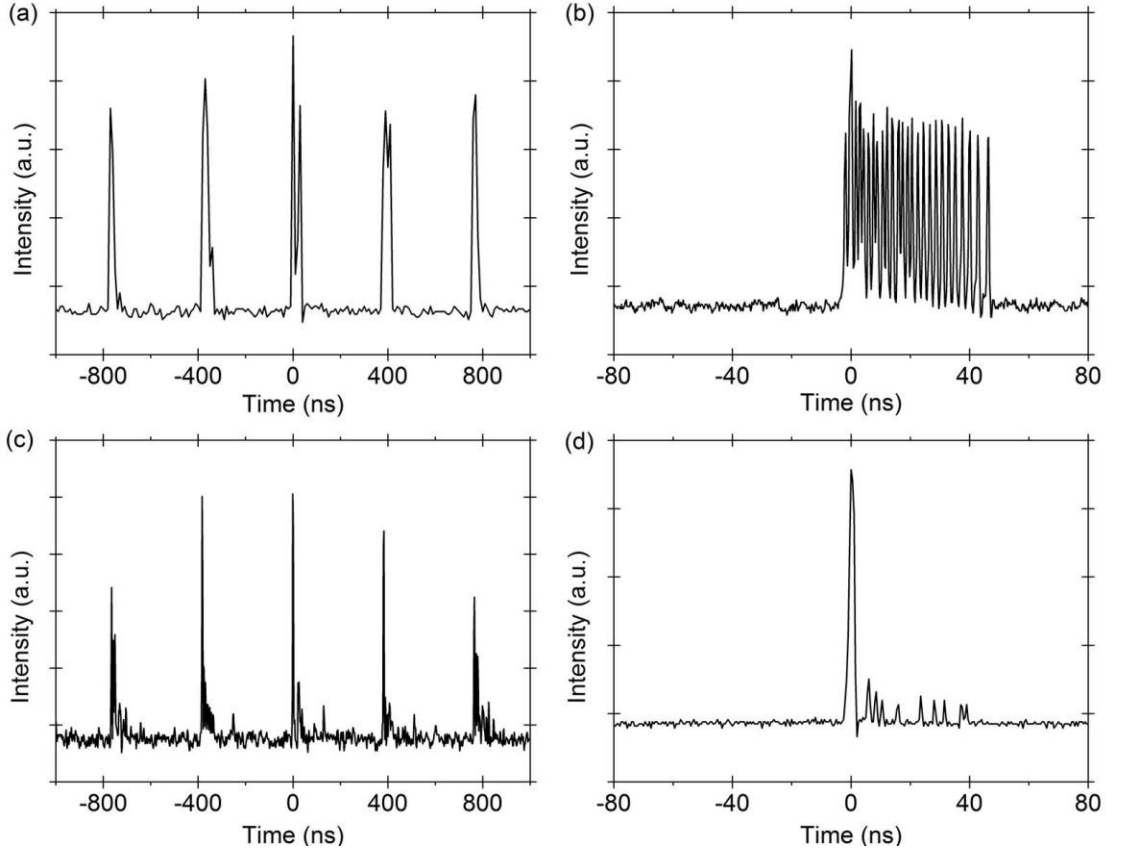


Figure 7. 5. The pulse train of noise-like pulses from Tm-doped mode-locked all-fiber lasers enabled by NPE. (a) and (b) are measured with one polarization state but with different time scales, (c) and (d) are measured with the other polarization state but with different time scales.

7.3 The Laser Stability and Repeatability

For the laser emits at short-wavelength and long-wavelength of tunable range, it usually contains some noise so that exhibits spectral content at other wavelengths. For the laser stability, the laser away from the edge of the tunable range (e.g. 1860 – 1960 nm) is the most stable. It produces the stable pulse trains, keeps single-pulse emission over several hours, is insensitive to environmental perturbation, and has a broad pump power range to stay in single-pulse regime. While the laser near the edge of the

tunable range is less stable, and the mode locking is less insensitive to the perturbations.

The tunable, switchable and multi-wavelength mode locking can be repeatable in the experiment, with the center wavelength maybe shifts a little from the values shown in this thesis, which is due to the NPE effect. If we want the laser emitting at shorter or longer wavelength range, the PCs are squeezed more, to change more on the refractive index of the fibers inside PCs. As different modes react differently to the change of refractive index, in this way the modes emitting at shorter or longer wavelength are selected to be emitted [113].

In this setup, the mode locking has many working states, including Q-switched mode-locked state, single-pulse state, multi-pulse state, and noise-like-pulse state. If other researchers implement a similar laser, they may observe the working states listed above.

Chapter 8

Conclusion and Future Works

8.1 The Conclusion

In conclusion, we have designed and demonstrated a thulium (Tm) doped mode-locked all-fiber laser with widely tunable operation and multi-wavelength emission based on nonlinear polarization evolution (NPE) technique.

Tm fiber is chosen as the gain medium as it has broad gain bandwidth, with higher pumping efficiency with 793 nm pumping, and the laser emission is in the eye-safe regime. The bidirectional pumping scheme, the NPE-induced transmission modulation on the net gain (saturated gain minus cavity loss), and the cavity loss management were implemented to enable the widely tunable operation. The NPE-induced transmission modulation is also responsible for the multi-wavelength emission and mode locking. The transmission of couplers and isolators are studied in order to know how it affects the net gain.

With this setup, we can achieve the tunable single-wavelength mode-locked all-fiber laser ranging from 1842 to 1978 nm. It is with 136 nm tunable range, which is the widest in such kind of laser, as far as we know. The tunable operation is enabled by NPE-induced transmission modulation, which forms spectral filters. By tuning the PCs, the emission wavelength of mode-locked laser will be tuned accordingly.

We also realize the tunable multi-wavelength mode-locked all-fiber laser. The tuning range is 52 nm, from 1864 to 1916 nm for dual-wavelength mode-locking, 49 nm, from 1863 to 1912 nm for tri-wavelength mode-locking, and 55 nm, from 1860 to 1915 nm for four-wavelength mode-locking, respectively, which is also the widest in such kind of laser. The multi-wavelength emission is enabled when the net gain has multiple peaks, functioning as a periodic band-pass filter, and the optical power was equally distributed among two or three or four peaks, to reduce the mutual mode competition. This multi-peak net gain is formed by the periodic modulation of cavity transmission, induced by NPE effect.

The dual- and tri- wavelength mode locking can be switchable with the full two-bit and three-bit binary control, respectively. This switchable operation is firstly demonstrated in such kind of laser. This could act as an optical binary system, which has potential applications in optical signal processing, optical switching devices and optical communication.

The quasi-five-wavelength Q-switched mode locking is working on the Q-switched mode-locked state, due to the insufficient intracavity pulse energy. To switch the Q-switched mode-locked state to stable mode-locked state, the intracavity pulse energy should be increased by either increase the pump power or avoid the gain filtering effect.

What is more, we study the sidebands of solitons in this laser cavity. There are two types of peak sidebands, one is Kelly sidebands due to the constructive interference between dispersive waves and solitons, and the other is modulation instability sidebands due to the parametric coupling between dispersive waves and solitons, which is a nonlinear effect and has the threshold pump power. The dip sidebands are due to the water absorption.

The noise-like pulses are also observed with a broad and smooth spectrum. There are many subpulses inside one pulse envelope, with different peak powers and pulse widths.

Various applications by this widely tunable multi-wavelength Tm-doped mode-locked all-fiber laser can be found in optical communications, spectroscopy, time-resolved measurement, and among others.

8.2 The Future Works

The tunable range and the number of emission wavelength can be further improved by engineering the gain profile of the gain fiber, to make it wide and flat. For the Tm-doped silica fiber, the short wavelength end of the tuning range is limited by reabsorption associated with the three-level nature of the Tm ion. At longer wavelengths, performance is limited by a lower thulium emission cross section and background absorption losses in the silica glass host material [114]. These issues need to be solved during the fabrication of Tm fiber. Meanwhile the gain profile should be flat, to reduce the gain difference between different longitudinal modes, to enable more laser emission at multiple wavelengths.

A high power tunable multi-wavelength Tm-doped fiber laser can be developed in some applications such as remote sensing and nonlinear spectroscopy. The power level in this setup is limited by the pump source. To increase the power, high power 793 nm laser diode can be adopted, or a master oscillator fiber amplifier system is adopted by using this setup as a seed laser. When building a high power system, the use of high-power optical components, and the cooling of this components and fibers, and the safety issue should be taken into consideration.

Technique to suppress the peak sidebands of solitons should be developed as it could cause the soliton instability, limit the further pulse narrowing [115], and reduce the amplification efficiency in an amplification system.

The tunable and multi-wavelength operation can be further extended to mid-infrared (mid-IR) regime, to enlarge the spectral range of current applications. Now the optical components used to construct a fiber laser cavity in mid-IR regime is only available with free-spaced form, and the pump source for the mid-IR laser emission is also limited. The development of a tunable and multi-wavelength mid-IR all-fiber laser will drive the development of fiber-based mid-IR components such as isolators and couplers.

Reference

1. "Synthetic stick absorption spectrum of a simple gas mixture corresponding to the Earth's atmosphere composition based on HITRAN data created using Hitran on the Web system.," https://en.wikipedia.org/wiki/Electromagnetic_absorption_by_water.
2. G. Whitenett, G. Stewart, H. Yu, and B. Culshaw, "Investigation of a tuneable mode-locked fiber laser for application to multipoint gas spectroscopy," *J. Light. Technol.* **22**, 813–819 (2004).
3. J. Ye, L. Yan, W. Pan, B. Luo, X. Zou, A. Yi, and X. S. Yao, "Two-dimensionally tunable microwave signal generation based on optical frequency-to-time conversion," *Opt. Lett.* **35**, 2606–2608 (2010).
4. Q. Ye, R. Huang, Q. Xu, H. Cai, R. Qu, and Z. Fang, "Numerical investigation of ultrashort complex pulse generation based on pulse shaping using a superstructure fiber bragg grating," *J. Light. Technol.* **27**, 2449–2456 (2009).
5. K. Kitagawa, "Single-shot multi-wavelength interferometry without carrier fringe introduction," *J. Electron. Imaging* **21**, 021107 (2012).
6. A. O'Keefe and D. a. G. Deacon, "Cavity ring-down optical spectrometer for absorption measurements using pulsed laser sources," *Rev. Sci. Instrum.* **59**, 2544–2551 (1988).
7. R. L. Swofford and A. C. Albrecht, "Nonlinear spectroscopy," *Annu. Rev. Phys. Chem.* **29**, 421–440 (1978).
8. S. a. Studenikin and M. Cocivera, "Time-resolved luminescence and photoconductivity of polycrystalline ZnO films," *J. Appl. Phys.* **91**, 5060–5065 (2002).
9. C. V. Shank, R. Yen, and C. Hirlimann, "Time-resolved reflectivity measurements of femtosecond-optical-pulse-induced phase transitions in silicon," *Phys. Rev. Lett.* **50**, 454–457 (1983).
10. Z. Sun, D. Popa, T. Hasan, F. Torrisi, F. Wang, E. J. R. Kelleher, J. C. Travers, V. Nicolosi, and A. C. Ferrari, "A stable, wideband tunable, near transform-limited, graphene-mode-locked, ultrafast laser," *Nano Res.* **3**, 653–660 (2010).
11. Z. C. Luo, A. P. Luo, and W. C. Xu, "Tunable and switchable multiwavelength passively mode-locked fiber laser based on SESAM and inline birefringence comb filter," *IEEE Photonics J.* **3**, 64–70 (2011).

12. X. Liu, X. Zhou, X. Tang, J. Ng, J. Hao, T. Y. Chai, E. Leong, and C. Lu, "Switchable and tunable multiwavelength erbium-doped fiber laser with fiber Bragg gratings and photonic crystal fiber," *IEEE Photonics Technol. Lett.* **17**, 1626–1628 (2005).
13. Z. Lv, H. Teng, R. Wang, L. Wang, J. Wang, and Z. Wei, "Tunable triple-wavelength mode-locked ytterbium fiber laser with birefringence filter," *Appl. Phys. B* **121**, 1–6 (2015).
14. X. Wang, Y. Zhu, P. Zhou, X. Wang, H. Xiao, and L. Si, "Tunable , multiwavelength Tm-doped fiber laser based on polarization rotation and four-wave- mixing effect," *Opt. Express* **21**, 25977–25984 (2013).
15. S. Huang, Y. Wang, P. Yan, J. Zhao, H. Li, and R. Lin, "Tunable and switchable multi-wavelength dissipative soliton generation in a graphene oxide mode-locked Yb-doped fiber laser," *Opt. Express* **22**, 11417–11426 (2014).
16. H. Zhang, D. Y. Tang, X. Wu, and L. M. Zhao, "Multi-wavelength dissipative soliton operation of an erbium-doped fiber laser," *Opt. Express* **17**, 12692–12697 (2009).
17. S. M. Kobtsev, S. V. Kukarin, and Y. S. Fedotov, "Wide-spectrally-tunable CW and femtosecond linear fiber lasers with ultrabroadband loop mirrors based on fiber circulators," *Laser Phys.* **20**, 347–350 (2010).
18. Z. W. Xu and Z. X. Zhang, "All-normal-dispersion multi-wavelength dissipative soliton Yb-doped fiber laser," *Laser Phys. Lett.* **10**, 085105 (2013).
19. X. Li, Y. Wang, Y. Wang, X. Hu, W. Zhao, X. Liu, J. Yu, C. Gao, W. Zhang, Z. Yang, C. Li, and D. Shen, "Wavelength-switchable and wavelength-tunable all-normal-dispersion mode-locked Yb-doped fiber laser based on single-walled carbon nanotube wall paper absorber," *IEEE Photonics J.* **4**, 234–241 (2012).
20. X. Li, X. Liu, D. Mao, X. Hu, and H. Lu, "Tunable and switchable multiwavelength fiber lasers with broadband range based on nonlinear polarization rotation technique," *Opt. Eng.* **49**, 094303 (2010).
21. X. H. Li, Y. S. Wang, W. Zhao, W. Zhang, Z. Yang, X. H. Hu, H. S. Wang, X. L. Wang, Y. N. Zhang, Y. K. Gong, C. Li, and D. Y. Shen, "All-normal dispersion, figure-eight, tunable passively mode-locked fiber laser with an invisible and changeable intracavity bandpass filter," *Laser Phys.* **21**, 940–944 (2011).
22. Q. Fang, K. Kieu, and N. Peyghambarian, "An all-fiber 2-um wavelength-tunable mode-locked laser," *IEEE Photonics Technol. Lett.* **22**, 1656–1658 (2010).

23. A. Y. Chamorovskiy, A. V. Marakulin, A. S. Kurkov, and O. G. Okhotnikov, "Tunable Ho-doped soliton fiber laser mode-locked by carbon nanotube saturable absorber," *Laser Phys. Lett.* **9**, 602–606 (2012).
24. R. Ramaswami, "Multiwavelength lightwave networks for computer communication," *Commun. Mag. IEEE* **31**, 78 – 88 (1993).
25. J. Marshall, G. Stewart, and G. Whitenett, "Design of a tunable L-band multi-wavelength laser system for application to gas spectroscopy," *Meas. Sci. Technol.* **17**, 1023–1031 (2006).
26. A. D. Kersey, "Multiplexed fiber optic sensors," *Proc. SPIE* **1797**, 161–185 (1992).
27. D. Milam and M. J. Weber, "Measurement of nonlinear refractive-index coefficients using time-resolved interferometry: Application to optical materials for high-power neodymium lasers," *J. Appl. Phys.* **47**, 2497–2501 (2014).
28. H. Malitson, I., "Interspecimen Comparison of the Refractive Index of Fused Silica," *J. Opt. Soc. Am.* **55**, 1205–1209 (1965).
29. S. M. J. Kelly, "Characteristic sideband instability of periodically amplified average soliton," *Electron. Lett.* **28**, 806–808 (1992).
30. G. Agrawal, "Optical pulse propagation in doped fiber amplifiers," *Phys. Rev. A* **44**, 7493–7501 (1991).
31. G. Agrawal, *Nonlinear Fiber Optics* (Academic Press, 2012), Vol. 2012.
32. O. Svelto and D. C. Hanna, *Principles of Lasers*, 5th editio (Springer Science+Business Media, 2010), Vol. 53.
33. E. P. Ippen, "Principles of passive mode locking," *Appl. Phys. B Lasers Opt.* **58**, 159–170 (1994).
34. H. A. Haus, "Mode-locking of lasers," *IEEE J. Sel. Top. Quantum Electron.* **6**, 1173–1185 (2000).
35. R. Ulrich and A. Simon, "Polarization optics of twisted single-mode fibers," *Appl. Opt.* **18**, 2241–2251 (1979).
36. L. E. Nelson, D. J. Jones, K. Tamura, H. a. Haus, and E. P. Ippen, "Ultrashort-pulse fiber ring lasers," *Appl. Phys. B Lasers Opt.* **65**, 277–294 (1997).
37. R. H. Stolen, J. Botineau, and A. Ashkin, "Intensity discrimination of optical pulses with birefringent fibers.," *Opt. Lett.* **7**, 512–514 (1982).

38. Z. Luo, A. Luo, W. Xu, H. Yin, J. Liu, Q. Ye, and Z. Fang, "Tunable multiwavelength passively mode-locked fiber ring laser using intracavity birefringence-induced comb filter," *IEEE Photonics J.* **2**, 571–577 (2010).
39. M. Endo, G. Ghosh, and Y. Tanaka, "Generation of tunable pulses below 345 fs using a passively mode-locked fiber ring laser with bulk components," *Jpn. J. Appl. Phys.* **35**, 906–908 (1996).
40. L. E. Nelson, E. P. Ippen, and H. A. Haus, "Broadly tunable sub-500 fs pulses from an additive-pulse mode-locked thulium-doped fiber ring laser," *Appl. Phys. Lett.* **67**, 19–21 (1995).
41. S. Pan and C. Lou, "Stable multiwavelength dispersion-tuned actively mode-locked erbium-doped fiber ring laser using nonlinear polarization rotation," *IEEE Photonics Technol. Lett.* **18**, 1451–1453 (2006).
42. R. M. Sova, K. Chang-Seok, and J. U. Kang, "Tunable dual-wavelength all-PM fiber ring laser," *Photonics Technol. Lett. IEEE* **14**, 287–289 (2002).
43. X. Zhao, Z. Zheng, L. Liu, Y. Liu, Y. Jiang, X. Yang, and J. Zhu, "Switchable, dual-wavelength passively mode-locked ultrafast fiber laser based on a single-wall carbon nanotube modelocker and intracavity loss tuning," *Opt. Express* **19**, 1168–1173 (2011).
44. Z. Zhang, L. Zhan, K. Xu, J. Wu, Y. Xia, and J. Lin, "Multiwavelength fiber laser with fine adjustment, based on nonlinear polarization rotation and birefringence fiber filter," *Opt. Lett.* **33**, 324–326 (2008).
45. X. Feng, H. Tam, and P. K. A. Wai, "Stable and uniform multiwavelength erbium-doped fiber laser using nonlinear polarization rotation," *Opt. Express* **14**, 8205–8210 (2006).
46. Z. C. Luo, A. P. Luo, and W. C. Xu, "Multiwavelength picosecond and single wavelength femtosecond pulses emission in a passively mode-locked fiber laser using a semiconductor saturable absorber mirror and a contrast ratio tunable comb filter.," *Appl. Opt.* **50**, 2831–2835 (2011).
47. M. A. Chernysheva, A. A. Krylov, P. G. Kryukov, and E. M. Dianov, "Nonlinear amplifying loop-mirror-based mode-locked thulium-doped fiber laser," *IEEE Photonics Technol. Lett.* **24**, 1254–1256 (2012).
48. W. Peng, F. Yan, Q. Li, S. Liu, T. Feng, and S. Tan, "A 1.97 μm multiwavelength thulium-doped silica fiber laser based on a nonlinear amplifier loop mirror," *Laser Phys.*

- Lett. **10**, 115102 (2013).
49. X. Jin, X. Wang, X. Wang, and P. Zhou, "Tunable multiwavelength mode-locked Tm/Ho-doped fiber laser based on a nonlinear amplified loop mirror," *Appl. Opt.* **54**, 8260–8264 (2015).
 50. S. Liu, F. Yan, T. Feng, B. Wu, Z. Dong, and G. Chang, "Switchable and spacing-tunable dual-wavelength thulium-doped silica fiber laser based on a nonlinear amplifier loop mirror," *Appl. Opt.* **53**, 5522–5526 (2014).
 51. S.-K. Liaw, K.-C. Hsu, and N.-K. Chen, "Tunable erbium-doped fiber lasers using various inline fiber filters," *Engineering* **02**, 585–593 (2010).
 52. X. Liu and Y. Cui, "Flexible pulse-controlled fiber laser," *Sci. Rep.* **5**, 9399 (2015).
 53. K. Yin, B. Zhang, G. Xue, L. Li, and J. Hou, "High-power all-fiber wavelength-tunable thulium doped fiber laser at 2 μm ," *Opt. Express* **22**, 19947–19952 (2014).
 54. X. Liu, D. Han, Z. Sun, C. Zeng, H. Lu, D. Mao, Y. Cui, and F. Wang, "Versatile multi-wavelength ultrafast fiber laser mode-locked by carbon nanotubes," *Sci. Rep.* **3**, 2718 (2013).
 55. G. Anzueto-Sanchez, J. Castellon-Urbe, and A. Martine-Rios, "Wavelength-Dependent Selective Loss for Wavelength Switching Operation of an Erbium-Doped Fiber Ring Laser," *Opt. Rev.* **18**, 301–304 (2011).
 56. J. H. Lim, K. S. Lee, J. C. Kim, and B. H. Lee, "Tunable fiber gratings fabricated in photonic crystal fiber by use of mechanical pressure," *Opt. Lett.* **29**, 331–333 (2004).
 57. K. Kieu and M. Mansuripur, "Tuning of fiber lasers by use of a single-mode biconic fiber taper," *Opt. Lett.* **31**, 2435–2437 (2006).
 58. Z. Q. Luo, J. Z. Wang, M. Zhou, H. Y. Xu, Z. P. Cai, and C. C. Ye, "Multiwavelength mode-locked erbium-doped fiber laser based on the interaction of graphene and fiber-taper evanescent field," *Laser Phys. Lett.* **9**, 229–233 (2012).
 59. Z. Luo, Y. Huang, J. Wang, H. Cheng, Z. Cai, and C. Ye, "Multiwavelength dissipative-soliton generation in Yb-fiber laser using graphene-deposited fiber-taper," *IEEE Photonics Technol. Lett.* **24**, 1539–1542 (2012).
 60. "Fabry–Pérot interferometer," https://en.wikipedia.org/wiki/Fabry%E2%80%93P%C3%A9rot_interferometer.
 61. N. Park, J. W. Dawson, K. J. Vahala, and C. Miller, "All fiber, low threshold, widely

- tunable single-frequency, erbium-doped fiber ring laser with a tandem fiber Fabry-Perot filter," *Appl. Phys. Lett.* **59**, 2369–2371 (1991).
62. J. Tian, Y. Yao, J. J. Xiao, X. Yu, and D. Chen, "Tunable multiwavelength erbium-doped fiber laser based on intensity-dependent loss and intra-cavity loss modulation," *Opt. Commun.* **285**, 2426–2429 (2012).
 63. X. Wang, T. Zhu, L. Chen, and X. Bao, "Tunable Fabry-Perot filter using hollow-core photonic bandgap fiber and micro-fiber for a narrow-linewidth laser.," *Opt. Express* **19**, 9617–9625 (2011).
 64. J. Masson, R. St-gelais, S. Member, A. Poulin, Y. Peter, and S. Member, "Tunable fiber laser using a MEMS-based in plane Fabry-Pérot filter," *IEEE J. Quantum Electron.* **46**, 1313–1319 (2010).
 65. S. Li and K. T. Chan, "Actively mode-locked erbium fiber ring laser using a Fabry-Perot semiconductor modulator as mode locker and tunable filter," *Appl. Phys. Lett.* **74**, 2737 (1999).
 66. J. M. Sierra-Hernandez, R. Rojas-Laguna, E. Vargas-Rodriguez, J. M. Estudillo-Ayala, D. Jauregui-Vazquez, a D. Guzmán-Chávez, and P. Zaca-Moran, "A tunable multi-wavelength erbium doped fiber laser based on a Mach-Zehnder interferometer and photonic crystal fiber," *Laser Phys.* **23**, 125103 (2013).
 67. M. R. K. Soltanian, H. Ahmad, a. Khodaie, I. S. Amiri, M. F. Ismail, and S. W. Harun, "A Stable Dual-wavelength Thulium-doped Fiber Laser at 1.9 μm Using Photonic Crystal Fiber," *Sci. Rep.* **5**, 14537 (2015).
 68. J. E. Antonio-Lopez, A. Castillo-Guzman, D. A. May-Arrioja, R. Selvas-Aguilar, and P. Likamwa, "Tunable multimode-interference bandpass fiber filter," *Opt. Lett.* **35**, 324–326 (2010).
 69. A. Castillo-Guzman, J. E. Antonio-Lopez, R. Selvas-Aguilar, D. A. May-Arrioja, J. Estudillo-Ayala, and P. LiKamWa, "Widely tunable erbium-doped fiber laser based on multimode interference effect," *Opt. Express* **18**, 591–597 (2010).
 70. S. Zhao, P. Lu, D. Liu, and J. Zhang, "Switchable multiwavelength thulium-doped fiber ring lasers," *Opt. Eng.* **52**, 086105 (2013).
 71. T. V. A. Tran, K. Lee, S. B. Lee, and Y. Han, "Switchable multiwavelength erbium doped fiber laser based on a nonlinear optical loop mirror incorporating multiple fiber Bragg gratings," *Opt. Express* **16**, 1460–1465 (2008).

72. Y.-G. Han, T. V. A. Tran, and S. B. Lee, "Wavelength-spacing tunable multiwavelength erbium-doped fiber laser based on four-wave mixing of dispersion-shifted fiber," *Opt. Lett.* **31**, 697–699 (2006).
73. Y.-G. Han and S. B. Lee, "Flexibly tunable multiwavelength erbium-doped fiber laser based on four-wave mixing effect in dispersion-shifted fibers.," *Opt. Express* **13**, 10134–10139 (2005).
74. R. L. Shubochkin, V. A. Kozlov, A. L. G. Carter, and T. F. Morse, "Tunable thulium-doped all-fiber laser," *IEEE Photonics Technol. Lett.* **10**, 944–945 (1998).
75. H. Zhang, D. Y. Tang, L. M. Zhao, Q. L. Bao, K. P. Loh, B. Lin, and S. C. Tjin, "Compact graphene mode-locked wavelength-tunable erbium-doped fiber lasers: From all anomalous dispersion to all normal dispersion," *Laser Phys. Lett.* **7**, 591–596 (2010).
76. Y. S. Fedotov, S. M. Kobtsev, R. N. Arif, A. G. Rozhin, C. Mou, and S. K. Turitsyn, "Spectrum-, pulsewidth-, and wavelength-switchable all-fiber mode-locked Yb laser with fiber based birefringent filter," *Opt. Express* **20**, 17797–17805 (2012).
77. C. S. Jun and B. Y. Kim, "Mode-locking and Q-switching in multi-wavelength fiber ring laser using low frequency phase modulation.," *Opt. Express* **19**, 6290–6295 (2011).
78. S. Wang, P. Lu, S. Zhao, D. Liu, W. Yang, and J. Zhang, "2- μ m switchable dual-wavelength fiber laser with cascaded filter structure based on dual-channel Mach–Zehnder interferometer and spatial mode beating effect," *Appl. Phys. B* DOI:10.1007/s00340–014–5868–0 (2014).
79. X. Feng, P. K. a. Wai, H. Y. Tam, C. Lu, and B. Guan, "Switchable multiwavelength erbium-doped fiber laser employing wavelength-dependent loss," *Opt. Fiber Technol.* **17**, 138–140 (2011).
80. K. Scholle, S. Lamrini, P. Koopmann, and P. Fuhrberg, "2 μ m laser sources and their possible applications," in *Frontiers in Guided Wave Optics and Optoelectronics* (InTech, 2010), pp. 471–500.
81. V. (Vartan) Ter-Mikirtychev, *Fundamentals of Fiber Lasers and Fiber Amplifiers* (Springer, 2014).
82. S. D. Agger and J. H. Povlsen, "Emission and absorption cross section of thulium doped silica fibers," *Opt. Express* **14**, 50–57 (2006).
83. N. Simakov, A. Hemming, W. A. Clarkson, J. Haub, and A. Carter, "A cladding-pumped, tunable holmium doped fiber laser," *Opt. Express* **21**, 187–191 (2013).

84. D. Creeden, B. R. Johnson, G. A. Rines, and S. D. Setzler, "High power resonant pumping of Tm-doped fiber amplifiers in core- and cladding-pumped configurations," *Opt. Express* **22**, 29067–29080 (2014).
85. M. Johnson, "Single-mode-fiber birefringent filters.," *Opt. Lett.* **5**, 142–144 (1980).
86. Y. Yen and R. Ulrich, "Birefringent optical filters in single-mode fiber," *Opt. Lett.* **6**, 278–280 (1981).
87. K. Ozgören and F. O. Ilday, "All-fiber all-normal dispersion laser with a fiber-based Lyot filter.," *Opt. Lett.* **35**, 1296–1298 (2010).
88. R. Ulrich, S. C. Rashleigh, and W. Eickhoff, "Bending-induced birefringence in single-mode fibers.," *Opt. Lett.* **5**, 273–275 (1980).
89. S. C. Rashleigh, "Wavelength dependence of birefringence in highly birefringent fibers.," *Opt. Lett.* **7**, 294–296 (1982).
90. "PANDA PM Specialty Fibers,"
[https://www.corning.com/media/worldwide/csm/documents/PANDA PM and RC PANDA Specialty Fiber.pdf](https://www.corning.com/media/worldwide/csm/documents/PANDA_PM_and_RC_PANDA_Specialty_Fiber.pdf).
91. G. Sobon, J. Sotor, I. Pasternak, A. Krajewska, W. Strupinski, and K. M. Abramski, "All-polarization maintaining, graphene-based femtosecond Tm-doped all-fiber laser," *Opt. Express* **23**, 9339–9346 (2015).
92. Z. Yan, X. Li, Y. Tang, P. P. Shum, X. Yu, Y. Zhang, and Q. J. Wang, "Tunable and switchable dual-wavelength Tm-doped mode-locked fiber laser by nonlinear polarization evolution," *Opt. Express* **23**, 4369–4376 (2015).
93. Z. Yan, B. Sun, X. Li, J. Luo, P. P. Shum, X. Yu, Y. Zhang, and Q. J. Wang, "Widely tunable Tm-doped mode-locked all-fiber laser," *Sci. Rep.* **6**, 27245 (2016).
94. Z. Yan, Y. Tang, B. Sun, T. Liu, X. Li, P. S. Ping, X. Yu, Y. Zhang, and Q. J. Wang, "Switchable multi-wavelength Tm-doped mode-locked fiber laser," *Opt. Lett.* **40**, 1916–1919 (2015).
95. C. Hönninger, R. Paschotta, F. Morier-Genoud, M. Moser, and U. Keller, "Q-switching stability limits of continuous-wave passive mode locking," *J. Opt. Soc. Am. B* **16**, 46–56 (1999).
96. N. J. Smith, K. J. Blow, and I. Andonovic, "Sideband generation through perturbations to the average soliton model," *J. Light. Technol.* **10**, 1329–1333 (1992).

97. S. M. J. Kelly, K. Smith, K. J. Blow, and N. J. Doran, "Average soliton dynamics of a high-gain erbium fiber laser," *Opt. Lett.* **16**, 1337–1339 (1991).
98. D. Tang, L. Zhao, X. Wu, and H. Zhang, "Soliton modulation instability in fiber lasers," *Phys. Rev. A* **80**, 023806 (2009).
99. L. S. Rothman, I. E. Gordon, A. Barbe, D. C. Benner, P. F. Bernath, M. Birk, V. Boudon, L. R. Brown, A. Campargue, J. P. Champion, K. Chance, L. H. Coudert, V. Dana, V. M. Devi, S. Fally, J. M. Flaud, R. R. Gamache, A. Goldman, D. Jacquemart, I. Kleiner, N. Lacome, W. J. Lafferty, J. Y. Mandin, S. T. Massie, S. N. Mikhailenko, C. E. Miller, N. Moazzen-Ahmadi, O. V. Naumenko, A. V. Nikitin, J. Orphal, V. I. Perevalov, A. Perrin, A. Predoi-Cross, C. P. Rinsland, M. Rotger, M. Šimečková, M. A. H. Smith, K. Sung, S. A. Tashkun, J. Tennyson, R. A. Toth, A. C. Vandaele, and J. Vander Auwera, "The HITRAN 2008 molecular spectroscopic database," *J. Quant. Spectrosc. Radiat. Transf.* **110**, 533–572 (2009).
100. Y. Takushima, K. Yasunaka, Y. Ozeki, and K. Kikuchi, "87 nm bandwidth noise-like pulse generation from erbium-doped fibre laser," *Electron. Lett.* **41**, 7–8 (2005).
101. J. C. Hernandez-Garcia, O. Pottiez, J. M. Estudillo-Ayala, and R. Rojas-Laguna, "Numerical analysis of a broadband spectrum generated in a standard fiber by noise-like pulses from a passively mode-locked fiber laser," *Opt. Commun.* **285**, 1915–1919 (2012).
102. J. C. Hernandez-Garcia, O. Pottiez, R. Grajales-Coutiño, B. Ibarra-Escamilla, E. a. Kuzin, J. M. Estudillo-Ayala, and J. Gutierrez-Gutierrez, "Generation of long broadband pulses with a figure-eight fiber laser," *Laser Phys.* **21**, 1518–1524 (2011).
103. Q. Wang, T. Chen, M. Li, B. Zhang, Y. Lu, and K. P. Chen, "All-fiber ultrafast thulium-doped fiber ring laser with dissipative soliton and noise-like output in normal dispersion by single-wall carbon nanotubes," *Appl. Phys. Lett.* **103**, 011103 (2013).
104. L. M. Zhao and D. Y. Tang, "Generation of 15-nJ bunched noise-like pulses with 93-nm bandwidth in an erbium-doped fiber ring laser," *Appl. Phys. B* **83**, 553–557 (2006).
105. L. M. Zhao, D. Y. Tang, T. H. Cheng, H. Y. Tam, and C. Lu, "120nm Bandwidth noise-like pulse generation in an erbium-doped fiber laser," *Opt. Commun.* **281**, 157–161 (2008).
106. M. Horowitz and Y. Silberberg, "Control of noiselike pulse generation in erbium-doped fiber lasers," *IEEE Photonics Technol. Lett.* **10**, 1389–1391 (1998).

107. M. Horowitz, Y. Barad, and Y. Silberberg, "Noiselike pulses with a broadband spectrum generated from an erbium-doped fiber laser," *Opt. Lett.* **22**, 799–801 (1997).
108. X. He, A. Luo, Q. Yang, T. Yang, X. Yuan, S. Xu, Q. Qian, D. Chen, Z. Luo, W. Xu, and Z. Yang, "60nm bandwidth, 17nJ noiselike pulse generation from a thulium-doped fiber ring laser," *Appl. Phys. Express* **6**, 112702 (2013).
109. S. Lin, S. Hwang, and J. Liu, "Supercontinuum generation in highly nonlinear fibers using amplified noise-like optical pulses," *Opt. Express* **22**, 4152–4160 (2014).
110. A. Zaytsev, C. Lin, Y. You, and C. Chung, "Supercontinuum generation by noise-like pulses transmitted through normally dispersive standard single-mode fibers," *Opt. Express* **21**, 16056 – 16062 (2013).
111. Y. Takushima, "High average power, depolarized super-continuum generation using a 1.55- μ m ASE noise source," *Opt. Express* **13**, 5871–5877 (2005).
112. J. C. Hernandez-Garcia, O. Pottiez, and J. M. Estudillo-Ayala, "Supercontinuum generation in a standard fiber pumped by noise-like pulses from a figure-eight fiber laser," *Laser Phys.* **22**, 221–226 (2011).
113. K. S. Chiang, "Stress-induced birefringence fibers designed for single-polarization single-mode operation," *J. Light. Technol.* **7**, 436–441 (1989).
114. T. S. McComb, R. A. Sims, C. C. C. Willis, P. Kadwani, V. Sudesh, L. Shah, and M. Richardson, "High-power widely tunable thulium fiber lasers," *Appl. Opt.* **49**, 6236–6242 (2010).
115. M. L. Dennis and I. N. Duling, "Role of dispersion in limiting pulse width in fiber lasers," *Appl. Phys. Lett.* **62**, 2911–2913 (1993).

Publications

Journal Papers

1. **Z. Yan**, B. Sun, X. Li, J. Luo, Perry P. Shum, X. Yu, Y. Zhang, and Q. J. Wang, “Widely tunable Tm-doped mode-locked all-fiber laser”, *Scientific Reports* 6, 27245, 2016.
2. J. Luo, B. Sun, J. Liu, **Z. Yan**, N. Li, E. L. Tan, Q. J. Wang and X. Yu, “Mid-IR supercontinuum pumped by femtosecond pulses from thulium doped all-fiber amplifier”, *Optics Express* 24, 13939-13945, 2016.
3. **Z. Yan**, Y. Tang, B. Sun, T. Liu, X. Li, Perry P. Shum, X. Yu, Y. Zhang, and Q. J. Wang, “Switchable multi-wavelength Tm-doped mode-locked fiber laser”, *Optics Letters* 40, 1916-1919, 2015.
4. **Z. Yan**, X. Li, Y. Tang, Perry P. Shum, X. Yu, Y. Zhang, and Q. J. Wang, “Tunable and switchable dual-wavelength Tm-doped mode-locked fiber laser by nonlinear polarization evolution”, *Optics Express* 23, 4369-4376, 2015.
5. X. Li, X. Yu, Z. Sun, **Z. Yan**, B. Sun, Y. Cheng, X. Yu, Y. Zhang, and Q. J. Wang, "High-power graphene mode-locked Tm/Ho co-doped fiber laser with evanescent field interaction", *Scientific Reports* 5, 16624, 2015.
6. L. Sun, X. Wang, K. Zhang, J. Zou, **Z. Yan**, X. Hu and Q. Zhang, “Bi-functional electrode for UV detector and supercapacitor”, *Nano Energy* 15, 445-452, 2015.
7. X. Li, Y. Tang, **Z. Yan**, Y. Wang, B. Meng, G. Liang, H. Sun, X. Yu, Y. Zhang, X. Cheng, and Q. J. Wang, “Broadband saturable absorption of graphene oxide thin film and its application in pulsed fiber lasers”, *IEEE Journal of Selected Topics in Quantum Electronics* 20, 1101107, 2014.
8. Y. Tang, X. Li, **Z. Yan**, Y. Xia, Z. Ying, and Q. J. Wang, “50-W 2- μ m nanosecond all-fiber-based thulium-doped fiber amplifier”, *IEEE Journal of Selected Topics in Quantum Electronics* 20, 3100707, 2014.
9. Y. Tang, X. Yu, X. Li, **Z. Yan**, and Q. J. Wang, “High power Q switching thulium fiber laser with single-layer graphene”, *Optics Letters* 39, 614-617, 2014.

Conference Proceedings

1. **Z. Yan**, X. Li, B. Sun, J. Luo, Perry P. Shum, X. Yu, Y. Zhang, and Q. J. Wang, “Widely tunable multi-wavelength Tm-doped mode-locked fiber laser”, Proc. SPIE 9728, Fiber Lasers XIII: Technology, Systems, and Applications, 972812, 2016, doi:10.1117/12.2213974.

Conference Talks

1. **Z. Yan**, X. Li, B. Sun, J. Luo, Perry P. Shum, X. Yu, Y. Zhang, and Q. J. Wang, “Widely tunable multi-wavelength Tm-doped mode-locked fiber laser”, SPIE Photonics West, 9728-40, United States, 2016. (SPIE travel scholarship award)
2. **Z. Yan**, X. Li, B. Sun, X. Yu, Q. J. Wang, "Dip-type sidebands in Tm-doped soliton fiber laser", International Conference on Materials for Advanced Technology together with Photonics Global Conference ICMAT15-A-4071, Singapore, 2015. (Best paper award)
3. **Z. Yan**, X. Li, Y. Tang, P. Shum, X. Yu, Y. Zhang, Q. J. Wang, “Simulation of mid-IR supercontinuum generation in fluoride fiber pumped by noise-like pulse”, International Conference on Materials for Advanced Technology ICMAT13-A-2634, Singapore, 2013.